

JTG

**Recommended Industry Standards of
the People's Republic of China**
中华人民共和国行业推荐性标准

JTG/T 3360-01—2018 (EN)

**Specifications for Wind-Resistant Design of
Highway Bridges**

公路桥梁抗风设计规范

(英文版)

Issue date: November 19, 2018

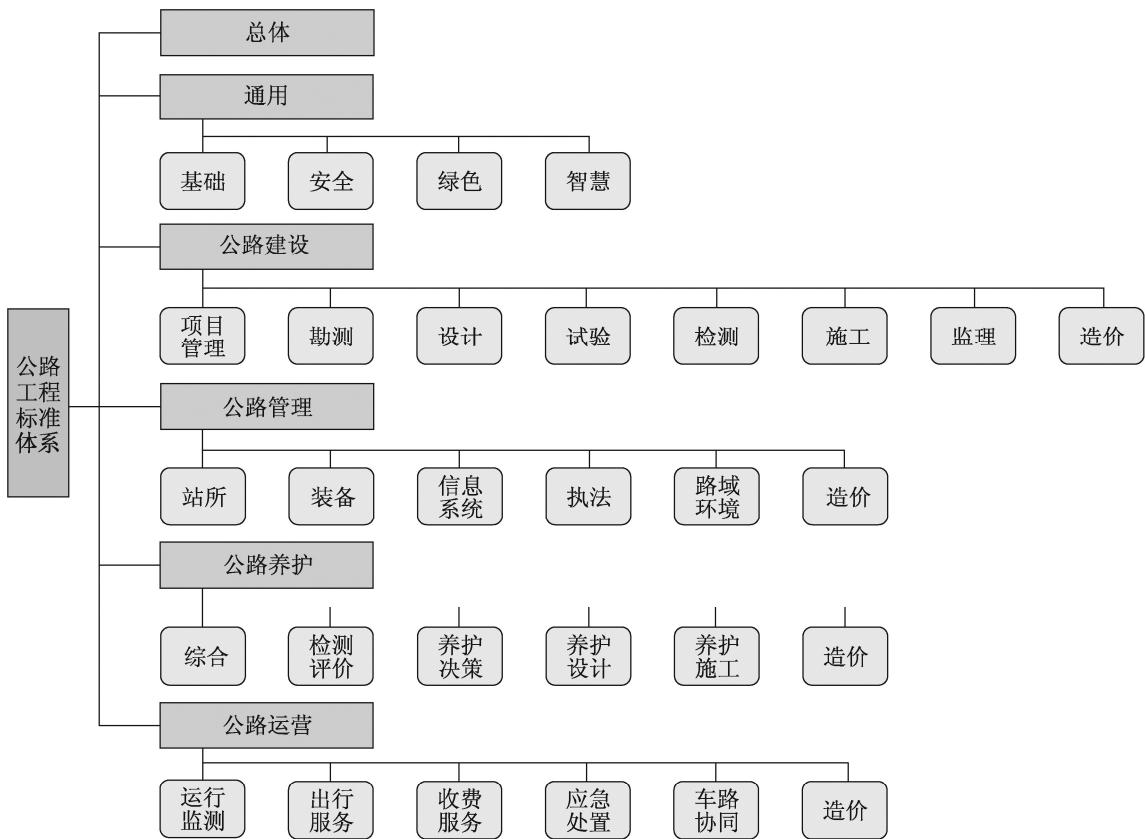
Effective date: March 01, 2019

Issued by the Ministry of Transport of the People's Republic of China

英文版编译出版说明

标准是人类文明进步的成果,是世界通用的技术语言,促进世界的互联互通。近年来,中国政府大力开展标准化工作,通过标准驱动创新、协调、绿色、开放、共享的共同发展。在丝绸之路经济带与 21 世纪海上丝绸之路,即“一带一路”倡议的指引下,为适应日益增长的全球交通运输发展的需求,增进世界连接,促进知识传播与经验分享,中华人民共和国交通运输部组织编译并发布了一系列中国公路行业标准英文版。

中华人民共和国交通运输部发布的公路工程行业标准代号为 JTG,体系范围涵盖公路工程从规划建设到养护和运营管理全过程所需要的设施、技术、管理与服务标准,也包括相关的安全、环保和经济方面的评价等标准。



中国的公路标准体系有效地支撑了中国公路桥梁的快速发展,包含了多项桥梁相关的设计、施工、养护标准。目前有关桥梁设计的规范有:《公路桥涵设计通用规范》、《公路钢筋混凝土及预应力混凝土桥涵设计规范》、《公路圬工桥涵设计规范》、《公路钢结构桥梁设计规范》、《公路钢混组合桥梁设计与施工规范》、《公路斜拉桥设计规范》、《公路悬索桥设计规范》、《公路钢管混凝土拱桥设计规范》、《公路装配式混凝土桥梁设计规范》、《公路桥梁抗风设计规范》、《公路桥梁抗撞设计规范》、《公路桥梁景观设计规范》等。其中,《公路桥梁抗风设计规范》是公路工程行业唯一的抗风设计推荐性标准,对保障公路桥梁结构安全与耐久性具有极其重要的作用,在中国交通建设行业得到了非常广泛的应用。

1996 年我国编制并出版了第一部《公路桥梁抗风设计指南》,在此基础上,编制了《公路桥梁抗风设计规范》(JTG/T D60 -01—2004)(以下简称《规范》04 版),并于 2004 年颁布实施。尔后,对《规范》04 版进行了全面修订,形成了本次编译的《公路桥梁抗风设计规范》(JTG/T 3360 -01—2018)中文版,于 2018 年 11 月发布,2019 年 3 月 1 日实施。

《公路桥梁抗风设计规范》(JTG/T 3360 -01—2018)确立了“安全可靠、技术先进、经济合理”的设计原则,采用了基于性能的设计思想以及以分项系数表达的极限状态设计方法,完善了风荷载计算体系和抗风极限状态设计方法,确保桥梁在设计使用年限内满足抗风稳定性、行车安全及舒适性、结构耐久性要求,为各类公路桥梁工程提供标准化抗风设计框架,推动大跨径桥梁抗风设计的精细化发展。

本规范英文版的编译发布便是希望将中国的工程经验和技術成果与各国同行进行交流分享,为其他国家类似建设条件的公路桥涵建设提供参考借鉴。

本规范英文版的编译工作由中华人民共和国交通运输部委托福州大学主持完成,并由中华人民共和国交通运输部公路局组织审定。

本规范英文的内容与现行中文版一致,如出现异议时,以中文版为准。

感谢中文版编者陈艾荣和马如进教授在本规范英文编译与审定期间给予的指导与支持。

如在执行过程中发现问题或有任何修改建议,请函告英文版主编单位(地址:福建省福州市福州大学城乌龙江北大道 2 号,邮政编码:350108,电子邮箱:zhchen@fzu.edu.cn),以便修订时研用。

英文版主编单位:福州大学

英文版主编:陈昭晖

英文版参编人员:陈宝春,Ahad Javanmardi

英文版主审:Khaled Sennah

英文版参与审查人员:张慧斌,郭彦霖,董延峰,黄李骥,赵姬,Krishna Shrestha

交通运输部信息公开
浏览专用

The People's Republic of China

Ministry of Transport

Public Notice

No.79

**Public Notice on Issuing of the *Specifications for Wind-resistant
Design of Highway Bridges***

The *Specifications for Wind-Resistant Design of Highway Bridges* (JTG/T 3360-01—2018) is hereby issued as one of the industry standards for highway engineering to become effective on March 1, 2019. The former edition of the *Specifications* (JTG/T D60-01—2004) and its English version shall be superseded from the same date.

The general administration and final interpretation of the *Specifications for Wind-Resistant Design of Highway Bridges* (JTG/T 3360-01—2018) belong to the Ministry of Transport, while particular interpretation for application and routine administration of the *Specifications* shall be provided by Tongji University.

Comments, suggestions and inquiries are welcome and should be addressed to Tongji University (Room 313, Department of Bridge Engineering, Tongji University, No. 1239 Siping Road, Shanghai 200092, China).

It is hereby announced.

The Ministry of Transport of the People's Republic of China

November 19, 2018

Introduction to English Version

Standards reflect the achievement of civilization, provide common languages for technical communications and improve global connectivity. In recent years, the Chinese government has been proactively implementing standardization to stimulate innovation, coordination, greenness and opening up for shared development in China and worldwide. To align with the Belt One Road Initiative for mutual development, the Ministry of Transport of the People's Republic of China organized the compilation and publication of international version of Chinese transportation industry standards and specifications to meet the increasing demands for international cooperation in transportation, enhance global connectivity, promote knowledge dissemination and sharing of experience.

JTG is the designation referring to the standards and specifications of highway transportation industry, issued by the Ministry of Transport of the People's Republic of China. This system encompasses the entire lifecycle of highway engineering projects, from planning and construction to maintenance and operation management. It includes standards for the facilities, technologies, management, and services required throughout these processes, as well as standards related to safety, environmental protection, and economic evaluation.

In the highway standard system, it includes a number of standards for design, construction and maintenance of bridges, which have effectively supported the rapid development of highway bridges in China. The current bridge design specifications include: *General Specifications for Design of Highway Bridges and Culverts*, *Specifications for Design of Highway Reinforced Concrete and Prestressed Concrete Bridges and Culverts*, *Code for Design of Highway Masonry Bridges and Culverts*, *Specifications for Design of Highway Cable-stayed Bridge*, *Specifications for Design of Highway Suspension Bridge*, *Specifications for Design of Highway Concrete-filled Steel Tubular Arch Bridges*, *Specifications for Design of Highway Precast Concrete Bridges*, *Specifications for Wind-Resistant Design of Highway Bridges*, *Specifications for Collision Design of Highway Bridges*, *Specifications for*

technology, and economic rationality. It incorporates a performance-based design philosophy and employs a limit state design methodology featuring partial factors. The *Specifications* refines the wind load calculation system and wind-resistant limit state design methodology. This ensures bridges meet requirements for wind stability, traffic safety and ride comfort, as well as structural durability throughout their design life. The *Specifications* provides a standardized wind-resistant design framework for all categories of highway bridge projects, advancing the refined wind-resistant design for long-span bridges.

The release of the English version of the *Specifications* aims to share the engineering experience and technical achievements from China and provide references for other countries to build highway bridges and culverts with similar construction conditions.

The editing of the English version was conducted by Fuzhou University under the authorization of the Ministry of Transport of the People's Republic of China and approved by the Highway Department, the Ministry of Transport of the People's Republic of China.

The contents and numbering of the chapters, sections, clauses and sub-clauses in the English version are consistent with those in the Chinese version. In the event of any ambiguity or discrepancy between the English version and the Chinese version of the *Specifications*, the Chinese version shall prevail.

Gratitude is given here to Profs. Chen Airong and Ma Rujin, the editors of the Chinese version, for the valuable guidance and comments during the review of the English version.

Feedbacks are welcome and will be taken into account in future editions. Please address them to the editing organization for the English version in writing (Address: No. 2, Wulongjiang North Avenue, Fuzhou University Town, Fuzhou, Fujian, China, Postal Code: 350108, E-mail: zhchen@fzu.edu.cn).

Chief editing organization for English version:

Fuzhou University

Chief editor for English version:

Chen Zhaohui

Associate editors for English version:

Chen Baochun, Ahad Javanmardi

Review editor for English version:

Khaled Sennah

Associate review editors for English version:

Zhang Huiyu, Guo Yanlin, Dong Yanfeng, Huang Liji, Zhao Ji,
Krishna Shrestha

交通运输部信息公开
浏览专用

Foreword to Chinese Version

The revision of the *Wind-resistant Design Specification for Highway Bridges* (JTG/T D60-01—2004, hereinafter referred to as the “*Specification 2004*”), pursuant to the Notice on Planning of Compilation and Revision Programs of Highway Engineering Industry Standards and Specifications in 2013 (Transport Highway Document [2013] No. 169) issued by the General Office of the Ministry of Transport of the People’s Republic of China, was carried out by the chief editing organization for Chinese version, Tongji University.

The *Specifications* constitutes a comprehensive revision of the *Specifications 2004*. Upon approval, it is issued and implemented as the *Specifications for Wind-Resistant Design of Highway Bridges* (JTG/T 3360-01—2018).

This revision of the *Specifications* systematically summarizes the experience gained from highway bridge construction in China since the implementation of the *Specifications 2004*. Building on the comprehensive integration of recent advancements in bridge wind resistance research and design practices in China, dedicated supporting research projects were conducted to address specific technical challenges. The revision also refers to international standards, research findings and practices, including Eurocodes, British Standard BS 5400, American highway bridge design specifications, and specifications or guidelines of Japan and Denmark. After multiple rounds of consultations and revisions, the final draft was reviewed and approved by the competent authorities of the Ministry of Transport and relevant departments.

The main contents of this revision include: adding provisions on basic requirements, wind-induced traffic safety, virtual wind tunnel testing, and wind observation at bridge sites; revising the basic wind speed map and wind speed value tables of China; adjusting provisions for determining wind speed parameters; supplementing provisions on design turbulence intensity; modifying and expanding

provisions for determining wind loads; supplementing estimation of fundamental frequencies for dynamic characteristics of stay cables and hangers and revising the content on determining damping ratios; revising provisions on wind-resistant ultimate limit state and serviceability limit state designs; and supplementing provisions on vibration damping device design.

The *Specifications* was drafted by Chen Airong for Chapters 1, 2, and 3; by Chen Airong and Ma Rujin jointly for Chapters 4, 9, and Appendix A; by Ma Rujin for Chapters 5 and 6; by Chen Airong and Wang Dalei jointly for Chapters 7 and 8; by Wang Dalei and Ma Rujin jointly for Chapter 10; by Wang Dalei for Chapter 11; by Wang Dalei and Liu Gao jointly for Appendix B; by Wang Dalei and Ai Huilin jointly for Appendix C; and by Ai Huilin, Liu Gao and Liu Tiancheng jointly for Appendix D.

Feedback is welcome and will be taken into account in future editions. Please address them to the chief editing organization for the Chinese version (Chen Airong, Address: Room 313 Department of Bridge Engineering, Tongji University, No. 1239, Siping Road, Shanghai 200092, China; Tel. No. : 021-65981871, Fax No. : 021-65984211; Email : a.chen@tongji.edu.cn).

Chief editing organization for Chinese version:

Tongji University

Associate editing organizations for Chinese version:

CCCC Highway Consultants Co. , Ltd.

Shanghai Norma Civil Technology Co. Ltd.

CCCC Highway Bridges National Engineering Research Center Co. , Ltd.

Chief editor for Chinese version:

Chen Airong

Associate editors for Chinese version:

Ma Rujin Wang Dalei Liu Gao Ai Huilin Liu Tiancheng

Chief review editor for Chinese version:

Ji Lin

Other review editors for Chinese version:

Chen Zhengqing	Liao Haili	Li Long'an	Yuan Hong
Peng Yuancheng	Han Dazhang	Ma Biao	Zhou Liang
Mao Zhaoxiang	Xu Fuyou	Liu Zhiwen	Ma Renle
Li Jiawu	Wang Sishun	Wu Huaiyi	

Participating personnel:

Li Qiheng Cui Chuanjie

交通运输部信息公开
浏览专用

Contents

	Page
1 General Provisions	1
2 Terms and Symbols	3
2.1 Terms	3
2.2 Symbols	9
3 Basic Requirements	11
3.1 General	11
3.2 Wind-Resistant Design Objectives and Performance Requirements	13
3.3 Combination of Wind Loads and Other Actions	16
3.4 Wind-Resistant Design Process for Bridges	17
4 Wind Speed Parameters	19
4.1 Basic Wind Speed	19
4.2 Reference Wind Speed	20
4.3 Design Turbulence Intensity	30
5 Wind Loads	33
5.1 General	33
5.2 Equivalent Static Gust Wind Speed	34
5.3 Equivalent Static Gust Load on Main Girder	40
5.4 Equivalent Static Gust Wind Loads on Piers, Towers, Stay Cables, Suspension Cables, and Hangers	50
5.5 Buffeting Inertial Load and Its Effects	58
5.6 Wind Loads during Construction	61
6 Dynamic Characteristics	63
6.1 General	63
6.2 Finite Element Modeling Principles for Dynamic Characteristics Analysis	63

	Page
6.3 Estimation of Fundamental Frequencies of Cable-stayed Bridges	66
6.4 Estimation of Fundamental Frequencies of Suspension Bridges	67
6.5 Estimation Formulas for Frequencies of Stay Cables and Hangers	70
6.6 Damping Ratios of Bridges	73
7 Wind-Resistant Ultimate Limit State Design	75
7.1 General	75
7.2 Aerostatic Stability	75
7.3 Galloping Stability	81
7.4 Wake Galloping	85
7.5 Flutter Stability	87
7.6 Vortex Resonance	99
7.7 Wind-induced Stability Verification during Construction	99
8 Wind-Resistant Serviceability Limit State Design	101
8.1 General	101
8.2 Vortex Resonance	101
8.3 Buffeting	106
8.4 Stay Cables and Hangers	106
8.5 Wind-induced Vibration Serviceability Criteria	112
9 Wind-induced Vibration Control	114
9.1 General	114
9.2 Girders	115
9.3 Towers and High Piers	118
9.4 Stay Cables and Hangers	119
10 Wind-induced Traffic Safety	124
10.1 General	124
10.2 Assessment of Wind-induced Traffic Safety	124
10.3 Design of Wind Barriers	130
	132
Appendix A Wind Risk Region Map and Wind Speed Distribution	
Map for Bridges in China	134
A.1 Wind Risk Region Map for Bridges in China	134
A.2 Basic Wind Speed Distribution in China	134

	Page
A.3 Wind Speeds for Different Return Periods in Major Regions of China	134
A.4 Probabilistic Distribution Models and Parameter Values of Wind Speed at Meteorological Stations across China	134
Appendix B Basic Requirements for Wind Observation at Bridge Site in China	135
B.1 General Rules	135
B.2 Wind Observation Period, Measurement Points and Parameters	136
B.3 Wind Observation Data Analysis	137
Appendix C Requirements for Wind Tunnel Testing	140
C.1 General	140
C.2 Aerostatic Force Testing	143
C.3 Sectional Model Vibration Testing	144
C.4 Bridge Tower Model Testing	147
C.5 Full-bridge Aeroelastic Model Testing	149
C.6 Sectional Model Testing for Wind-rain-induced Vibration of Stay Cables	150
C.7 Bridge Site Topographic Wind Environment Model Testing	151
C.8 Wind Environment Testing for Traffic Safety on Bridge Deck	151
Appendix D Requirements for Virtual Wind Tunnel Testing	153
D.1 General	153
D.2 Virtual Wind Tunnel Test Area and Boundary Conditions	158
D.3 Mesh Generation	161
D.4 Numerical Solution	164
D.5 Requirements for Virtual Wind Tunnel Testing	166
Explanation on Wording in the <i>Specifications</i>	169

1 General Provisions

1.0.1 The *Specifications* is developed for regulating and guiding the wind-resistant design of highway bridges in accordance with the principles of safety and reliability, advanced technology, and economic rationality.

Commentary

In recent years, the construction of bridges in China and other countries has developed rapidly, which has benefited from the advancing theory and technology of wind-resistant design for various types of bridges. Recent experience and research outcomes on wind-resistant design for bridges in the world were incorporated in this revision, in which the performance-based design philosophy and the limit state design methodology expressed with partial factors are adopted.

1.0.2 The *Specifications* is applicable for the wind-resistant design of highway bridges except for beam bridges with a main span longer than 350 m, arch bridges with a main span longer than 600 m, cable-stayed bridges with a main span longer than 1200 m and suspension bridges with a main span longer than 2000 m.

1.0.3 Within the design life, the wind-resistant performance of bridge structures and members shall conform to the following requirements:

- 1 Under the design wind actions or their combinations with other actions, the specified requirements for strength, stiffness, and static stability shall be met.
- 2 Under the design wind actions, the specified requirements for aerostatic stability and aerodynamic stability shall be met.

- 3 Under the design wind actions or their combinations with other actions, the specified requirements for durability, fatigue, safety, and comfort for moving vehicles and pedestrians shall be met.

1.0.4 Proper structural system of bridges and aerodynamic shapes of members shall be selected in accordance with the wind environment at the bridge site, bridge type, span and other factors. Whenever necessary, aerodynamic countermeasures or additional damping measures shall be provided to improve the wind resistance of the bridge structures.

1.0.5 In addition to the requirements in the *Specifications*, the wind-resistant design of highway bridges shall also comply with the provisions in the current relevant national and industrial standards.

2 Terms and Symbols

2.1 Terms

2.1.1 Basic wind speed

The annual maximum mean wind speed averaged over 10 minutes with a return period of 100 years (having a probability of exceedance of 63.2% in 100 years) at a height of 10 m above the ground surface in flat open country terrain.

2.1.2 Basic wind speed at bridge site

The annual maximum mean wind speed averaged over 10 minutes with a return period of 100 years (having a probability of exceedance of 63.2% in 100 years) at a height of 10 m above the ground or water surface of the bridge site.

2.1.3 Reference wind speed

The annual maximum mean wind speed averaged over 10 minutes with a return period of 100 years (having a probability of exceedance of 63.2% in 100 years) at the reference height of a bridge or a member.

2.1.4 Bridge reference wind speed

Reference wind speed at the reference height of the bridge girders.

2.1.5 Wind attack angle

The angle between the main flow direction of the wind and the horizontal plane.

2.1.6 Wind yaw angle

The angle between the horizontal projection of the main flow direction of the wind and the vertical plane normal to the bridge axis, as illustrated in Figure 2.1.6.

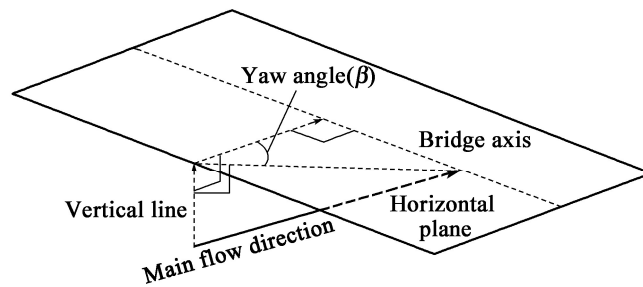


Figure 2.1.6 Definition schematic for wind yaw angle

2.1.7 Gust factor

The ratio of the instantaneous wind speed with an averaging time of 1 ~ 3 s to the mean wind speed with an averaging time of 10 minutes, as shown in Figure 2.1.7.

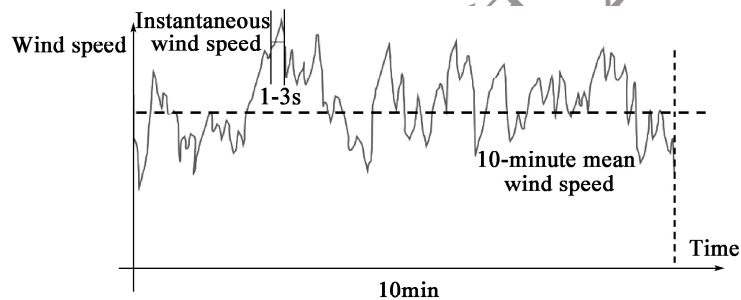


Figure 2.1.7 Definition schematic for gust factor

2.1.8 Turbulence intensity

A parameter to represent the temporal and spatial variation of fluctuating wind speed, which is the ratio of the standard deviation of the turbulent component of wind speed to the mean wind speed.

2.1.9 Wind action W1

The wind action corresponding to a 10-year return period (having a probability of exceedance of 65.1% in 10 years).

2.1.10 Wind action W2

The wind action corresponding to a 100-year return period (having a probability of exceedance of 63.2% in 100 years).

2.1.11 Equivalent static gust wind factor

A scale factor for wind speed under along-wind loading considering turbulence intensity, spatial correlation of fluctuation, loaded length (or height), and height of structural members above the ground or water surface.

2.1.12 Terrain roughness height

A parameter representing the roughness of the ground surface or the height and density of objects on the ground within the atmospheric boundary layer.

2.1.13 Aerodynamic force

A generic term for all aerodynamic wind-induced forces on structures and members.

2.1.14 Aerodynamic force coefficient

A dimensionless parameter to represent the aerodynamic force on structures and members subjected to wind actions.

2.1.15 Aerostatic force

The static force induced by the mean wind on structures and members. For main girders under the transverse wind load, it can be resolved into three static force components. These are lateral force, vertical force, and torsional moment with respect to body axes; and drag force, lift force, and torsional moment with respect to wind axes. Correspondingly, their aerodynamic force coefficients are referred to as lateral force coefficient, vertical force coefficient, and torsional moment coefficient with respect to body axes; and drag coefficient, lift coefficient, and torsional moment coefficient with respect to wind axes.

2.1.16 Static stability

The ability of structures or members to maintain equilibrium under static loads.

2.1.17 Aerostatic stability

The ability of bridges to maintain equilibrium under aerostatic forces without the occurrence of aerostatic instability. The aerostatic instability is a phenomenon of instability or divergence with augmenting motions caused by the force increment when additional aerodynamic forces produced by the deformation of the structures under aerostatic forces exceed the structural resistance. It includes aerostatic lateral buckling and aerostatic torsional divergence.

2.1.18 Aerostatic lateral buckling

An instability phenomenon that occurs when the lateral static wind load exceeds the critical lateral buckling load of bridge girders.

2.1.19 Aerostatic torsional divergence

A phenomenon of divergence with augmenting angle of rotation that occurs when the incremental aerodynamic moment generated by the additional wind attack angle, which results from torsional deformation of bridge girders, exceeds the incremental structural resistance moment under the action of static torsional moment.

2.1.20 Aerodynamic instability

An instability phenomenon of divergent self-excited vibration with gradually or suddenly increasing amplitude that occurs when bridges or members in motion continually absorb energy through the feedback mechanism of air flow. Flutter and galloping are two main types of aerodynamic instability.

2.1.21 Flutter

An instability phenomenon of divergent self-excited vibration with gradually or suddenly increasing torsion deflection that occurs when bridges or members in motion continually absorb energy through the feedback mechanism of air flow.

2.1.22 Galloping

An instability phenomenon of divergent self-excited vibration with gradually increasing cross-wind bending deflection that occurs when bridges or members in motion continually absorb energy through the feedback mechanism of air flow.

2.1.23 Wake galloping

A galloping phenomenon occurring in the downstream structures or members positioned within a certain distance parallel to upstream ones, induced by the wake flow from the upstream structures or members.

2.1.24 Vortex resonance

A resonance phenomenon induced by vortex shedding force when the frequency of vortex shedding, generated when wind flows through structures, is close to or equal to the natural frequency of the structures or members.

2.1.25 Buffeting

A random vibration of structures or members under the fluctuating wind force, the fluctuating force from the wakes of upstream structures, or the fluctuating force induced by turbulence when wind flows around structures.

2.1.26 Buffeting inertial load

Inertial force induced by the buffeting of structures.

2.1.27 Wind-rain-induced vibration

A galloping phenomenon occurs on stay cables or hangers under the combined action of wind and rain.

2.1.28 Parametric resonance

A phenomenon of augmenting transverse vibration of stay cables induced by small motions of bridge

decks or towers along the chord length of the cables.

2.1.29 Linear internal resonance

A phenomenon of augmenting transverse vibration of stay cables induced by small motions of bridge decks or towers normal to the chord length of the cables.

2.1.30 Critical wind speed for aerostatic instability

The lowest onset wind speed for lateral buckling and torsional divergence in structures, which is correspondingly referred to as the critical wind speed for aerostatic lateral buckling and the critical wind speed for aerostatic torsional divergence.

2.1.31 Flutter critical wind speed

The lowest onset wind speed for the flutter of structures or members.

2.1.32 Galloping critical wind speed

The lowest onset wind speed for galloping of structures or members.

2.1.33 Onset wind speed for vortex resonance

The lowest wind speed for vortex resonance of structures or members.

2.1.34 Wind tunnel

A tube-like testing equipment used for various aerodynamic tests based on the similarity principles, which is operated to simulate air flows around a test object with artificially generated and controlled air flows of a certain flow characteristics.

2.1.35 Virtual wind tunnel

A simulation technique based on the fundamental principle of computational fluid dynamics used for simulation, computing and analysis of the flow around structures or members, aerodynamics, and aeroelasticity in a wind field, which is a uniform flow or a turbulent flow field generated by computer simulation.

2.1.36 Wind tunnel testing

An experiment to acquire wind environment parameters and structural aerodynamics and to verify the wind resistance through investigations on air flows and their interaction with structures and members in a wind tunnel.

2.1.37 Virtual wind tunnel testing

An experiment to acquire wind environment parameters and structural aerodynamics and to verify the wind resistance through investigations on air flows and their interaction with structures and

members in a virtual wind tunnel.

2.1.38 Sectional model testing

An experiment to acquire wind-induced responses and verify the wind resistance of structures by using rigid models fabricated or simulated from representative sections of the structures or members.

2.1.39 Aerostatic force testing

An experiment to acquire the aerostatic forces of structures or members.

2.1.40 Sectional model vibration testing

An experiment to test the vibrational responses of structures or members using sectional models.

2.1.41 Bridge tower model testing

An experiment to test aerostatic forces or vibration responses of bridge towers using bridge tower models.

2.1.42 Full-bridge aeroelastic model testing

An experiment to acquire wind-induced responses and verify the wind resistance of structures by using three-dimensional elastic models fabricated or simulated from the bridge structures according to a certain similarity condition.

2.1.43 Bridge site topographic wind environment testing

An experiment to acquire wind parameters and their distributions at the bridge site, considering the influences of topographic features and buildings at the site and within a certain area surrounding the site.

2.1.44 Wind environment testing for traffic safety on bridge deck

An experiment to acquire the wind speed profile and the flow characteristics within the vertical clearance for moving vehicles on the bridge deck, considering the influences of bridge towers, abutment structures, arch ribs, trusses, and other members on the moving vehicles.

2.1.45 Wind-induced vibration control

Techniques to improve the wind resistance of structures or members, including aerodynamic countermeasures, supplemental damping measures, and additional structure measures, etc.

2.1.46 Wind barrier

A structure installed on bridge girders to reduce the influence of lateral wind speed over the bridge deck so that traffic safety and ride comfort on the bridge deck are improved. It generally consists of

posts, strips, anchorages, and damping devices.

2.1.47 Solidity ratio of wind barrier

Ratio of the solid area in the front elevation of the wind barrier to the overall area in the outline of the wind barrier.

2.2 Symbols

- B ——Characteristic width of the main girder
 b ——Half of the characteristic width of the main girder
 D ——Characteristic depth of the main girder
 D_c ——Outer diameter of the stay cable or hanger
 H ——Height of the tower
 f ——Frequency
 F_p ——Wind load per unit length
 F_g ——Equivalent static gust load per unit length
 F_H ——Horizontal wind load per unit length in the body axis system
 F_V ——Vertical wind load per unit length in the body axis system
 F_D ——Along-wind load per unit length in the wind axis system
 F_L ——Cross-wind load per unit length in the wind axis system
 g ——Acceleration of gravity
 G_v ——Equivalent static gust factor
 I_f ——Flutter stability index
 I_u, I_v, I_w ——Design longitudinal, transverse and vertical turbulence intensity, respectively
 I_y, I_z ——Moment of inertia about the principal centroidal axis of the cross-section
 I_d ——St. Venant torsional constant of the cross-section
 I_m ——Mass moment of inertia per unit length of main girder
 I_ω ——Warping torsional constant of section
 L ——Main span length of bridge
 l ——Length of stay cable or hanger
 m ——Mass per unit length of structure
 r ——Radius of gyration of cross-section
 U_{10} ——Basic wind speed
 U_{s10} ——Basic wind speed at the bridge site
 U_{cg} ——Galloping critical wind speed
 U_d ——Reference wind speed
 U_f ——Flutter critical wind speed
 U_g ——Equivalent static gust wind speed

U_{sd} ——Design wind speed at the construction stage
 U_{vh} ——Onset wind speed for vertical vortex resonance
 U_{vt} ——Onset wind speed for torsional vortex resonance
 U_z ——Wind speed at the height Z above the ground or water surface
 Z ——Reference height of member
 z_0 ——Terrain roughness height
 α ——Wind attack angle
 α_0 ——Terrain roughness factor
 β ——Wind yaw angle
 δ ——Logarithmic decrement
 δ_0 ——Gradient height of wind profile
 η_α ——Shape factor
 η_s ——Factor for attack angle effect
 μ ——Ratio of structural density to air density
 ρ ——Air density
 ζ_s ——Damping ratio of structure

3 Basic Requirements

3.1 General

3.1.1 Both the static and dynamic actions of wind shall be considered in the wind-resistant design of bridges. The design and verification for the ultimate limit state and serviceability limit state shall also be conducted according to different requirements for wind-resistant performance.

Commentary

Effects of wind actions on bridge structures are generally classified as static effect, aerostatic effect and dynamic effect. Static effect mainly includes deformation and internal forces generated in structures, as well as static instability. Aerostatic effect is the aerostatic instability of structures induced by the wind, for example, aerostatic torsional divergence and aerostatic lateral buckling. Dynamic effect includes vibrations with limited amplitudes, such as buffeting and vortex resonance, as well as aerodynamic instability, such as flutter and galloping. Table 3-1 shows the classification of wind effects on bridge structures.

Table 3-1 Classification of wind effects on bridge structures

Classification of effect		Action
Static effect	Internal force and deformation	Static action of wind load or static action of the combination of wind load and other loads
	Static instability	
Aerostatic effect	Aerostatic torsional divergence	Static torsional moment of wind
	Aerostatic lateral buckling	Combined action of static resistance and torsional moment of wind

continued

Classification of effect			Action
Dynamic effect	Buffeting		Random excitation of turbulent wind
	Vortex resonance		Vortex-induced force when the frequency of vortex shedding is close to that of the structure
	Galopping		Action of negative aerodynamic damping caused by the self-excited force associated with structural vibration
	Flutter	Torsional flutter	Action of aerodynamic damping and stiffness caused by the self-excited force associated with structural vibration
		Flexural-torsional flutter	

3.1.2 Potential wind-induced vibrations of bridges shall be assessed based on factors such as wind environment at the bridge site, bridge type, span length, structural system, and geometries of structures or members.

Commentary

Table 3-2 provides simplified assessment criteria for potential wind-induced vibrations in cable-stayed bridges, suspension bridges, and steel girder bridges, as specified in *Wind Resistant Design Manual for Highway Bridges* in Japan.

Table 3-2 Simplified assessment criteria for potential wind – induced vibrations in bridges

Bridge type	Form of main girder	Assessment criterion	Potential wind-induced vibration
Suspension bridge Cable-stayed bridge	Truss	$L \cdot U_d/B > 350$	Flutter
	Open section	$L \cdot U_d/B > 350$	Flutter
		$L \cdot U_d/B > 330, B/D < 5, I_u < 0.15,$ Steel girder	Galopping
		$L \cdot U_d/B > 200, I_u < 0.20$	Vortex resonance
	Closed section	$L \cdot U_d/B > 520$	Flutter
		$L \cdot U_d/B > 330, B/D < 5, I_u < 0.15,$ Steel girder	Galopping
		$L \cdot U_d/B > 200, I_u < 0.20$	Vortex resonance
Steel girder bridge	Plate girder or box girder	$L \cdot U_d/B > 330, B/D < 5, I_u < 0.15$	Galopping
		$L \cdot U_d/B > 200, I_u < 0.20$	Vortex resonance

3.1.3 When it is determined that there is a fatigue issue with a structure or member under wind actions, the design for fatigue resistance shall be performed.

3.1.4 If it is determined that wind at the bridge deck level has impacts on traffic safety and ride comfort, the corresponding wind-induced traffic safety shall be assessed and designed in accordance with the provisions in Chapter 10 of the *Specifications*.

3.2 Wind-Resistant Design Objectives and Performance Requirements

3.2.1 Wind risk regions for bridges shall be classified based on the basic wind speed as specified in Table 3.2.1. The risk regions may be determined in accordance with Appendix A.1 of the *Specifications*.

Table 3.2.1 Criteria for classification of wind risk regions for bridges

Risk region	Basic wind speed U_{10}
R1	$U_{10} \geq 32.6 \text{ m/s}$
R2	$24.5 \text{ m/s} \leq U_{10} < 32.6 \text{ m/s}$
R3	$U_{10} < 24.5 \text{ m/s}$

Commentary

Statistical analysis of data from all 761 meteorological stations in China indicates that the mean value of basic wind speed is 29.1 m/s. Based on the magnitude of basic wind speed, bridge locations are classified into three risk regions of R1, R2 and R3, which have comparable probability levels corresponding to their wind speed ranges. Also, considering that meteorological wind scales have been widely accepted, the three risk regions are aligned with the wind scales, namely, R1 corresponds to Wind Scale 12 or higher, R2 corresponds to Wind Scale 10-11, and R3 corresponds to Wind Scale 9 or lower. Table 3-3 lists the meteorological wind scales and their corresponding wind speed ranges.

Table 3-3 Wind scales and their corresponding wind speed ranges

Wind scale	Sea state		Conditions of coastal fishing vessels	Conditions on land	Range of wind speed (m/s)
	Wave height (m)				
	Normal	Very high			
0	—	—	Calm	Calm. Smoke rises vertically.	0 ~ 0.2
1	0.1	0.1	Ordinary fishing boats wobbly slightly.	Smoke drift indicates wind direction, but wind vanes cease moving.	0.3 ~ 1.5

continued

Wind scale	Sea state		Conditions of coastal fishing vessels	Conditions on land	Range of wind speed (m/s)
	Wave height (m)				
	Normal	Very high			
2	0.2	0.3	2 ~ 3km Fishing boats sailed can move with wind for 2 ~ 3 km/h.	Wind can be felt on faces, leaves rustle, and the wind vane can be moved by wind.	1.6 ~ 3.3
3	0.6	1.0	5 ~ 6km Fishing boats gradually felt the tuckering and moved with wind for 5 ~ 6 km/h.	Leaves and small twigs are in constant motion, wind extends light flags.	3.4 ~ 5.4
4	1.0	1.5	Fishing boats in full sail lean to one side.	Dust and loose paper are raised up, small branches are moved.	5.5 ~ 7.9
5	2.0	2.5	Reefing on fishing boats (i.e. part of the sail is reefed).	Small trees in leaf begin to sway, crested wavelets form on inland waters.	8.0 ~ 10.7
6	3.0	4.0	Reefing on fishing boats is doubled, and be aware of the risks associated with fishing.	Large branches are in motion, power lines whistle, and umbrellas are difficult to use.	10.8 ~ 13.8
7	4.0	5.5	Fishing boats are moored in the harbor, and those at sea are anchored in situ.	Whole trees are in motion, and inconvenience is felt when walking against the wind.	13.9 ~ 17.1
8	5.5	7.5	Fishing boats near the harbor are stayed.	Twigs break off trees, and progress is generally impeded.	17.2 ~ 20.7
9	7.0	10.0	Sailing of steamboats is difficult.	Chimney pots and states are removed, and slight structural damage occurs.	20.8 ~ 24.4
10	9.0	12.5	Sailing of steamboats is dangerous.	Seldom experienced on land, trees are uprooted, or buildings suffer damage.	24.5 ~ 28.4
11	11.5	16.0	Sailing of steamboats is extremely dangerous.	Seldom experienced on land, accompanied by widespread damage.	28.5 ~ 32.6
12	14.0	—	Waves are raging.	Very rarely experienced, accompanied by devastation.	> 32.6

3.2.2 The wind-resistant design of bridges shall be determined based on the wind actions W1 and W2. The corresponding wind speeds and design objectives shall comply with the provisions in Table 3.2.2.

Table 3.2.2 Wind actions and objectives for wind-resistant design of bridges

Wind action	Design wind speed	Design objectives
W1	<p>Design wind speed with a 10-year return period (having a probability of exceedance of 65.1% in 10 years).</p> <p>When the wind speed on main girders determined by is larger than 25 m/s, 25 m/s is used.</p>	<p>The specified requirements for strength, stiffness, static stability and durability shall be met when the wind action is combined with vehicular load and other actions.</p> <p>The specified requirements for fatigue, safety and ride comfort of moving vehicles and pedestrians shall be met.</p> <p>Vortex resonance that affects normal operation of bridges shall not occur within the wind speed range corresponding to wind action W1 or below.</p>
W2	<p>Design wind speed with a 100-year return period (having a probability of exceedance of 63.2% in 100 years).</p>	<p>The specified requirements for strength, stiffness and static stability shall be met.</p> <p>The specified requirements for aerostatic stability and aerodynamic stability shall be met.</p> <p>Vortex resonance shall not occur within the wind speed ranges corresponding to wind actions W1 and W2.</p>

Commentary

The wind speeds corresponding to the wind actions W1 and W2 are those with return periods of 10 years (i. e. , a probability of exceedance of 65.1% in 10 years) and 100 years (i. e. , a probability of exceedance of 63.2% in 100 years), respectively. The relationship between the probability of exceedance, P_T , within the design reference period and the return period, t_R , can be expressed using Eq. (3-1).

$$P_T(t \leq t_L) = 1 - (1 - p)^{t_L} \quad (3-1)$$

where;

$P_T(t \leq t_L)$ ——probability of exceedance within the design reference period;

t_L ——design reference period (year);

p ——annual probability of exceedance, which is generally taken as $1/t_L$.

The wind action W1 reflects the concept of frequent loads. A 10-year return period (i. e. , a probability of exceedance of 65.1% in 10 years) is taken as the basis for determining the wind speed under the wind action W1 in the *Specifications*. Additionally, a wind speed of 25 m/s at the girder elevation is specified as the wind speed limit under the combination of wind and vehicular loads.

3.2.3 The design parameters for wind-resistant performance of bridges shall be determined in accordance with Table 3.2.3.

Table 3.2.3 Design parameters for wind-resistant performance of bridges

Wind action	Action effect	Design parameters	Design situation
W1	Wind effect	Internal force, stress, static stability, etc.	Ultimate limit state
		Deflection, crack width, etc.	Serviceability limit state
	Vortex resonance	Vibration amplitude, acceleration, onset wind speed, equivalent stress range	Serviceability limit state
W2	Wind effect	Internal force, stress, static stability, etc.	Ultimate limit state
	Aerostatic stability	Critical wind speed	
	Vortex resonance	Onset wind speed	
	Flutter	Critical wind speed	
	Galloping	Critical wind speed	

3.3 Combination of Wind Loads and Other Actions

3.3.1 The combination of wind loads and other actions shall comply with the provisions in the current *General Specifications for Design of Highway Bridges and Culverts* (JTG D60) and shall adhere to the following principles;

- 1 When the wind load is combined with the vehicular load and relevant actions, the wind

load shall be determined by the wind action W1.

- 2 When a relevant limit state design is performed for the wind action W2, the vehicular load shall not be included in the action combination.

3.3.2 Partial factors and factor for the combination of wind load combined with other actions shall be determined by the following principles:

- 1 For the ultimate limit state design under fundamental combinations where wind load serves as the primary variable action, the wind speed shall be selected according to the wind action W2, the vehicular load shall not be included, and the partial factor, γ_{Q_1} , for the wind load shall be 1.4.
- 2 For the ultimate limit state design under fundamental combinations where vehicular load or other variable actions serve as the primary variable action, the wind speed shall be selected according to the wind action W1, the partial factor, γ_{Q_1} , for the wind load shall be 1.1, and the factor for combination, ψ_c , shall be 1.0.
- 3 For the serviceability limit state design, the wind speed shall be selected according to the wind action W2, both the factor, ψ_j , for the frequent value of the wind load and the factor, ψ_q , for the quasi-permanent value of the wind load shall be 1.0.

Commentary

It is specified in the *General Specifications for Design of Highway Bridges and Culverts* (JTG D60) that the fundamental combination is the combination of design values of permanent and variable actions. In practical applications, one action is selected as the primary variable action, while other actions are involved in the combination. There are two possible combination scenarios for wind load: 1) the wind load acts as the primary action, and 2) the wind load combined with vehicular load or other actions serves as the primary action. Design wind speeds for these two scenarios are selected according to the two wind actions, respectively.

3.4 Wind-Resistant Design Process for Bridges

3.4.1 Wind-resistant design process for bridges may be carried out according to Figure 3.4.1.

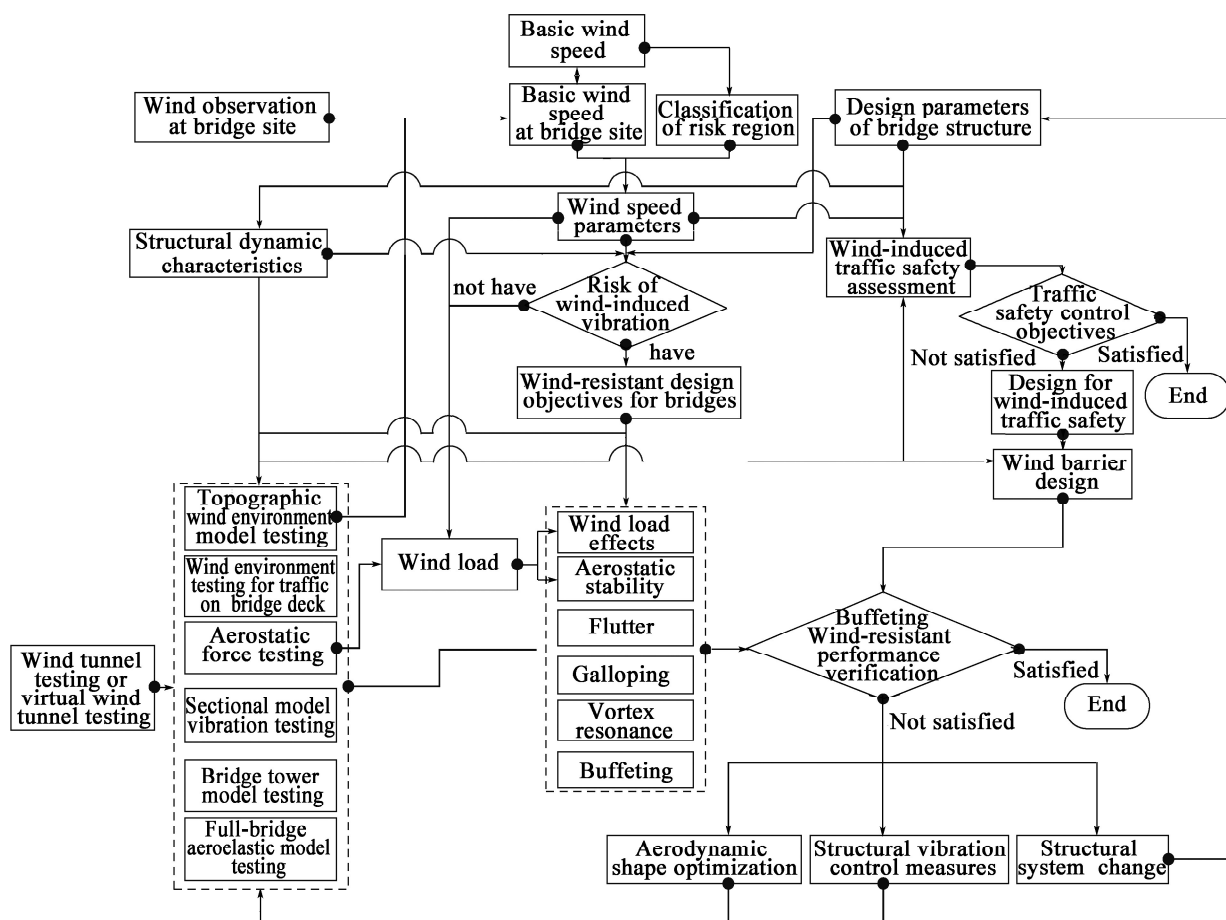


Figure 3.4.1 Wind-resistant design process for bridges

Commentary

The wind-resistant design of bridges is involved throughout all stages of bridge design and can be implemented in phases according to the risk region of the bridge site and structural characteristics. For structures or members insensitive to the dynamic effects of wind, only the static effects of wind can be considered in the design. For structures or members sensitive to the dynamic effects of wind, wind-resistant design under static and dynamic actions of wind needs to be carried out simultaneously. For bridges where wind has an impact on traffic safety, the issue of wind-induced traffic safety needs to be considered.

4 Wind Speed Parameters

4.1 Basic Wind Speed

4.1.1 If there are sufficient continuous wind observation data provided by meteorological stations in the area of the bridge location, the probability distribution model of 10-minute annual maximum mean wind speed from the local meteorological stations should be used to estimate the mathematical expectation of the wind speed with a return period of 100 years (i.e., a probability of exceedance of 63.2% in 100 years), which is taken as the basic wind speed, U_{10} .

4.1.2 If wind observation data are unavailable, the basic wind speed in the area of the bridge location may be taken as the larger value obtained from Appendix A.2 or Appendix A.3 in the *Specifications*.

Commentary

The wind speed given in Appendixes A.2 and A.3 of the *Specifications* were obtained based on the wind speed data recorded by 761 meteorological stations in China from their establishment to 2015. The historical data from the meteorological stations covers the period from 1953 to 2015. To obtain these basic wind speed values and other wind speed values with different return periods, the missing data were imputed by the predictive mean matching method, the extreme wind speed of each station was determined by the fourth-order linear moment test method, and the optimal probability model and distribution parameters were fitted, and the calculation was performed according to different return periods on the basis of achieving a 99% confidence level.

4.1.3 The wind speed probability distribution model and its parameter values of each meteorological station in China may be selected in accordance with Appendix A.4 of the *Specifications*.

Commentary

Since there are large differences in the regional distribution of the historical data of each meteorological station in China, and the probability distribution models are different, it is not reasonable to use a single extreme distribution type for the calculation of extreme wind speed. In order to fully consider the statistical characteristics of the parent sample data, it is necessary to select the optimal probability model according to the distribution conditions, and then predict the extreme wind speed. The fourth-order linear moment test method determines the optimal probability density model function according to the minimum absolute value of the difference between the probability density distribution function and the fourth-order linear moment coefficient between the sample. In the calculation of the extreme wind speed, the optimal distribution function as well as the corresponding location parameters, scale parameters and shape parameters are determined from the generalized extreme value distribution, Pearson Type III distribution, generalized logistic distribution, generalized Pareto distribution and generalized normal distribution, and the basic wind speed is predicted by using the optimal model and the parameters.

The probability distribution model in Appendix A. 4 of the *Specifications* is fitted from the historical data of meteorological stations. The wind speed values with different return periods obtained by this model may differ from those in Appendix A. 2 and Appendix A. 3 of the *Specifications*, because the wind speed values in Appendix A. 2 and Appendix A. 3 of the *Specifications* have been corrected for correlation with adjacent meteorological stations.

4.1.4 When the basic wind speed, U_{10} , obtained from the statistical analysis of meteorological stations or Appendix A of the *Specifications* is less than 24.5 m/s, U_{10} shall be taken as 24.5 m/s.

Commentary

In order to ensure the fundamental wind-resistant capacity of bridges, according to the principle of capacity-based design, the minimum requirement for the basic wind speed of 24.5 m/s is stipulated in the *Specifications*.

4.2 Reference Wind Speed

4.2.1 Terrain roughness factor, α_0 , and terrain roughness height, z_0 , may be selected in accordance with Table 4.2.1. When the roughness varies around the bridge location, they may be determined by the following method:

- 1 When two terrain categories have significantly different roughness within the considered range, their average terrain roughness factor may be adopted.
- 2 When there are two similar terrain categories within the considered range, the one with the smaller terrain roughness factor may be used. When the terrain categories on the upstream and downstream sides of a bridge are different, the value may be taken according to the side with the smaller terrain roughness factor.
- 3 The influence range of the terrain roughness factor may be selected from Figure 4. 2. 1 according to the maximum height, h_a , and length, l_a , of the structural member.

Table 4. 2. 1 Terrain categories

Terrain category	Terrain condition	Terrain roughness factor, α_0	Terrain roughness height, z_0 (m)
A	Sea, coast, open water, desert	0. 12	0. 01
B	Fields, countryside, jungles, flat open areas and areas with few low-rise buildings	0. 16	0. 05
C	Areas with dense trees and low-rise buildings, areas with few mid- and high-rise buildings, and gentle hills	0. 22	0. 3
D	Areas with dense mid- and high-rise buildings, undulating hilly areas	0. 30	1. 0

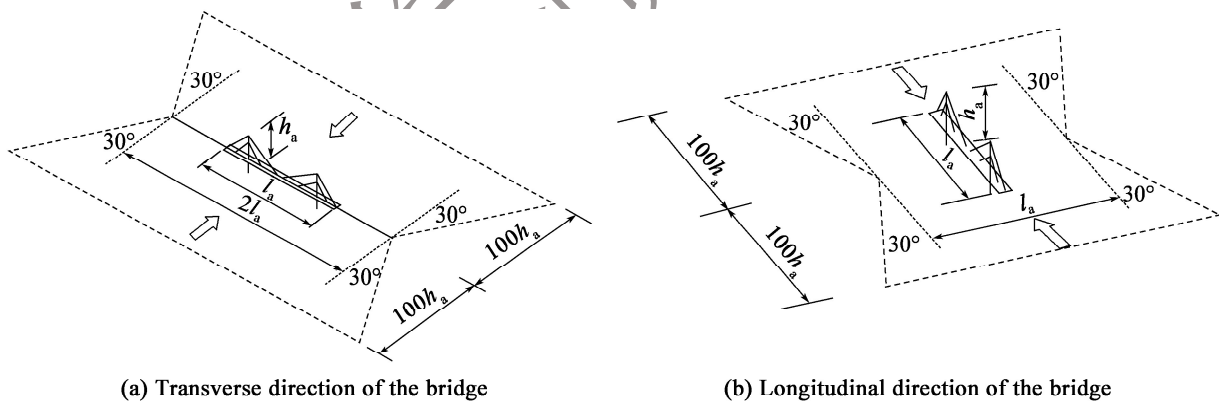


Figure 4. 2. 1 Determination of influence range of terrain roughness factor

Commentary

Within the atmospheric boundary layer, wind speed gradually increases with height above the ground. The increase of wind speed with height depends mainly on the terrain category and the

vertical temperature gradient. It is generally believed that at heights of 300 m ~ 500 m above the ground surface, the wind speed is no longer affected by the terrain category, that is, the so-called “gradient wind speed” is reached, and the height is termed the gradient height, δ_0 . The terrain roughness factors, α_0 , of various terrain categories in the *Specifications* are 0.12, 0.16, 0.22 and 0.30, respectively; the terrain roughness heights, z_0 , are 0.01 m, 0.05 m, 0.3 m and 1.0 m, respectively; and the gradient heights, δ_0 , are 300 m, 350 m, 400 m and 450 m, respectively. Figure 4-1 shows the variation law of the wind speed profile and the corresponding gradient height for different terrain categories, and the wind speed is considered to be constant when the gradient height is reached.

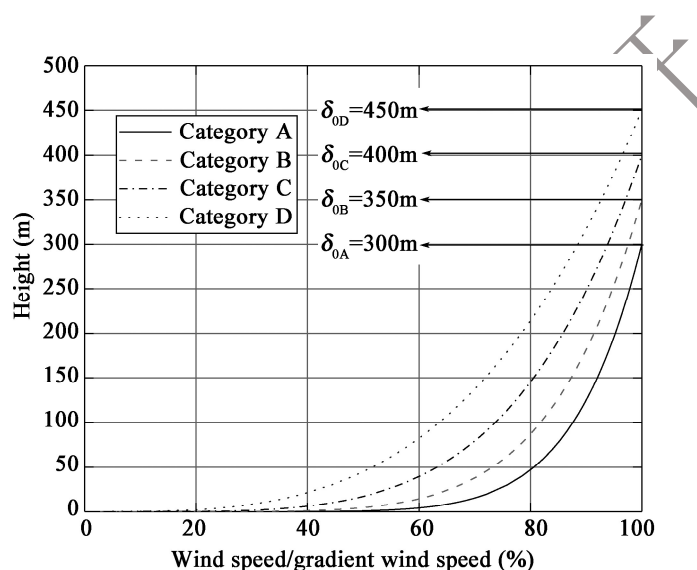


Figure 4-1 Curves of wind speed distribution along height for four terrain categories

4.2.2 The reference height, Z , of each bridge member may be taken from Table 4.2.2.

Table 4.2.2 Method for determining reference height Z

Member	Suspension bridge, cable-stayed bridge	Arch bridge	Other bridge types
Main girder	Average height of the deck at the main span of the girder above the water or ground surface		Take the greater of the following two values: ① Average height of support + (maximum elevation of bridge deck-average elevation of support) $\times 0.8$; ② Design height of the bridge.
Hanger, stay cable or suspension cable	Average height of the member above the water or ground surface	Height of the midpoint of the hanger above the water or ground surface	—

continued

Member	Suspension bridge, cable-stayed bridge	Arch bridge	Other bridge types
Tower (pier, column)	65% of the height of the tower (pier, column) above the water or ground surface	Height of the midpoint of the column from the water or ground surface	65% of the height of the tower (pier, column) above the water or ground surface
Arch rib	—	Height of the arch crown from the water or ground surface	—

Note: The water surface is referenced to the lowest water level of the river or sea surface.

4.2.3 The reference height, Z , of bridges spanning deep river valleys or mountain valleys and their members may be selected according to Figure 4.2.3 and the following method:

- 1 The reference height, Z , of the main girder of a bridge may be determined using Eq. (4.2.3):

$$Z = \frac{2}{3} \times Z_h \quad (4.2.3)$$

where,

Z_h ——height of the bridge deck above the water surface or the valley bottom.

- 2 The reference height, Z , for the member other than the main girder may be taken as the distance between the midpoint of the member or the position at 65% of the height of the tower and the starting height for calculation or the ground surface.

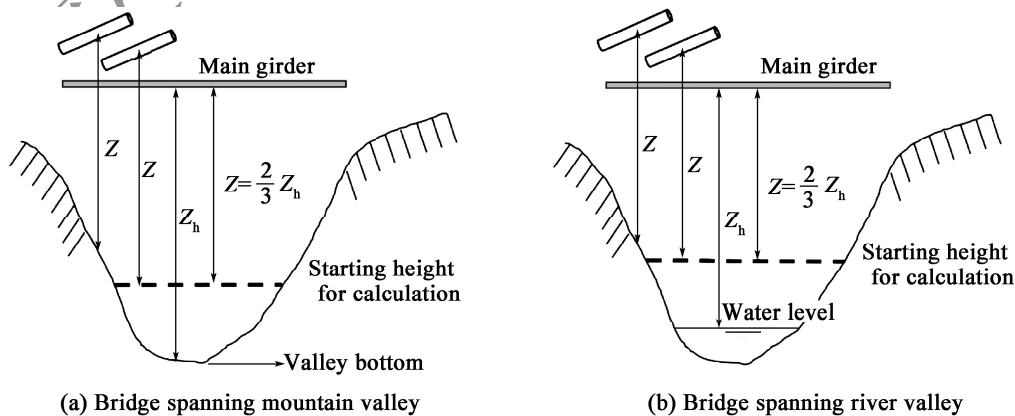


Figure 4.2.3 Schematic of reference heights for bridges spanning deep river valley or mountain valley

Commentary

The reference height of the main girder of a bridge spanning a river valley or mountain valley is obtained based on the principle of equivalent displacement under transverse wind load on the bridge. This method has been verified to be reasonable through its applications in several existing bridges.

4.2.4 The basic wind speed at bridge site, U_{s10} , may be calculated according to the terrain category of the bridge site using Eq. (4.2.4):

$$U_{s10} = k_c U_{10} \quad (4.2.4)$$

where,

k_c ——transition factor for basic wind speed based on terrain category, which is taken from Table 4.2.4;

U_{10} ——basic wind speed (m/s).

Table 4.2.4 Transition factor, k_c , for basic wind speed based on terrain category

Terrain category	A	B	C	D
Transition factor, k_c	1.174	1.0	0.785	0.564

Commentary

According to the definition of basic wind speed, U_{10} is the wind speed at a height of 10 m above the ground surface of Terrain Category B in the bridge location area. However, the basic wind speed at bridge site, U_{s10} , is the wind speed at a height of 10 m above the ground or water surface at the bridge site, and their transition is based on maintaining the consistency of the wind speeds at the gradient height. For example, Terrain Category A has a gradient height, δ_0 , of 300 m, while that of Terrain Category B is 350 m. Based on the consistency of the gradient wind speeds for these two terrain categories, the following is obtained:

$$U_{s10} \left(\frac{300}{10} \right)^{0.12} = U_{10} \left(\frac{350}{10} \right)^{0.16} \quad (4-1)$$

Then,

$$U_{s10} = 1.174 U_{10} \quad (4-2)$$

For Terrain Categories C and D, the corresponding transition factors can be obtained to be 0.785 and 0.564, respectively, by the same method.

4.2.5 When wind observation data at the bridge site are insufficient, or when the meteorological station in the area where the bridge is located is far from the bridge site and the topography is quite different from that of the nearby meteorological station, a wind observation station at the bridge site should be set up for important bridges sensitive to wind actions, and wind observation should be conducted in accordance with the provisions of Appendix D in the *Specifications* to obtain the basic wind speed at bridge site. When the basic wind speed at the bridge site, U_{s10} , obtained from wind observations, is converted to a basic wind speed, U_{10} , less than 24.5 m/s, the basic wind speed is taken as 24.5 m/s.

Commentary

The basic wind speed at the bridge site can be determined by wind observations. Table 4-1 shows ten cases where the basic wind speeds at bridge sites were obtained through wind observations.

Table 4-1 Cases of determining basic wind speed at bridge site through wind observations

Bridge	Bridge type	Main span (m)	Terrain feature
Sutong Yangzi River Bridge	Cable-stayed bridge	1088	Wide river surface
Edong Yangzi River Bridge	Cable-stayed bridge	926	River surface
Jiangshun Bridge in Guangzhou	Cable-stayed bridge	700	River surface
Hong Kong-Zhuhai-Macau Bridge	Cable-stayed bridge	458	Wide sea surface
Runyang Yangzi River Suspension Bridge	Suspension bridge	1490	River surface
Aizhai Bridge	Suspension bridge	1176	Canyon
Baling River Bridge	Suspension bridge	1088	Canyon
Taizhou Yangzi River Bridge	Suspension bridge	1080	River surface
Sidu River Bridge	Suspension bridge	900	Canyon
Beipanjiang Bridge (Zhensheng Highway)	Suspension bridge	636	Canyon

4.2.6 The reference wind speed of a bridge or member at the reference height Z may be calculated using Eqs. (4.2.6-1) and (4.2.6-2) :

$$U_d = k_f \left(\frac{Z}{10} \right)^{\alpha_0} U_{s10} \quad (4.2.6-1)$$

$$\text{or } U_d = k_f k_i k_h U_{10} \quad (4.2.6-2)$$

where,

U_d ——reference wind speed of a bridge or member at the reference height Z (m/s) ;

α_0 ——terrain roughness factor at the bridge site, which may be selected according to Table 4.2.1 ;

k_f ——wind risk factor, which is determined according to the wind risk regions for bridges and Table 4.2.6-1;

Table 4.2.6-1 Wind risk factor, k_f

Risk region	R1	R2	R3
Basic wind speed, U_{10} , (m/s)	$U_{10} > 32.6$	$24.5 < U_{10} \leq 32.6$	$U_{10} \leq 24.5$
Wind risk factor, k_f	1.05	1.02	1.00

k_t ——terrain condition factor, which may be taken as 1.0 for flat and open terrain, and may be 1.2 ~ 1.5 for canyon mouth or mountain pass. For important bridges, it may be obtained by wind tunnel testing or virtual wind tunnel testing and shall not be less than 1.0;

k_h ——correction factor for transition between terrain categories and height of wind speed, which may be selected from Table 4.2.6-2 according to the reference height of members, and also may be determined using Eqs. (4.2.6-3) ~ (4.2.6-6). When the calculated factor is smaller than 1.0 or larger than 1.77, the value in Table 4.2.6-2 shall be selected.

Table 4.2.6-2 Correction factor, k_r , for transition between terrain categories and height of wind speed

Reference height, Z (m)	Terrain category			
	A	B	C	D
5	1.08	1.00	0.86	0.79
10	1.17	1.00	0.86	0.79
15	1.23	1.07	0.86	0.79
20	1.28	1.12	0.92	0.79
30	1.34	1.19	1.00	0.85
40	1.39	1.25	1.06	0.85
50	1.42	1.29	1.12	0.91
60	1.46	1.33	1.16	0.96
70	1.48	1.36	1.20	1.01
80	1.51	1.40	1.24	1.05
90	1.53	1.42	1.27	1.09
100	1.55	1.45	1.30	1.13
150	1.62	1.54	1.42	1.27
200	1.68	1.62	1.52	1.39
250	1.73	1.67	1.59	1.48
300	1.77	1.72	1.66	1.57
350	1.77	1.77	1.71	1.64
400	1.77	1.77	1.77	1.71
450	1.77	1.77	1.77	1.77

$$k_{hA} = 1.174 \left(\frac{Z}{10} \right)^{0.12} \quad (4.2.6-3)$$

$$k_{hB} = 1.0 \left(\frac{Z}{10} \right)^{0.16} \quad (4.2.6-4)$$

$$k_{hC} = 0.785 \left(\frac{Z}{10} \right)^{0.22} \quad (4.2.6-5)$$

$$k_{hD} = 0.564 \left(\frac{Z}{10} \right)^{0.30} \quad (4.2.6-6)$$

Commentary

The variation of wind speed with height is complex and is affected by both the terrain category and the temperature. In practice, logarithmic or exponential formulas are commonly used to describe the variation of wind speed with height. In the *Specifications*, the exponential rule is used to represent the distribution of wind speed along the height. Considering that areas with high basic wind speeds are typically prone to strong winds and frequent typhoons, a risk factor for wind-resistant design is proposed in the *Specifications*, and it is determined based on the risk region categorization. The risk factors for wind-resistant design corresponding to R1, R2, and R3 are equivalent to wind speed increase factors for wind speed with return periods of 150 years, 120 years and 100 years, respectively.

4.2.7 The terrain roughness factor for bridges spanning river valleys or mountain valleys may be determined based on Terrain Category C or D. When the bridge structure is sensitive to wind-induced vibrations, it should be determined through wind tunnel testing and/or virtual wind tunnel testing on simulated terrains, and shall also comply with the relevant provisions in Appendix B.7 and Appendix C.5 of the *Specifications*.

Commentary

Wind observations and wind tunnel tests for topographic wind environment at multiple bridge sites spanning valleys or mountain valleys have shown that the wind speed distribution at these bridge sites generally conforms to that of Terrain Category C or D. Table 4-2 lists the terrain categories obtained through wind tunnel testing and/or virtual wind tunnel testing for several bridges.

Table 4-2 Examples of methods for determining terrain category of several bridges spanning river valleys or mountain valleys

Bridge	Bridge type	Main span (m)	Terrain	Determination method			Terrain category
				Wind tunnel testing	Virtual wind tunnel testing	Wind observation at bridge site	
Beipanjiang Bridge (Zhensheng Highway)	Suspension bridge	636	Canyon	✓	✓	✓	D
Beipanjiang Bridge (Hangrui Highway)	Cable-stayed bridge	720	Canyon		✓		D
Dimu River Bridge	Suspension bridge	538	Canyon		✓		D
Sidu River Bridge	Suspension bridge	900	Canyon	✓	✓		D
Baling River Bridge	Suspension bridge	1088	Canyon	✓	✓	✓	D
Aizhai Bridge	Suspension bridge	1176	Canyon	✓	✓	✓	D
Yachi River Bridge	Suspension bridge	800	Canyon		✓	✓	D
Hezhang Bridge in Guizhou	Beam bridge	180	River valley		✓		C

4.2.8 In the absence of correlation data between wind speeds at the bridge site and surrounding meteorological stations, the reference wind speed, U_d , for the bridge or its members may be determined based on the principle that the gradient wind speeds at the bridge site and surrounding meteorological stations are consistent and according to Eqs. (4.2.8-1) and (4.2.8-2):

$$U_d = \lambda_z U_{\delta s} \quad (4.2.8-1)$$

$$U_{\delta s} = \sum_{i=1}^n \eta_i U_{\delta i} = \eta_1 U_{\delta 1} + \eta_2 U_{\delta 2} + \cdots + \eta_n U_{\delta n} \quad (4.2.8-2)$$

where,

λ_z ——scale factor for wind speed at reference height Z , which is the proportional coefficient between the wind speed at the reference height and the gradient wind speed at the bridge site, and may be obtained through wind tunnel testing and/or virtual wind tunnel testing on simulated terrain;

$U_{\delta s}$ ——gradient wind speed at bridge site (m/s);

n ——number of meteorological stations near the bridge site, which shall not be less than 3;

$U_{\delta i}$ ——gradient wind speed at the i th meteorological station ($i = 1, 2, \cdots, n$) (m/s);

η_i ——weighting coefficient for the gradient wind speed at the i th meteorological station.

Assuming the distance between the i th meteorological station and the bridge site is d_i ($i = 1, 2, \cdots, n$), η_i may be determined according to Eq. (4.2.8-3).

Commentary

Taking a mountain bridge as an example, the wind speed distribution along different heights and the gradient wind speed were obtained through topographic wind environment simulation tests. The scale factor, λ_z , between the wind speed at the deck elevation and the gradient wind speed is 0.63. The distances from the bridge site to three neighboring meteorological stations are 50 km, 37 km and 43 km, respectively. The basic wind speeds at these three stations are 23.7 m/s, 24.5 m/s and 25.2 m/s, respectively. Based on the topographic features of the meteorological stations, the corresponding gradient wind speeds are estimated to be 41.9 m/s, 43.4 m/s and 44.6 m/s, respectively. According to Eq. (4.2.8-2), the gradient wind speed at the bridge site is calculated to be 43.4 m/s. Finally, with $\lambda_z = 0.63$, the reference wind speed for the main girder is determined to be 27.3 m/s.

4.2.9 The design wind speed at the construction phase may be determined using Eq. (4.2.9):

$$U_{sd} = k_{sf} U_d \quad (4.2.9)$$

where,

U_{sd} ——design wind speed at the construction phase (m/s);

k_{sf} ——wind risk factor during the construction period, which generally may be selected from Table 4.2.9, and may also be determined through risk assessment based on the specific conditions of the bridge and different wind-resistant design objectives.

Table 4.2.9 Wind risk factor, k_{sf} , during the construction period

Construction duration (Year)	Risk region		
	R1	R2	R3
≤ 3	0.88	0.84	0.78
> 3	0.92	0.88	0.84

Commentary

Wind-resistant design for bridges during construction needs to account for factors such as risk region, construction duration, wind-resistant design objectives, and magnitude of risk loss. Considering that the probability of encountering extreme wind speeds during the construction period cannot be equated with that during the service period, the design wind speed at the construction phase is generally determined by combining the construction duration with the probability of not

exceeding the design wind speed for the completed bridge (e. g. , 80%). The probability of not exceeding can be expressed as:

$$P = (1 - 1/R)^T \tag{4-3}$$

where ,

- P ——Non-exceedance probability ;
- T ——Construction duration (year) ;
- R ——Return period (year).

The wind risk factor during construction is comprehensively determined based on Tables 4-3 and 4-4. It is also advisable to adopt risk management methodologies to reasonably determine the wind risk factor during construction, taking into account risk assessment, identification of key wind-resistant states of bridges, rational arrangement of construction schedule, and different wind-resistant design objectives.

Table 4-3 Relationship between return period, R , of wind speed, non-exceedance probability, P , and construction duration, T

Non-exceedance probability	Construction duration, T					
	1 year	2 years	3 years	5 years	10 years	20 years
0.95	20.0	39.5	59.0	98.0	195	390
0.90	10.0	19.5	29.0	48.0	95.4	190
0.85	6.7	12.8	19.0	31.3	62.0	124
0.80	5.0	9.5	14.0	22.9	45.3	90.1
0.70	3.5	6.1	8.9	14.5	28.5	56.6
0.60	2.5	4.4	6.4	10.3	20.1	39.7
0.50	2.0	3.4	4.8	7.7	14.9	29.4

Table 4-4 Reference table of wind risk factors at different return periods of wind speed

Return period of wind speed (Year)	5	10	20	30	50	100
k_{sf}	0.78	0.84	0.88	0.92	0.95	1

4.3 Design Turbulence Intensity

4.3.1 The design turbulence intensity of bridges may be calculated using Eqs. (4.3.1-1) ~ (4.3.1-3). For the longitudinal fluctuating wind speed component, the design turbulence intensity,

I_u , may alternatively be selected from Table 4.3.1.

$$I_u = \frac{1}{\ln\left(\frac{Z}{z_0}\right)} \quad (4.3.1-1)$$

$$I_v = 0.88I_u \quad (4.3.1-2)$$

$$I_w = 0.50I_u \quad (4.3.1-3)$$

where,

I_u ——design longitudinal turbulence intensity;

I_v ——design cross-wind turbulence intensity;

I_w ——design vertical turbulence intensity;

Z ——reference height of the bridge structure or member (m);

z_0 ——terrain roughness height of the bridge site (m).

Table 4.3.1 Design longitudinal turbulence intensity, I_u

Height (m)	Terrain category			
	A	B	C	D
10 < Z ≤ 20	0.14	0.17	0.25	0.29
20 < Z ≤ 30	0.13	0.16	0.23	0.29
30 < Z ≤ 40	0.12	0.15	0.21	0.28
40 < Z ≤ 50	0.12	0.15	0.20	0.26
50 < Z ≤ 70	0.11	0.14	0.18	0.24
70 < Z ≤ 100	0.11	0.13	0.17	0.22
100 < Z ≤ 150	0.10	0.12	0.16	0.19
150 < Z ≤ 200	0.10	0.12	0.15	0.18

Commentary

Turbulence intensity is the most fundamental parameter to characterize the degree of variation of wind speed with time and space. The incoming wind has a horizontal component (X direction) with a wind speed of U , and its average wind speed is \bar{U} ; the transverse wind speed is V , and the vertical wind speed is W , with their mean wind speeds being \bar{V} and \bar{W} , respectively. Generally, $\bar{V} = \bar{W} = 0$ can be assumed. Let u , v , and w be the fluctuating components of U , V , and W , respectively, and σ_u , σ_v , and σ_w be the standard deviations of U , V , and W , respectively, as shown in Figure 4-2, then the turbulence intensities of the fluctuating wind speed in these three directions are defined as:

$$I_u = \frac{\sigma_u}{\bar{U}} \quad (4-4)$$

$$I_v = \frac{\sigma_v}{\bar{U}} \quad (4-5)$$

$$I_w = \frac{\sigma_w}{\bar{U}} \quad (4-6)$$

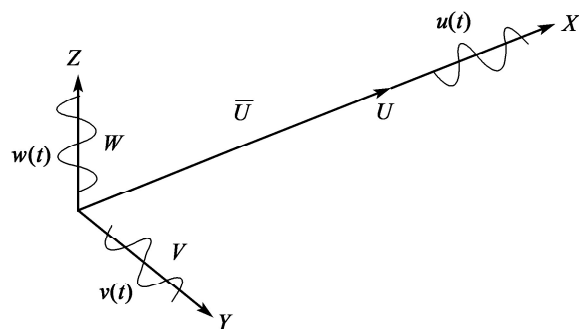


Figure 4-2 Definition schematic for fluctuating wind components u , v , and w

5 Wind Loads

5.1 General

5.1.5 Wind loads acting on bridge structures or members shall consider both static wind effects and dynamic wind effects.

Commentary

Both static and dynamic effects can be generated when wind acts on bridge structures or members. The characteristics of wind-induced structural response under wind action are related to the magnitude of structural stiffness. When the structural stiffness is low, the dynamic response characteristics gradually appear, leading to relatively significant dynamic effects. In the wind-resistant design, the dynamic action and its effects need to be considered for lightweight and flexible bridges or members.

5.1.2 The along-wind load on bridge structures or members may be calculated using the equivalent static gust wind load method specified in this chapter. When the dynamic effects of wind action on the bridge are determined to be significant, necessary wind tunnel testing, virtual wind tunnel testing and corresponding numerical analysis shall be conducted to obtain cross-wind loads and their effects on the bridge structures or members.

Commentary

Natural wind is generally decomposed into mean wind and fluctuating wind components. Structures under the action of natural wind will experience both mean wind effects and fluctuating wind effects. The fluctuating wind effects consist of background response and resonance response

components, as shown in Figure 5-1. The energy distribution corresponding to the shaded area A is similar to that of wind speed, representing the power spectrum without considering the structural resonance response. The energy distribution corresponding to the shaded area B is the power spectrum of the structural resonance response. When the structural stiffness is sufficiently high, the resonance response component becomes negligible.

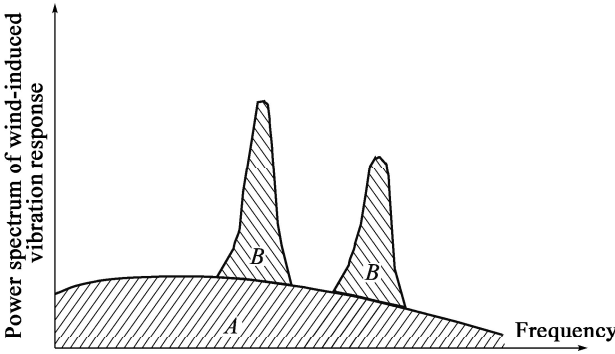


Figure 5-1 Schematic for decomposition of power spectrum of wind – induced vibration response

Along-wind loads are expressed in the form of equivalent static gust wind loads in the *Specifications* by taking into account factors such as the spatial correlation of wind. Detailed wind load response analysis is required for cross-wind load responses, special structures, or special construction phases of structures (e. g. , bridges in balanced cantilever construction state).

5.2 Equivalent Static Gust Wind Speed

5.2.1 The equivalent static gust wind speed, U_g , may be calculated using Eq. (5.2.1) :

$$U_g = G_v U_d \quad (5.2.1)$$

where,

G_v ——equivalent static gust factor, which may be selected from Table 5.2.1 ;

U_d ——reference wind speed (m/s).

Table 5.2.1 Equivalent static gust factor, G_v

Terrain category	Horizontal wind loaded length (m)												
	≤20	60	100	200	300	400	500	650	800	1000	1200	1500	≥2000
A	1.29	1.28	1.26	1.24	1.23	1.22	1.21	1.2	1.19	1.18	1.17	1.16	1.15
B	1.35	1.33	1.31	1.29	1.27	1.26	1.25	1.24	1.23	1.22	1.21	1.20	1.18
C	1.49	1.48	1.45	1.41	1.39	1.37	1.36	1.34	1.33	1.31	1.30	1.29	1.26
D	1.56	1.54	1.51	1.47	1.44	1.42	1.41	1.39	1.37	1.35	1.34	1.32	1.30

Note: (1) In the completed bridge state, the horizontal wind loaded length is the full length of the main bridge.

- (2) The wind loaded length of a multi – span continuous bridge with multiple units is determined by the length of its individual structural unit.
- (3) For a bridge under cantilever construction, the horizontal wind loaded length is selected based on the length of the assembled main girder in that construction state.

Commentary

The gust wind speed that takes into account the spatial correlation of wind on structures or components is defined as the equivalent static gust wind speed in the *Specifications*. When considering the along-wind load on structures or members, the equivalent static gust wind load is used in the analysis. The equivalent static gust factor is essentially a wind speed scaling factor when applying the along-wind load that accounts for factors such as turbulence intensity, spatial correlation of fluctuating wind, loaded length (height), and the height of structural members above the ground or water surface.

For the horizontal structural member in Figure 5-2, the wind pressure per unit length at position x and time t is given by:

$$P(x, t) = \frac{1}{2} \rho C_H D (U + u(x, t))^2 = \bar{P} + \frac{2\bar{P}}{U} u(x, t) \quad (5-1)$$

where,

\bar{P} —— the mean wind pressure calculated based on the 10-minute mean wind speed.

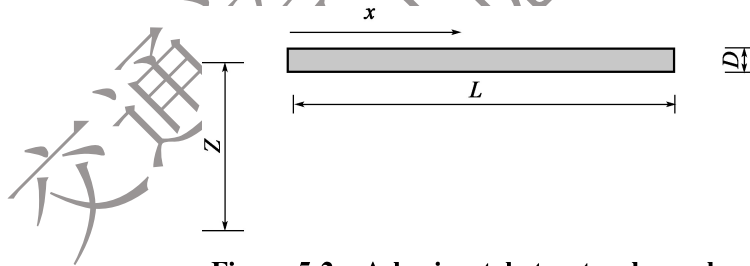


Figure 5-2 A horizontal structural member

Then, the total pressure on the member is:

$$P_{t0} = \int_0^L P(x, t) dx = \bar{P} + \int_0^L \frac{2\bar{P}}{U} u(x, t) dx = \bar{P} + P(t) \quad (5-2)$$

$P(t)$ is the fluctuating wind pressure. While

$$S_p(n) = \left(\frac{2\bar{P}}{U} \right)^2 |J_H(n)|^2 S_u(n) \quad (5-3)$$

where,

$S_p(n)$ ——spectral density function of fluctuating wind pressure, $P(t)$;

$S_u(n)$ ——spectral density function of fluctuating wind speed;

$|J_H(n)|^2$ ——joint acceptance function, expressed as

$$|J_H(n)|^2 = \frac{1}{l^2} \int_0^l \int_0^l e^{\frac{-K_1 n}{U} |x_1 - x_2|} dx_1 dx_2 \quad (5-4)$$

K_1 is the correlation coefficient of fluctuating wind, and is generally taken to be 7 ~ 21. The standard deviation of the fluctuating wind pressure is:

$$\sigma_p = \left(\int_0^\infty S_p(n) dn \right)^{\frac{1}{2}} \quad (5-5)$$

According to Davenport's theory, the expected value of the maximum wind pressure is:

$$E[P_{10, \max}] = \bar{P} + g_f \sigma_p \quad (5-6)$$

$$g_f = \sqrt{2 \ln(vT)} + \frac{0.5772}{\sqrt{2 \ln(vT)}} \quad (5-7)$$

$$v = \left[\int_0^\infty n^2 S_p(n) dn \right]^{\frac{1}{2}} / \sigma_p \quad (5-8)$$

Hence, the equivalent static gust wind pressure factor can be obtained, which is the ratio of the expected value of the maximum wind pressure to the 10-minute mean wind pressure:

$$G_p = \frac{E[P_{10, \max}]}{\bar{P}} = 1 + g_f \cdot \sigma_p / \bar{P} \quad (5-9)$$

The equivalent static gust factor is:

$$G_v = \frac{U_g}{U_z} = \sqrt{G_p} \quad (5-10)$$

The equivalent static gust factor, G_v , for different averaging times, can be obtained through the following method. Since the expected maximum value of $u(t)$ is derived from a series of measurements, the actual spectrum, $S_u(n)$, is limited by the finite observation time T and the finite response time τ of the recording instrument, forming a spectral window where the low-frequency components are truncated by T and the high-frequency components are dependent on τ . Given that the averaging time T for mean wind is typically 10 minutes, the low-frequency cutoff is negligible, while the high-frequency components can be considered by replacing the instantaneous expected maximum value with the average expected maximum value over a short averaging time τ .

The average maximum wind speed within the finite response time, T , can be obtained using Eqs. (5-11) ~ (5-12):

$$U_g(\tau) = G_V(\tau) \cdot U \quad (5-11)$$

$$G_V(\tau) = \sqrt{1 + g(\tau) \cdot \sigma_p(\tau)/P} \quad (5-12)$$

In the equations, $g(\tau)$ and $\sigma_p(\tau)$ can be calculated according to the aforementioned Eqs. (5-7) and (5-5), but the spectral density function $S_u(n)$ of the fluctuating wind speed needs to be replaced using Eq. (5-13).

$$S_u(n, \tau) = S_u(n) \chi(n, \tau) \quad (5-13)$$

$$\chi(n, \tau) = \sin^2(\pi n \tau) / (\pi n \tau)^2 \quad (5-14)$$

The equivalent static gust factors for different reference wind speeds, terrain categories, several correlation coefficients and various deck elevations were calculated for the *Specifications* based on the Kaimal horizontal wind spectrum. Calculations indicate that for the same terrain category, the equivalent static gust factor varies little with changes in the reference wind speed and shows only minor variations with changes in the deck elevation. It also exhibits minimal changes with variations in the horizontal correlation coefficient, but is significantly influenced by changes in the terrain category. Table 5-1 presents the equivalent static gust factors for different averaging times, while Tables 5-2 and 5-3 provide the equivalent static gust factors for different heights and different reference wind speeds, respectively.

Table 5-1 Equivalent static gust factors for different averaging times

Averaging time (s)	Horizontal wind loaded length (m)											
	100	200	300	400	500	650	800	1000	1200	1500	1800	2100
1	1.31	1.29	1.27	1.26	1.25	1.24	1.23	1.22	1.21	1.20	1.19	1.18
3	1.28	1.26	1.25	1.24	1.23	1.22	1.21	1.20	1.20	1.19	1.18	1.17
5	1.26	1.25	1.24	1.23	1.22	1.21	1.20	1.19	1.19	1.18	1.17	1.16
10	1.22	1.21	1.21	1.20	1.20	1.19	1.18	1.18	1.17	1.16	1.15	1.15
20	1.18	1.18	1.17	1.17	1.16	1.16	1.15	1.15	1.14	1.14	1.13	1.13
30	1.16	1.15	1.15	1.14	1.14	1.14	1.13	1.13	1.13	1.12	1.12	1.12
60	1.11	1.11	1.11	1.11	1.11	1.10	1.10	1.10	1.10	1.09	1.09	1.09
180	1.06	1.06	1.06	1.06	1.06	1.06	1.06	1.06	1.06	1.05	1.05	1.05
300	1.04	1.04	1.04	1.04	1.04	1.04	1.04	1.04	1.04	1.04	1.04	1.04

Note: The calculation conditions in the table are: Terrain Category B, a reference height of 40 m for members, and a reference wind speed of 40 m/s.

For the equivalent static gust wind load, the averaging time of wind speed is taken as 1 ~ 3 s. For typical long-span bridges, the bridge height is generally in the range of 30 ~ 70 m, and the

reference wind speed is usually between 20 and 50 m/s. It is recommended in the *Specifications* to adopt the result for an averaging time of 1 s, a reference height of 40 m for the bridge deck, and a correlation coefficient of 7 for the fluctuating wind, as shown in Table 5-4.

Table 5-2 Equivalent static gust factors for different reference heights

Height of bridge deck above the water or ground surface (m)	Horizontal wind loaded length (m)											
	100	200	300	400	500	650	800	1000	1200	1500	1800	2100
20	1.32	1.30	1.28	1.26	1.25	1.24	1.22	1.21	1.20	1.19	1.18	1.17
40	1.31	1.29	1.27	1.26	1.25	1.24	1.23	1.22	1.21	1.20	1.19	1.18
60	1.30	1.28	1.27	1.26	1.25	1.24	1.23	1.22	1.21	1.20	1.19	1.19
80	1.30	1.28	1.27	1.26	1.25	1.24	1.23	1.22	1.21	1.20	1.20	1.19

Note: The calculation conditions in the table are: Terrain Category B, averaging time $\tau = 1$ s, and reference wind speed of 40 m/s.

Table 5-3 Equivalent static gust factors for different reference wind speeds

Reference wind speed (km/h)	Horizontal wind loaded length (m)											
	100	200	300	400	500	650	800	1000	1200	1500	1800	2100
20	1.30	1.28	1.26	1.25	1.24	1.23	1.22	1.21	1.20	1.19	1.18	1.17
30	1.31	1.28	1.27	1.26	1.25	1.23	1.22	1.21	1.20	1.19	1.19	1.18
40	1.31	1.29	1.27	1.26	1.25	1.24	1.23	1.22	1.21	1.2	1.19	1.18
50	1.31	1.29	1.28	1.26	1.25	1.24	1.23	1.22	1.21	1.2	1.19	1.19

Note: The calculation conditions in the table are: Terrain Category B, averaging time $\tau = 1$ s, and reference wind speed of 40 m/s.

Table 5-3 Equivalent static gust factors for different terrain categories

Terrain category	Horizontal wind loaded length (m)													
	< 20	60	100	200	300	400	500	650	800	1000	1200	1500	1800	2100
A	1.29	1.28	1.26	1.24	1.23	1.22	1.21	1.20	1.19	1.18	1.17	1.16	1.16	1.15
B	1.35	1.33	1.31	1.29	1.27	1.26	1.25	1.24	1.23	1.22	1.21	1.20	1.19	1.18
C	1.49	1.48	1.45	1.41	1.39	1.37	1.36	1.34	1.33	1.31	1.30	1.29	1.27	1.26
D	1.56	1.54	1.51	1.47	1.44	1.42	1.41	1.39	1.37	1.35	1.34	1.32	1.31	1.30

Note: The calculation conditions in the table are: averaging time $\tau = 1$ s, reference height of 40 m for members, and reference wind speed of 40 m/s.

5.2.2 Equivalent static gust factors for bridge towers and piers may be taken from Table 5.2.2 according to the height of the members.

Table 5.2.2 Equivalent static gust factors for bridge towers and piers, G_v

Terrain category	Structural height (m)							
	<40	60	80	100	150	200	300	400
A	1.19	1.18	1.17	1.16	1.14	1.13	1.12	1.11
B	1.24	1.22	1.20	1.19	1.17	1.16	1.14	1.13
C	1.33	1.29	1.27	1.26	1.23	1.21	1.18	1.16
D	1.48	1.42	1.39	1.36	1.31	1.28	1.24	1.22

Commentary

For the vertical member shown in Figure 5-3, at the height z and time t , the wind pressure per unit length is:

$$P(z, t) = \frac{1}{2} \rho C_H B (U(z) + u(z, t))^2 = \bar{P}(z) + \frac{2\bar{P}(z)}{U} u(z, t) \quad (5-15)$$

Then, the total pressure on the member is:

$$P_{h0} = \int_0^h P(z, t) dz = \int_0^h (\bar{P}(z) + \frac{2\bar{P}(z)}{U} u(z, t)) dz \quad (5-16)$$

$$S_p(n, z) = \left(\frac{2\bar{P}(z)}{U} \right)^2 |J_H(n, z)|^2 S_u(n) \quad (5-17)$$

where,

$S_p(n, z)$ — spectral density function of fluctuating wind pressure $P(z, t)$ at height z ;

n — frequency of wind (Hz);

$S_u(n)$ — spectral density function of fluctuating wind speed at height z , which is taken as the Davenport wind speed spectrum keeping constant along the height, and is expressed as:

$S_u(n) = 4K^2 v_{10} x^2 / (n (1 + x^2)^{\frac{4}{3}})$, where $x = 1200n/U_{10}$, U_{10} is the mean wind speed at the height of 10 m, and K is a factor related to the ground surface roughness.

$|J_H(n, z)|^2$ — $|J_H(n, z)|^2 = \frac{1}{h^2} \int_0^h \int_0^h e^{\frac{ik_n}{i(1+z)} |z_1 - z_2|} dz_1 dz_2$, and is

the joint acceptance function at height z , in which K_1 is the correlation coefficient of fluctuating wind and is taken as 7.

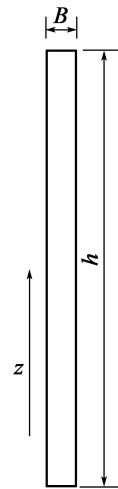


Figure 5-3 Illustration of a vertical structural member

The equivalent static gust factor is also calculated under the conditions of an averaging time of 1 s, a basic wind speed of 40 m/s, and a correlation coefficient of 7 for the fluctuating wind.

5.3 Equivalent Static Gust Load on Main Girder

5.3.1 The along-wind equivalent static gust load, F_g , per unit length of the main girder under the transverse wind load may be calculated using Eq. (5.3.1):

$$F_g = \frac{1}{2} \rho U_g^2 C_H D \quad (5.3.1)$$

where,

F_g ——along-wind equivalent static gust wind load acting on the unit length of main girder (N/m);

ρ ——air density (kg/m^3), which may be taken as 1.25 kg/m^3 ;

U_g ——equivalent static gust wind speed (m/s);

C_H ——lateral force coefficient of the main girder;

D ——characteristic depth of the main girder (m).

Commentary

In the body axis coordinate system shown in Figure 5-4, the aerostatic force acting on the unit length of the main girder is decomposed into the average wind loads in three directions, which are expressed as:

Aerodynamic lateral force:

$$F_H = \frac{1}{2} \rho U^2 C_H D \quad (5-18)$$

Aerodynamic vertical force:

$$F_V = \frac{1}{2} \rho U^2 C_V B \quad (5-19)$$

Aerodynamic torsional moment:

$$M = \frac{1}{2} \rho U^2 C_M B^2 \quad (5-20)$$

where

B ——characteristic width of the main girder (m);

C_V ——vertical force coefficient of the main girder;

C_M ——torsional force coefficient of the main girder.

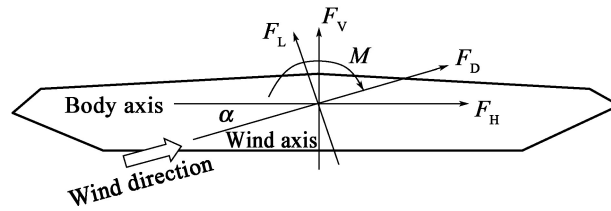


Figure 5-4 Wind axis and body axis coordinate systems and their aerodynamic force directions

The mean wind loads in three directions can also be expressed in the form of wind axis, and are generally represented by drag coefficient, C_D , lift coefficient, C_L and torsional force coefficient, C_M . The coefficients of forces in the three directions are able to convert between the body axis and the wind axis, and the conversion relationship is determined using Eqs. (5-21) and (5-22):

$$C_H = C_D \cos(\alpha) - \frac{B}{D} C_L \sin(\alpha) \quad (5-21)$$

$$C_V = \frac{D}{B} C_D \sin(\alpha) + C_L \cos(\alpha) \quad (5-22)$$

where,

C_D ——drag coefficient of main girder on wind axis;

C_L ——lift coefficient of main girder on wind axis;

α ——wind attack angle($^{\circ}$).

Air density is significantly influenced by atmospheric pressure and temperature, exhibiting noticeable variations. A typical characteristic is that the atmospheric pressure is low and the air is thin at high altitudes, and the air density is also relatively low. Additionally, when atmospheric pressure remains constant, air density increases as temperature decreases. The relationship between air density, temperature, and atmospheric pressure is shown in Table 5-5.

Table 5-5 Relationship between air density, ρ , temperature, and atmospheric pressure (kg/m^3)

Temperature	0.7 atm	0.8 atm	0.9 atm	1 atm	1.1 atm	1.2 atm
-30 °C	1.017	1.162	1.307	1.453	1.598	1.743
-25 °C	0.996	1.139	1.281	1.423	1.566	1.708
-20 °C	0.977	1.116	1.256	1.395	1.535	1.674
-15 °C	0.958	1.095	1.231	1.368	1.505	1.642
-10 °C	0.939	1.074	1.208	1.342	1.476	1.611
-5 °C	0.922	1.054	1.185	1.317	1.449	1.581
0 °C	0.905	1.034	1.164	1.293	1.422	1.552

continued

Temperature	0.7 atm	0.8 atm	0.9 atm	1 atm	1.1 atm	1.2 atm
5 °C	0.889	1.016	1.143	1.270	1.397	1.524
10 °C	0.873	0.998	1.123	1.247	1.372	1.497
15 °C	0.858	0.981	1.103	1.226	1.348	1.471
20 °C	0.843	0.964	1.084	1.205	1.325	1.446
25 °C	0.829	0.948	1.066	1.185	1.303	1.421
30 °C	0.816	0.932	1.049	1.165	1.282	1.398

Note: atm denotes standard atmospheric pressure, which is 101325 Pa.

5.3.2 When the main span of a bridge is less than or equal to 200 m, the lateral force coefficient C_H of certain forms of girder sections may be determined by the following method:

- 1 The lateral force coefficient, C_H , of main girders with I-shaped, Π -shaped or box section may be calculated using Eq. (5.3.2-1):

$$C_H = \begin{cases} 2.1 - 0.1 \left(\frac{B}{D} \right) & 1 \leq \frac{B}{D} < 8 \\ 1.3 & 8 \leq \frac{B}{D} \end{cases} \quad (5.3.2-1)$$

where,

B ——characteristic width of the main girder (m);

D ——projected height of the main girder (m).

- 2 When the main girder section of a bridge has inclined webs, the lateral force coefficient, C_H , may be reduced according to the angle of inclination of the web plates. The reduction coefficient, η_c , for the lateral force coefficient corresponding to the angle of inclination of the web plates may be determined using Eq. (5.3.2-2):

$$\eta_c = \begin{cases} 1 - 0.005 \times \beta_d & 0^\circ \leq \beta_d < 60^\circ \\ 0.7 & \beta_d \geq 60^\circ \end{cases} \quad (5.3.2-2)$$

where,

β_d ——angle of inclination of web plate ($^\circ$), as shown in Figure 5.3.2-1.

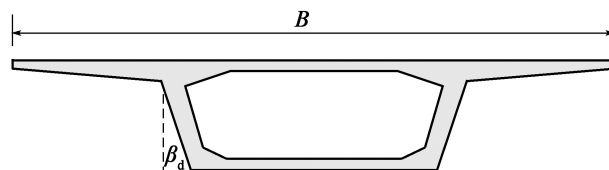


Figure 5.3.2-1 Definition schematic for angle of inclination of inclined web

- 3 The lateral force coefficient, C_H , for the superstructure of truss bridges may be selected from Table 5.3.2-1. When the superstructure consists of two or more trusses, the lateral force coefficient for each truss may be taken as ηC_H , where η is the shielding factor and may be adopted according to Table 5.3.2-2; the lateral force coefficient for the deck system may be taken as 1.3.

Table 5.3.2-1 Lateral force coefficient, C_H , for a truss

Solidity ratio	Rectangular and H-shaped members	Round members (d is diameter of member)	
		$dU_d \leq 6 \text{ m}^2/\text{s}$	$dU_d > 6 \text{ m}^2/\text{s}$
0.1	1.9	1.2	0.7
0.2	1.8	1.2	0.8
0.3	1.7	1.2	0.8
0.4	1.7	1.1	0.8
0.5	1.6	1.1	0.8

Note: The solidity ratio of the truss is the ratio of the net area to the overall area of the truss.

Table 5.3.2-2 Shielding factor for a truss, η

Spacing ratio	Solidity ratio				
	0.1	0.2	0.3	0.4	0.5
≤ 1	1.00	0.90	0.80	0.60	0.45
2	1.00	0.90	0.80	0.65	0.50
3	1.00	0.95	0.80	0.70	0.55
4	1.00	0.95	0.80	0.70	0.60
5	1.00	0.95	0.85	0.75	0.65
6	1.00	0.95	0.90	0.80	0.70

Note: The spacing ratio is the center-to-center distance between two trusses divided by the depth of the windward truss.

- 4 The lateral force coefficient, C_H , for the completed state of a streamlined closed-box girder bridge may be taken as 1.1. Correspondingly, for the construction state without guardrails and traffic barriers, the lateral force coefficient may be taken as 0.8. When additional measures such as wind barriers are installed, the lateral force coefficient should be determined through wind tunnel testing or virtual wind tunnel simulations.

Commentary

The depth and width of main girders with I-shaped, II-shaped or box sections can be determined by referring to Figures 5-5(a) ~ 5-5(c). When railings, wind barriers or sound barriers are attached

to the bridge deck, the girder depth can be determined by referring to Figure 5-5 (d).

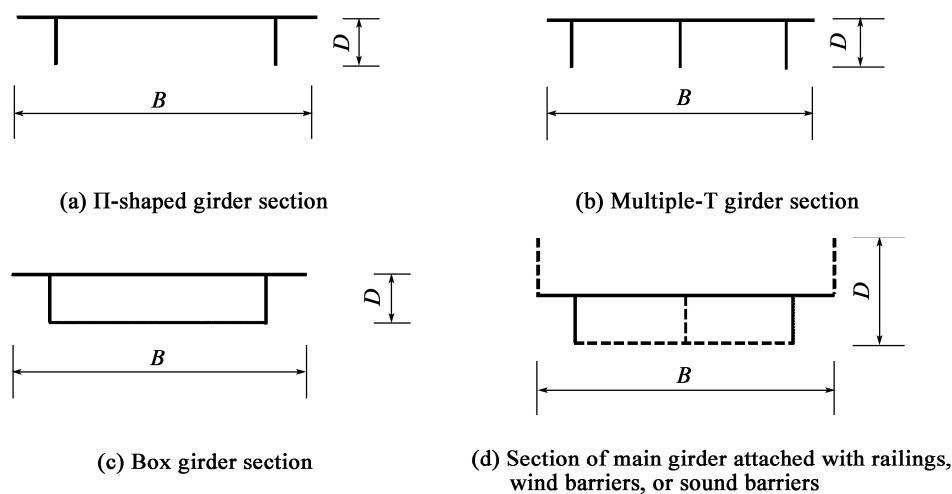


Figure 5-5 Schematic for determination of the depth of the main girder for wind load analysis

The lateral force coefficient of a truss girder is composed of two parts. One is the lateral force coefficient of the truss, and the other is the lateral force coefficient of the deck system. In the calculation of the drag coefficient for a single truss, the solidity ratio is the ratio of the net area to the overall area of the truss, which is the ratio of the shaded area to the area enclosed by $abcd$, as illustrated in Figure 5-6. For multiple trusses that are closely spaced, the shielding effect between trusses on wind loads needs to be considered.

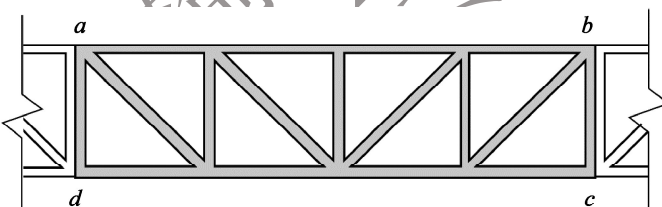


Figure 5-6 Schematic for the calculation of wind loads on a truss structure

The lateral force coefficient for a streamlined closed-box girder is influenced by the depth and width of the girder as well as the presence or absence of aerodynamic countermeasures. Based on the summary of existing bridges, the lateral force coefficient for streamlined closed-box girders is derived statistically in the *Specifications*. Table 5-6 shows the lateral force coefficients for some typical streamlined closed-box girders.

Table 5-6 Lateral force coefficients for streamlined closed-box girders

Bridge	Bridge type	Girder width (m)	Girder depth (m)	C_H for the completed bridge	C_H for a bridge under construction
Sutong Yangtze River Bridge	Cable-stayed bridge	41.0	4.0	0.979	0.353

continued

Bridge	Bridge type	Girder width (m)	Girder depth (m)	C_H for the completed bridge	C_H for a bridge under construction
Jiujiang Yangtze River Bridge	Cable-stayed bridge	38.9	3.6	0.992	0.773
Runyang Yangtze River Bridge (Suspension Bridge)	Suspension bridge	35.9	3.0	0.791	0.406
Zhujiang Huangpu Bridge (Suspension Bridge)	Suspension bridge	39.6	3.5	0.686	0.529
Zhujiang Huangpu Bridge (Cable-stayed Bridge)	Cable-stayed bridge	41.0	3.5	0.645	0.563
Jiangyin Yangtze River Bridge	Suspension bridge	36.9	3.0	1.063	/
Taizhou Yangtze River Bridge	Suspension bridge	39.1	3.5	0.839	/
Yichang Yangtze River Bridge	Suspension bridge	30.0	3.0	0.925	/

Note: The lateral force coefficients in this table are the maximum values for the wind attack angle between $-3^\circ \sim +3^\circ$.

5.3.3 When the main span of a bridge is larger than 200 m, the lateral force coefficients for truss girders and other girders with complex sections shall be determined through wind tunnel testing or virtual wind tunnel testing.

Commentary

The main truss girder has a relatively complex form, including single-layer and double-layer structures, and there are also significant differences in the truss spacing, depth, and overall width of the bridge. The lateral force coefficients of long-span truss bridges are generally obtained through aerostatic force testing. Table 5-7 presents the lateral force coefficients of ten completed truss girders.

Table 5-7 Lateral force coefficients of truss girders

Bridge	Bridgetype	Total width of main girder	Depth of truss (m)	C_H for the completed bridge	C_H for a bridge under construction
Second Dongting Lake Bridge	Suspension bridge	36.1	9.0	1.010	0.830

continued

Bridge	Bridgetype	Total width of main girder	Depth of truss (m)	C_H for the completed bridge	C_H for a bridge under construction
Beipanjiang Bridge (Zhensheng Highway)	Suspension bridge	28	7.57	1.049	0.950
Dimu River Bridge	Suspension bridge	27	4.5	0.982	/
Sidu River Bridge	Suspension bridge	26	6.5	1.036	/
Beipanjiang Bridge (Hangrui Highway)	Cable-stayed bridge	27	8.0	0.742	0.632
Shanghai Minpu Bridge	Cable-stayed bridge	44.0 (Top deck) 28.2 (Bottom deck)	11.62	0.886	0.810
Wuhan Tianxingzhou Yangtze River Bridge	Cable-stayed bridge (railway and highway)	30	15.2	0.894	0.848
nqing Yangtze River Bridge	Cable-stayed bridge (railway)	28	15	0.979	0.847
Tongling Yangtze River Bridge	Cable-stayed bridge (railway and highway)	35	15.5	0.709	0.563
Hanjiatuo Yangtze River Bridge in Chongqing	Cable-stayed bridge (railway)	18	14	0.835	0.789

Note: The lateral force coefficients in this table are the maximum values for the wind attack angle between $-3^\circ \sim +3^\circ$.

5.3.4 When the clear spacing between separated twin-deck bridges is less than 5 times the main girder width of the single-deck bridge, the aerodynamic interference effects between the twin decks of the bridge should be considered in the determination of the lateral force coefficient for the single-deck bridge.

Commentary

Figure 5-7 illustrates the configuration of the main girder for a twin-deck bridge. According to research findings on the aerostatic coefficients of rectangular, Π -shaped and streamlined sections with a width-to-depth ratio of 5, the aerodynamic interference factor for the drag coefficient of upstream bluff sections (rectangular and Π -shaped sections) is approximately 0.9 when the spacing ratio $0.02 \leq B_s/B \leq 1.0$, and approaches 1.0 when $B_s/B \geq 2.0$. For upstream streamlined sections, the aerodynamic interference factor for the drag coefficient approximately ranges from 0.51 to 0.90 when $0.02 \leq B_s/B \leq 1.0$, and approaches 0.82 when $B_s/B \geq 3.0$. For

downstream bluff sections (rectangular and Π -shaped sections), the aerodynamic interference factor for the drag coefficient increases linearly with the increasing spacing ratio, B_s/B , when $0.02 \leq B_s/B \leq 2.0$, and is approximately from 0.1 to 0.65. When $2.0 < B_s/B \leq 5.0$, the aerodynamic interference factor for the drag coefficient changes more gradually, approximately ranging from 0.65 to 0.80. For downstream streamlined girder sections, the aerodynamic interference factor for the drag coefficient is larger than that of the upstream section when $B_s/B < 3.0$, meaning that the drag coefficient of the downstream section is larger than that of the upstream section. When $B_s/B \geq 3.0$, the aerodynamic interference factor for the drag coefficient for the downstream streamlined girder section is 0.75.

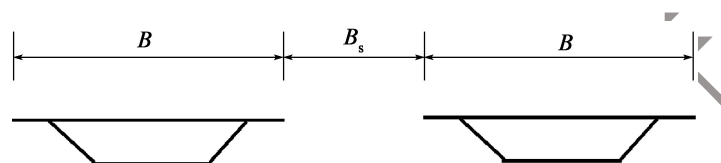


Figure 5-7 Schematic for main girder layout of a twin-deck bridge

5.3.5 For bridges with a span less than or equal to 200 m, the longitudinal wind load per unit length on main girders may be selected according to the following two scenarios:

- 1 For solid girders, it may be taken as 0.25 times the transverse wind load.
- 2 For truss girders, it may be taken as 0.50 times the transverse wind load.

5.3.6 For bridges with a span larger than 200 m, the longitudinal wind load per unit length may be calculated using Eq. (5.3.6) and based on the friction force generated between the wind and the surfaces of main girders:

$$F_{fr} = \frac{1}{2} \rho U_g^2 C_f s \quad (5.3.6)$$

where,

U_g ——equivalent static gust wind speed (m/s);

F_{fr} ——friction force per unit length (N/m);

C_f ——coefficient of friction, taken from Table 5.3.6;

s ——perimeter of main girder (m). For truss girder sections, it is the perimeter of the outer profile of the girder.

Table 5.3.6 Coefficients of friction, C_f

Conditions of upper and lower surfaces of main girder	Coefficients of friction, C_f
Smooth surfaces (smooth concrete or steel surfaces)	0.01
Rough surfaces (concrete surfaces)	0.02
Very rough surfaces (with ribs)	0.04

continued

Conditions of upper and lower surfaces of main girder		Coefficients of friction, C_f
Truss section	Single layer of carriageway	0.065
	Double layers of carriageway	0.10

Commentary

Studies have shown that the longitudinal wind load increases initially and then decreases as the wind yaw angle of wind increases. The most unfavorable longitudinal wind load does not occur in the longitudinal direction of the bridge but rather at a wind yaw angle of $45^\circ \sim 60^\circ$. Figure 5-8 shows the test results of the friction coefficient for a single-deck truss girder under the longitudinal wind load with different wind yaw angles obtained through sectional model testing. By conversion, the maximum friction coefficient is approximately 0.065. Wind tunnel tests on a sectional model of the double-deck truss girder of the Minpu Bridge have indicated a friction coefficient of 0.10. When using the coefficients in the table, the perimeter of the truss girder is determined based on the outer contour of the geometric space enclosed by the height and width of the truss.

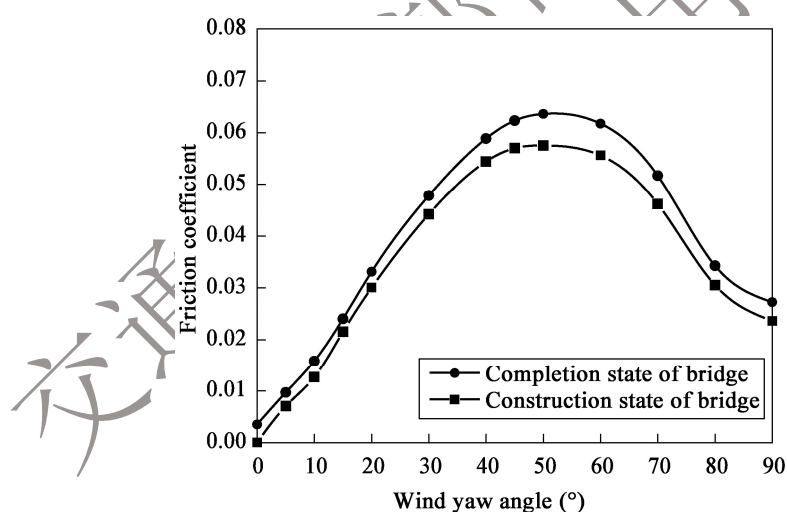


Figure 5-8 Test result of friction coefficients for a single-deck truss girder

5.3.7 Aerostatic coefficients of main girders should be determined based on the most unfavorable values with the wind attack angle in the range of $-3^\circ \sim +3^\circ$.

5.3.8 Under the wind action W1, when the wind load is combined with vehicular loads, the wind load on the main girder shall include the transverse load acting on the vehicles, and the

increment may be 1.5 kN/m. If wind barriers or sound barriers are installed, the transverse load on the vehicles may not be considered.

Commentary

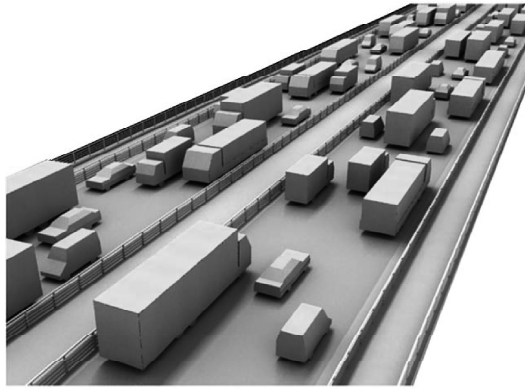
Under the wind action W1, when the wind load is combined with vehicular load, the wind effects on vehicles need to be considered. The wind effects on vehicles for various wind yaw angles are given in the AASHTO specifications, as shown in Table 5-8.

Table 5-8 Wind effects on vehicles in AASHTO specifications (basic wind speed of 24.6 m/s)

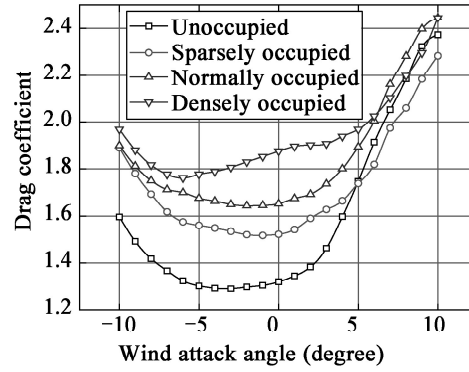
Wind yaw angle (°)	Wind load normal to bridge axis (kN/m)	Wind load parallel to bridge axis (kN/m)
0	1.459	0.0
15	1.284	0.175
30	1.197	0.350
45	0.963	0.467
60	0.496	0.554

Aerostatic force tests on sectional models with and without vehicles on the deck have shown that, for the wind effect on a closed box girder with a depth of 3.5 m, the transverse aerostatic coefficient increases by 42% considering the scenario with vehicles fully occupying the deck. Based on calculations for a 200 m long bridge with Terrain Category B and a wind speed of 25 m/s on the deck level, the transverse aerostatic coefficient increases by 1260 N/m, which is slightly less than the result obtained from the AASHTO specifications. Figure 5-9 schematically shows the vehicle arrangement for the sectional model testing considering moving vehicles on the deck and the test results of aerostatic coefficients.

In Eurocode, the transverse wind effects on the main girder due to the presence of vehicles are considered by adjusting the calculated depth of the girder. Taking a main girder with a width of 35 m and a depth of 3 m as an example, considering an additional vehicle height of 2.5 m, the calculated depths of the girder with and without the vehicles are 3 m and 5.5 m, respectively. The corresponding drag coefficient is taken as 1.0. If the turbulence intensity on the bridge deck is 0.15, the load increment is 1761 N/m, which is slightly larger than the calculated result according to the AASHTO specifications. Based on all the results from the test and both standards, an increment of 1.5 kN/m for the transverse wind load on the deck, considering the influence of vehicles, is adopted in the *Specifications*.



(a) Sectional model with randomly sequenced vehicles



(b) Aerostatic coefficients of the sectional model considering the influence of vehicles

Figure 5-9 Aerostatic coefficients of the main girder considering the influence of vehicles

5.4 Equivalent Static Gust Wind Loads on Piers, Towers, Stay Cables, Suspension Cables, and Hangers

5.4.1 Wind loads on piers, towers, and hangers, as well as equivalent static gust wind loads on stay cables and suspension cables under the transverse wind action, may be calculated using Eq. (5.4.1):

$$F_g = \frac{1}{2} \rho U_g^2 C_H A_n \quad (5.4.1)$$

where,

F_g ——wind load per unit length on member (N/m);

ρ ——air density (kg/m^3), which may be taken as 1.25 kg/m^3 ;

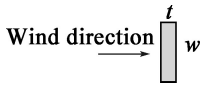
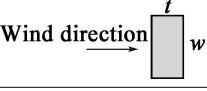
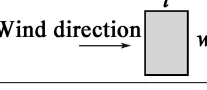
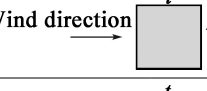

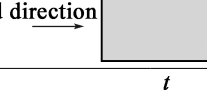
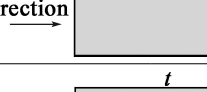
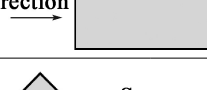
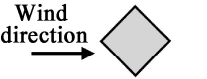


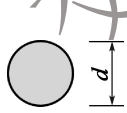
U_g ——equivalent static gust wind speed at the reference height of the member (m/s);

C_H ——drag coefficient of member;

A_n ——along-wind projected area of member per unit length (m^2/m), which is taken as the outer diameter of a stay cable, a suspension cable, and a hanger.

5.4.2 The drag coefficient, C_H , for piers or towers may be selected from Table 5.4.2-1, and that for individual members of steel structures may be selected from Table 5.4.2-2. For piers or towers with complex cross-sections, the drag coefficient may be obtained through wind tunnel testing or virtual wind tunnel testing, and the most unfavorable value within 30° wind yaw angles in the transverse or longitudinal direction of the bridge may be taken.

Table 5.4.2-1 Drag coefficients, C_H , of piers and towers

Cross-section	t/w	Ratio of height to width of pier or tower, h/w						
		1	2	4	6	10	20	40
	1/4	1.3	1.4	1.5	1.6	1.7	1.9	2.1
	1/3 ~1/2	1.3	1.4	1.5	1.6	1.8	2.0	2.2
	2/3	1.3	1.4	1.5	1.6	1.8	2.0	2.2
	1	1.2	1.3	1.4	1.5	1.6	1.8	2.0
	3/2	1.0	1.1	1.2	1.3	1.4	1.5	1.7
	2	0.8	0.9	1.0	1.1	1.2	1.3	1.4
	3	0.8	0.8	0.8	0.9	0.9	1.0	1.2
	4	0.8	0.8	0.8	0.8	0.8	0.9	1.1
	Square or Octagon	1.0	1.1	1.1	1.2	1.2	1.3	1.4
	12-sided polygon	0.7	0.8	0.9	0.9	1.0	1.1	1.3
	Circle with smooth surface where $dU_d \geq 6 \text{ m}^2/\text{s}$	0.5	0.5	0.5	0.5	0.5	0.6	0.6
	1. Circle with smooth surface where $dU_d \geq 6 \text{ m}^2/\text{s}$ 2. Circle with rough surface or projections	0.7	0.7	0.8	0.8	0.9	1.0	1.2

Notes: (1) In this table, t is the along-wind width of a cross-section, w is the windward width of a cross-section, d is the diameter of a circular cross-section, h is the height of a pier or tower.

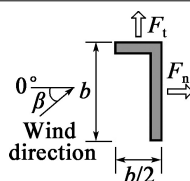
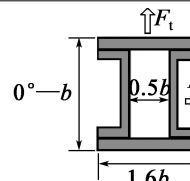
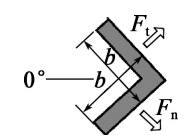
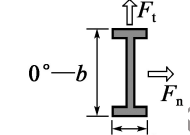
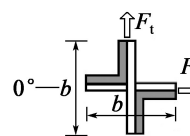
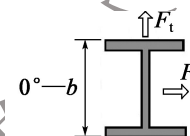
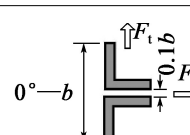
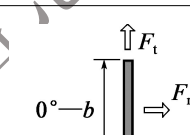
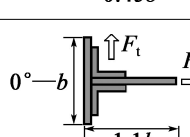
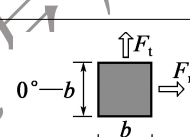
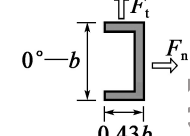
(2) After the erection of the superstructure, C_H shall be derived for a height-to-width ratio of 40.

(3) For a rectangular pier with radiused corners, the value of C_H shall be taken from the table above and then multiplied by either $(1 - 1.5r/w)$ or 0.5, whichever is greater, where r is the radius of the rounded corners.

(4) For a pier with triangular nose, C_H shall be calculated as the rectangle encompassing the outer edges of the pier.

(5) For a pier tapering with height, C_H shall be derived in segments based on the height of the pier. When calculating t/w , the average value of t/w for each segment shall be used, and the ratio of height to width shall be calculated using the total height of the pier divided by the average width of each segment.

Table 5.4.2-2 Drag coefficients of individual members in steel structures

Cross-section	Yaw angle of wind (°)						Cross-section	Yaw angle of wind (°)			
	β	0	45	90	135	180		β	0	45	90
	C_{fn}	+1.9	+1.8	+2.0	-1.8	-2.0		C_{fn}	+1.4	+1.2	0
	C_{fi}	+0.95	+0.8	+1.7	-0.1	+0.1		C_{fi}	0	+1.6	+2.2
	C_{fn}	+1.8	+2.1	-1.9	-2.0	-1.4		C_{fn}	+2.05	+1.95	+0.5
	C_{fi}	+1.8	+1.8	-1.0	+0.3	-1.4		C_{fi}	0	+0.6	+0.9
	C_{fn}	+1.75	+0.85	+0.1	-0.75	-1.75		C_{fn}	+1.6	+1.5	0
	C_{fi}	+0.1	+0.85	+1.75	+0.75	-0.1		C_{fi}	0	+1.5	+1.9
	C_{fn}	+1.6	+1.5	-0.95	-0.5	-1.5		C_{fn}	+2.0	+1.8	0
	C_{fi}	0	-0.1	+0.7	+1.05	0		C_{fi}	0	+0.1	+0.1
	C_{fn}	+2.0	+1.2	-1.6	-1.1	-1.7		C_{fn}	+2.0	+1.55	0
	C_{fi}	0	+0.9	+2.15	+2.4	+2.1		C_{fi}	0	+1.55	+2.0
	C_{fn}	+2.05	+1.85	0	-1.6	-1.8					
	C_{fi}	0	+0.6	+0.6	+0.4	0					

Commentary

The wind load on a rectangular cross-section is related to the ratio between the widths of the cross-section, t/w , and the ratio between the height of the member and the windward width, h/w . Without considering three-dimensional flow around the member, the drag coefficient for the two-dimensional rectangular cross-section reaches its maximum when t/w is within 0.65 ~ 0.70, and then gradually decreases with the increase of t/w . The variation of the drag coefficient with the ratio of height to windward width h/w is mainly due to the three-dimensional effect of airflow around the member. As the ratio h/w increases, the three-dimensional flow effect diminishes, causing the airflow to primarily pass around the member from both sides, which is approximately a

two-dimensional effect, and thus the drag coefficient increases. However, after the superstructure of the bridge is completed, the main girder weakens the three-dimensional flow effect. Therefore, it is specified in this clause that the drag coefficient is taken as the maximum value after the erection of the superstructure.

For piers or towers in the design for structures sensitive to wind loads, it is often necessary to obtain the drag coefficient of the cross-section through wind tunnel testing or virtual wind tunnel testing. However, the drag coefficient is significantly influenced by the wind yaw angle. To account for the most unfavorable effects, the most unfavorable value within wind yaw angles of $\pm 30^\circ$ in the transverse or longitudinal direction of the bridge is generally taken as the design value of the drag coefficient. The cross-section of the tower of the Sutong Yangtze River Bridge has chamfers, as shown in Figure 5-10. During the determination of wind loads, the drag coefficients at different wind yaw angles were analyzed and compared. Table 5-9 presents the results of virtual wind tunnel tests showing the variation of the drag coefficient of the tower column cross-section of the bridge with the wind yaw angle.

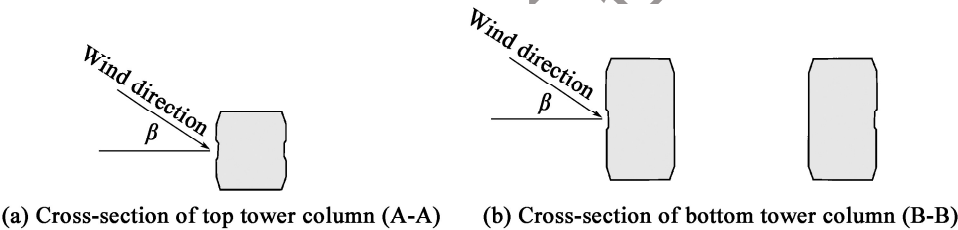


Figure 5-10 Schematic cross-sections of tower columns of Sutong Yangtze River Bridge

Table 5-9 Relationship between the drag coefficient of the tower column section of the Sutong Yangtze River Bridge and the wind yaw angle

Wind yaw angle(°)	A-A			B-B (windward side)			B-B (leeward side)		
	Drag coefficient (wind axis)	Lateral force coefficient	Longitudinal force coefficient	Drag coefficient (wind axis)	Lateral force coefficient	Longitudinal force coefficient	Drag coefficient (wind axis)	Lateral force coefficient	Longitudinal force coefficient
0	1.934	1.934	-0.021	2.217	2.217	-0.124	0.194	0.194	-0.122
3	2.233	2.250	-0.281	2.416	2.436	-0.332	0.537	0.534	0.075
10	1.991	2.082	-0.343	2.170	2.239	0.028	1.076	1.083	0.117
30	2.404	2.251	0.909	1.651	1.870	0.490	1.120	0.890	0.690
45	2.224	1.724	1.421	1.601	1.467	0.798	1.705	1.518	0.894
60	2.086	0.821	1.935	1.432	1.116	1.009	1.390	0.822	1.130
75	1.780	0.280	1.770	1.131	0.560	1.021	1.303	0.562	1.198
87	1.620	0.060	1.620	0.909	0.005	0.910	0.940	0.127	0.935
90	1.465	-0.087	1.465	0.874	0.063	0.874	0.920	0.013	0.920

5.4.3 Wind loads acting on piers or towers may be determined according to the wind speed at a height of 0.65 times the height of the piers or towers above the ground or water surface, and may also be determined according to the wind speed distribution specified in Clause 4.2.6 of the *Specifications* based on the terrain category.

Commentary

As shown in Figure 5-11, the tower is assumed to have a uniform cross-section with a windward width of w , a drag coefficient of C_D , and an equivalent height of h_0 , then the bending moment at the base of the tower is:

$$M = \int_0^h \left(\frac{1}{2} \rho \left[U_{s10} \left(\frac{x}{10} \right)^{\alpha_0} \right]^2 C_D w x dx \right. \quad (5-23)$$

The equivalent bending moment at the tower base is:

$$\tilde{M} = \frac{1}{2} \rho \left[U_{s10} \left(\frac{h_0}{10} \right)^{\alpha_0} \right]^2 C_D w h \frac{h}{2} \quad (5-24)$$

Let $M = \tilde{M}$, we have $h_0^{2\alpha} \frac{h^2}{2} = \int_0^h x^{2\alpha_0+1} dx$, then:

$$h_0 = \left(\frac{1}{1 + \alpha} \right)^{\frac{1}{2\alpha_0}} h \quad (5-25)$$

For four terrain categories A, B, C and D, the terrain roughness factors, α_0 , are 0.12, 0.16, 0.22 and 0.30, respectively. Hence, $h_0 = 0.624h$, $h_0 = 0.629h$, $h_0 = 0.636h$, and $h_0 = 0.646h$, respectively.

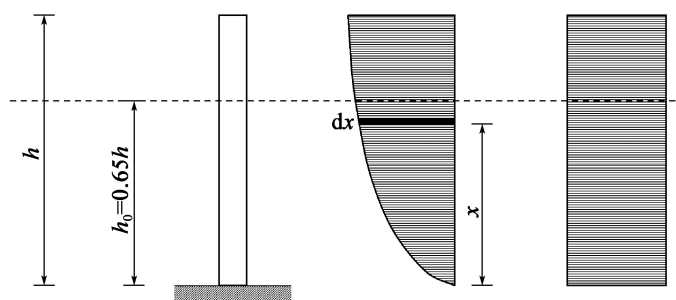


Figure 5-11 Principle of equivalence of wind load on tower structure and equivalent height

5.4.4 When the center-to-center distance between the suspension cables of a suspension bridge is 4 times or more than the diameter of the cables, the wind load on each cable should be considered separately, and a drag coefficient of 0.7 may be used for an individual suspension cable. When the center-to-center distance between suspension cables is less than 4 times their diameter, they may be calculated as one suspension cable, and a drag coefficient shall be 1.0. When the center-to-center distance between hangers is 4 times or more than their diameter, the drag coefficient of 1.0 may be used for each hanger.

5.4.5 For stay cables with smooth surfaces, dimpled surfaces, and helical fillets, the drag coefficient may be taken as 1.0 under the wind action W1, and 0.8 under the wind action W2. For stay cables with other shapes, arranged in parallel and with ice accretion, suspension cables as well as hangers, the drag coefficient should be obtained through wind tunnel testing or virtual wind tunnel testing.

Commentary

Wind tunnel tests on stayed cables of different diameters and with various additional aerodynamic countermeasures have shown that the aerodynamics of stay cables with a circular cross-section are significantly influenced by the Reynolds number, whereas stay cables with additional helical fillets and dimpled surfaces are minimally affected by the Reynolds number. Under the wind action W1, the design wind speed for stay cables of most bridges is generally above 20 m/s. Hence, the drag coefficient of stay cables is taken as 1.0, which can cover commonly used types of stay cables. Figure 5-12 shows the test results on the drag coefficients of stay cables with smooth surfaces and various additional aerodynamic countermeasures.

Generally, the drag coefficient of stay cables at high wind speeds is lower than that at low wind speeds. Table 5-10 presents the drag coefficients of stay cables at a wind speed of 55 m/s. Considering the influence of the Reynolds number, the drag coefficient is conservatively taken as 0.8.

In the northern regions with low temperatures and heavy snowfall in China and the southern regions prone to freezing rain, stay cables, suspension cables and hangers are susceptible to ice accretion due to climatic conditions. The ice accretion significantly alters their aerodynamic shapes and affects the aerostatic forces on the members. The aerostatic coefficients of ice-accreted cable members under special climatic conditions need to be determined through wind tunnel testing or virtual wind tunnel testing.

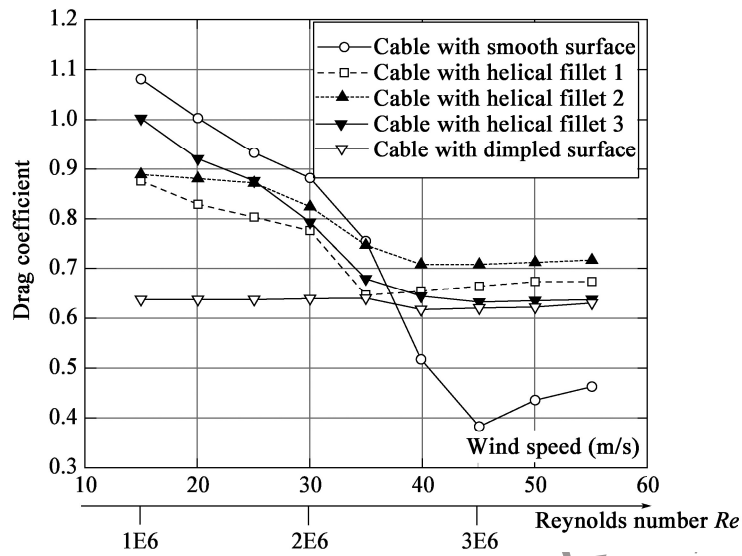


Figure 5-12 Drag coefficients of stay cables with smooth surface, helical fillets, and dimpled surface

Table 5-10 Comparison of drag coefficients of cross-wind stay cables (wind speed of 55 m/s)

Cable with smooth surface	Cable with dimpled surface	Cable with helical fillets								
		$t = 834$			$t = 1112$			$t = 1390$		
		$d = 2$	$d = 3$	$d = 4$	$d = 2$	$d = 3$	$d = 4$	$d = 2$	$d = 3$	$d = 4$
0.463	0.630	0.717	0.752	0.768	0.673	0.719	0.755	0.637	0.683	0.711

Note: In this table, t is the pitch of helical fillets (mm), and d is the diameter of helical fillets (mm).

5.4.6 The horizontal wind load per unit length on stay cables under the longitudinal wind action, F_g , shall be calculated according to Eq. (5.4.6):

$$F_g = \frac{1}{2} \rho U_g^2 C_D D_c \sin^2 \alpha_c \quad (5.4.6)$$

where,

F_g ——horizontal wind load per unit length on the stay cable under the longitudinal wind action;

C_D ——drag coefficient of stay cable, which is taken in accordance with Clause 5.4.5 of the *Specifications*;

D_c ——outer diameter of stay cable (m);

α_c ——inclination angle of stay cable($^\circ$).

Commentary

A wind tunnel test was conducted to investigate the aerostatic coefficients of stay cables with

different inclination angles under the wind action of various yaw angles. The results indicate that the longitudinal drag coefficient of the stay cables exhibits an approximately linear relationship with $\sin^2 \alpha_c$, as shown in Figure 5-13. Figure 5-14 illustrates the definition of the inclination angle of the stay cables.

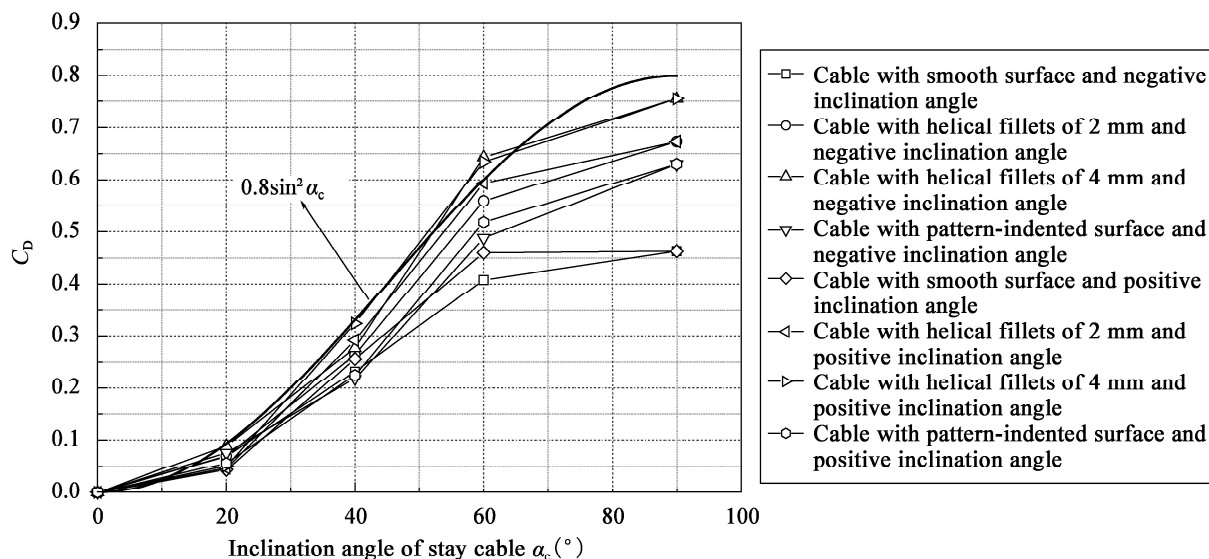


Figure 5-13 Longitudinal drag coefficient of stay cables with smooth surface, helical fillets, and dimpled surface

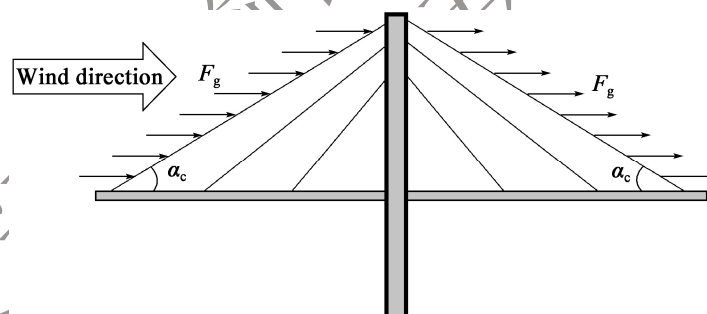


Figure 5-14 Definition schematic for inclination angle of stay cables and direction of wind load

5.4.7 Under the longitudinal wind action, the horizontal wind load per unit length in the longitudinal direction on suspension cables of suspension bridges may be taken as 0.15 times the transverse wind load. Whenever necessary, it may also be determined through wind tunnel testing or virtual wind tunnel testing.

Commentary

A virtual wind tunnel test study on the horizontal wind load in the longitudinal direction on suspension cables of a suspension bridge, considering factors such as inclination angle, wind yaw

angle and cable clamps, indicates that the horizontal wind load in the longitudinal direction on the suspension cable is related to the wind yaw angle and the inclination angle of the suspension cables. For safety purposes, the most unfavorable proportional relationship of 0.15 is adopted in the *Specifications*. Figure 5-15 illustrates the variation of the ratio between the longitudinal and transverse aerodynamic forces on the suspension cable with the wind yaw angle.

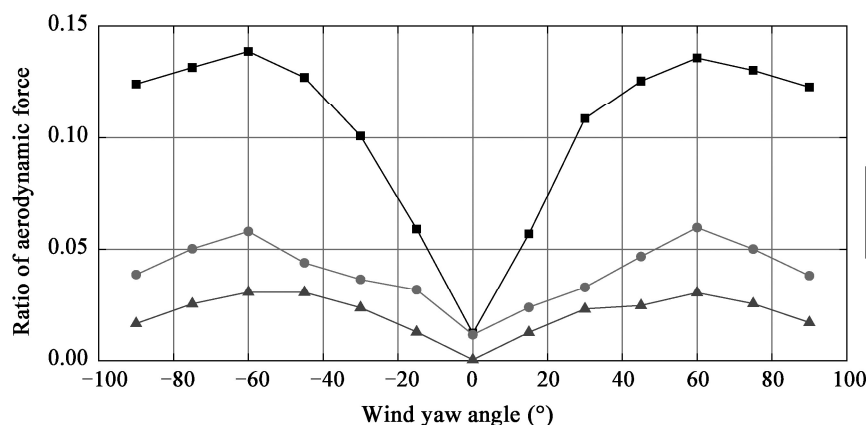


Figure 5-15 Relationship between the ratio of longitudinal and transverse aerodynamic forces on suspension cable and wind yaw angle

5.4.8 For arch ribs under wind loads, the drag coefficient of a single arch rib may be determined by referring to Clause 5.4.2 of the *Specifications*. When the arch rib consists of double or multiple chords with a spacing less than 5 times the width of a single chord, or when the cross-sectional shape of the main arch is complex, the drag coefficient should be determined through wind tunnel testing or virtual wind tunnel testing.

5.5 Buffeting Inertial Load and Its Effects

5.5.1 The buffeting inertial load of a certain mode of vibration for a structure or member may be obtained based on the acquired buffeting displacement of the mode and by comprehensively considering factors such as mass distribution, mode shape, and frequency.

Commentary

According to Newton's second law, the inertial force, $F_i(x)$, of a structure is proportional to its mass, $m(x)$, and acceleration, $a(x)$, that is $F_i(x) = m(x)a(x)$. After obtaining the vibrational displacement of each mode at position x through model testing or theoretical analysis, the corresponding acceleration at that position can be calculated, and the inertial load can be obtained by using the mass distribution.

5.5.2 Buffeting displacement may be obtained through frequency domain analysis, time domain analysis, wind tunnel testing or virtual wind tunnel testing, taking into account factors such as the possible participating modes, the spatial correlation of wind fluctuations and the cross-sectional characteristics of the member under the design wind speed.

Commentary

During the time-domain analysis, spatial fluctuating wind fields and wind forces are usually synthesized through wind field simulation methods and are applied to the structure to obtain its buffeting response. Statistical analysis is subsequently performed to obtain the buffeting response results. The frequency-domain analysis for buffeting typically treats atmospheric turbulence as a stationary random process. Based on the wind speed spectrum, along with the transfer function that accounts for the influence of the aerodynamic shape of the structural cross-section on the wind spectrum and aerodynamic force spectrum (i. e., the aerodynamic admittance), and considering the transfer function of the bridge structure, the statistical results of the buffeting response are finally obtained. Wind tunnel tests and virtual wind tunnel tests simulate the characteristics such as frequency, mode shape, damping ratio and aerodynamic shape of the structure to directly measure or analyze the buffeting response and its statistical results. Figure 5-16 schematically shows the computational principles of time-domain and frequency-domain analysis methods for buffeting.

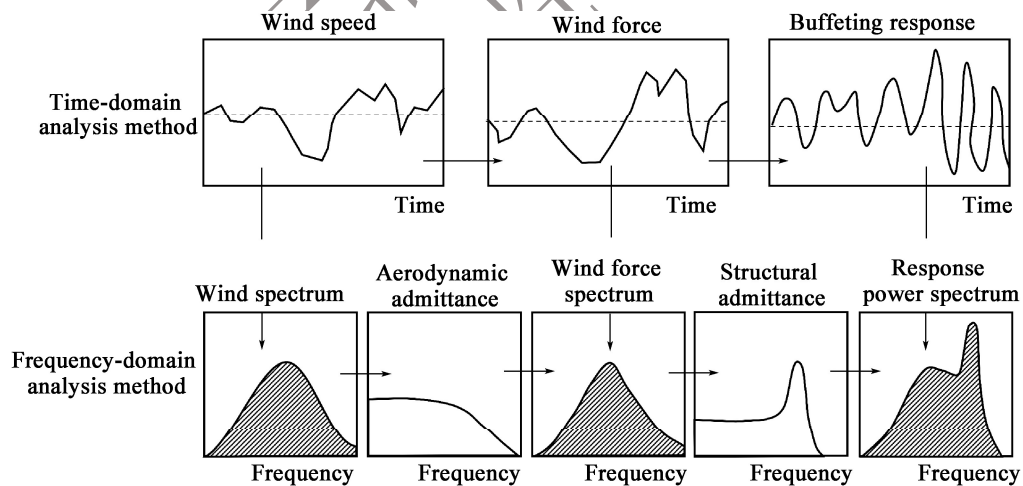


Figure 5-16 Schematic for computational principles of time-domain and frequency-domain analysis methods for buffeting

5.5.3 The inertial force per unit length corresponding to the i th mode shape of a bridge structure may be calculated using Eq. (5.5.3):

$$F_i(x) = k_p m(x) \sigma_i(x) (2\pi f_i)^2 \quad (5.5.3)$$

where,

$F_i(x)$ ——inertial force of the i th mode at position x of the bridge (N/m);

k_p ——peak factor, which is generally taken as 3.5;

$m(x)$ ——mass per unit length at position x of the bridge (kg/m);

$\sigma_i(x)$ ——standard deviation of buffeting displacement of the i th mode at position x of the bridge (m), which is usually derived from time domain or frequency domain analysis of buffeting, or through wind tunnel testing or virtual wind tunnel testing;

f_i ——frequency of the i th mode (Hz).

Commentary

Generally, buffeting response analysis is used to obtain statistical values of the vibration response, such as the root mean square displacement, and there is a certain proportional relationship between the extreme value and standard deviation of buffeting response, which can be represented by a peak factor. As shown in Figure 5-17, the peak factor is generally in a range of 3 ~ 4.5, and can be taken as 3.5. Its physical meaning can also be expressed using Eq. (5-26):

$$k_p = \frac{R_{\max} - R_{\min}}{2\sigma_R} \quad (5-26)$$

where,

R_{\max} ——maximum of buffeting response;

R_{\min} ——minimum of buffeting response;

σ_R ——standard deviation of buffeting response.

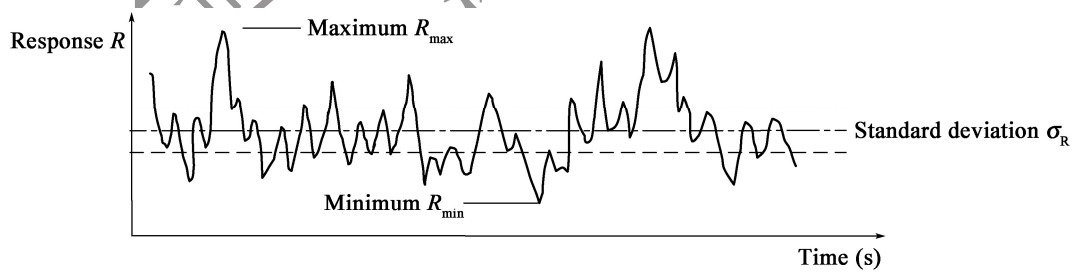


Figure 5-17 Physical meaning of peak factor

5.5.4 The effect of inertial forces on a bridge may be calculated by the SRSS (Square Root of the Sum of the Squares) modal combination method, taking into account the modes that are possible to be excited, as per Eq. (5.5.4):

$$R_s(x) = \sqrt{\sum_i R_i^2(x)} \quad (5.5.4)$$

where,

$R_s(x)$ ——effect of the buffeting inertial force at position x of the bridge;

$R_i(x)$ ——effect of the buffeting inertial force of the i th mode at position x of the bridge.

Commentary

Since resonance responses in multiple vibration modes of a structure are typically induced by wind loads, the modal combination method is often used to combine the effects of inertial forces of various modes in order to account for the contributions of each mode. In the calculation of buffeting responses, the SRSS method is commonly adopted to combine the effects of various vibration modes.

5.5.5 The extreme effect combination shall be conducted to combine the effects of buffeting inertial forces with the static wind effects at the design wind speed according to Eq. (5.5.5):

$$R_t(x) = R_m(x) \pm R_s(x) \quad (5.5.5)$$

where,

$R_t(x)$ ——extreme effect of wind at position x of the bridge;

$R_m(x)$ ——aerostatic effect of the mean wind at position x of the bridge.

5.5.6 When the effects of structural geometric nonlinearity are significant, time-domain analysis incorporating the nonlinear effects should be employed to evaluate the structural response under wind load.

5.6 Wind Loads during Construction

5.6.1 For large-span cable-stayed bridges and continuous bridges with fixed superstructure-pier connections during cantilever construction, detailed wind effect analyses in both transverse and longitudinal directions should be conducted for the maximum double-cantilever and maximum single-cantilever states. Wind tunnel testing or virtual wind tunnel testing may be implemented when necessary.

5.6.2 When applying transverse wind loads to bridges erected by the double-cantilever method, both symmetric and asymmetric loading conditions on the main girder shall be included. For asymmetric loading conditions, the wind load on one side of the main girder should be taken as 0.5 times that on the other side. Figure 5.6.2 illustrates the application of wind loads on the main girder.

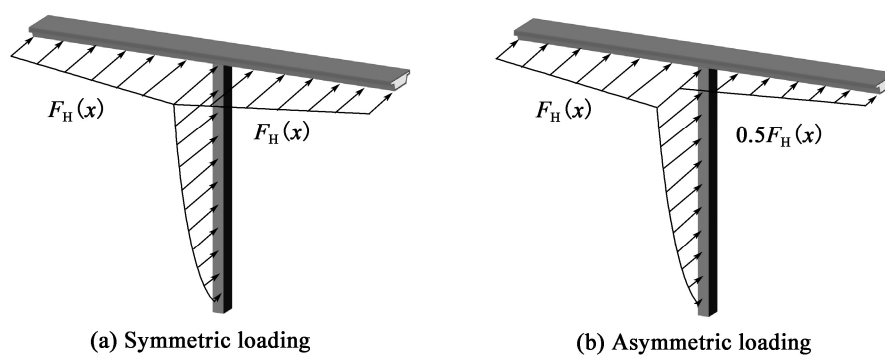


Figure 5.6.2 Application of transverse wind loads on main girder erected by balanced cantilever method

6 Dynamic Characteristics

6.1 General

6.1.1 Natural frequencies and corresponding mode shapes of bridges should be analyzed using the finite element method.

6.2 Finite Element Modeling Principles for Dynamic Characteristics Analysis

6.2.1 Finite element modeling for bridge structures shall match the structural stiffness characteristics, be appropriate for the constraint conditions, and be consistent with the distribution of mass and mass moment of inertia.

6.2.2 Finite element analysis for stay cables shall consider the sag effect. When the cable length exceeds 400 m, the stay cables shall be simulated using multiple elements. When a single element is used for simulation, the modulus of elasticity of the stay cable shall be modified and calculated using Eq. (6.2.2):

$$E_r = \frac{E_0}{1 + E_0 \frac{(\rho_c g l \cos \alpha_c)^2}{12 \sigma^3}} \quad (6.2.2)$$

where,

E_r ——modified modulus of elasticity of cable considering the sag effect (MPa);

E_0 ——modulus of elasticity of the cable material (MPa);

ρ_c ——density of cable (kg/m^3);

l ——length of cable (m);

α_c ——inclination angle of cable ($^\circ$);

σ ——mean stress of cable (MPa);

g ——gravitational acceleration, taken as 9.81 m/s^2 .

6.2.3 When the main girder of a bridge is modeled by beam elements, an appropriate model shall be selected based on the structural configuration of the main girder for equivalent simulation of its stiffness and mass distribution.

Commentary

For main girders with closed-box sections shown in Figures 6-1 (a) and 6-1 (b), a single-spine beam model can be adopted. For separated exterior girders with open-sections shown in Figures 6-1(c) and 6-1 (d), especially for cable-stayed bridges with parallel cable planes or suspension bridges, a triple-beam model can be used for the calculation of dynamic characteristics to better simulate the warping torsion effects of the main girder. Figure 6-2 schematically shows the single-spine beam and triple-beam models. When using the triple-beam model, the simulation of stiffness and mass for the interior girder and exterior girders is performed according to the following principles:

- 1 The cross-sectional area, A , and the moment of inertia, I_y , for lateral bending of the main girder are all concentrated in the interior girder, that is:

$$A_2 = I_{y2} = 0 \quad (6-1)$$

$$A_1 = A \quad (6-2)$$

$$I_{y1} = I_y \quad (6-3)$$

where,

A_1, A_2 ——cross-sectional area of interior girder and exterior girder, respectively (m^2);

I_{y1}, I_{y2} ——moment of inertia, I_y , for lateral bending of the interior girder and exterior girder, respectively (m^4).

- 2 The allocation of the moment of inertia, I_z , for vertical bending of the main girder, shall be based on the moment of inertia, I_{z2} , for vertical bending of the exterior girders to provide the necessary warping torsional constant, I .

$$I_{z1} + 2I_{z2} = I_z \quad (6-4)$$

$$2I_{z2} \cdot b_c^2 = I_\omega \quad (6-5)$$

where,

b_c ——half of the center-to-center distance between exterior girders (m);

I_{z1}, I_{z2} ——moment of inertia for vertical bending of interior girder and exterior girder, respectively (m^4);

I_w ——warping torsional constant of the main girder (m^6).

- 3 St. Venant torsional constant for open sections is relatively small and can be freely allocated to three girders, but the symmetry on both sides needs to be maintained.
- 4 The total mass m and the mass moment of inertia, I , can be concentrated on the interior girder, or they can be allocated to the three girders, with the required mass moment of inertia provided by the mass of the exterior girders, and calculated according to Eqs. (6-6) and (6-7):

$$m_1 + 2m_2 = m \quad (6-6)$$

$$2m_2 b_c^2 = I_m \quad (6-7)$$

where,

m_1, m_2 ——mass per unit length of interior girder and exterior girder, respectively (kg/m);

m ——mass per unit length of main girder (kg/m);

I_m ——mass moment of inertia per unit length of main girder ($\text{kg} \cdot \text{m}^2/\text{m}$).

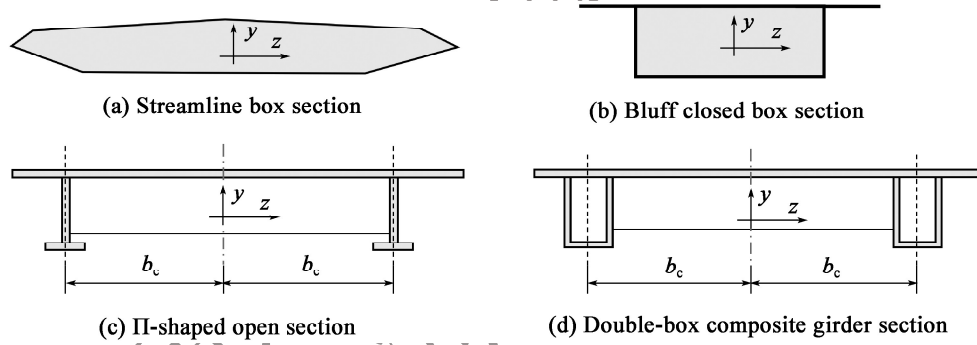


Figure 6-1 Typical cross-sections of main girder

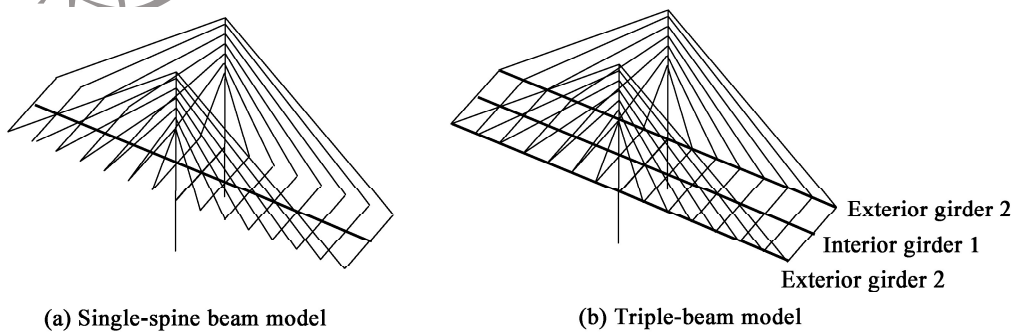


Figure 6-2 Schematics for single-spine beam and triple-beam finite element models

6.2.4 Dynamic characteristics analysis of long-span suspension bridges, cable-stayed bridges and arch bridges shall consider the influence of structural geometric nonlinearity.

Commentary

For long-span suspension bridges, cable-stayed bridges and arch bridges, the initial internal forces and changes in shape generated by the self-weight and dead loads of the structures will affect their stiffness. Especially, the geometric nonlinearity of suspension bridges has a significant impact on gravitational stiffness. Therefore, in the dynamic characteristics analysis, various nonlinear effects of the structures need to be considered first, and the reasonable initial configuration and initial internal forces should be determined. When analyzing the dynamic characteristics, the overall effect of the stiffness caused by initial stress, the stiffness caused by geometric deformation and structural stiffness needs to be considered. Based on this, the dynamic characteristics of the structures can be obtained through modal analysis.

6.3 Estimation of Fundamental Frequencies of Cable-stayed Bridges

6.3.1 The fundamental frequency of symmetric vertical bending, f_b , for a double-tower cable-stayed bridge may be estimated using Eq. (6.3.1-1) or Eq. (6.3.1-2):

For cable-stayed bridges without auxiliary piers:

$$f_b = \frac{110}{L} \quad (6.3.1-1)$$

For cable-stayed bridges with auxiliary piers:

$$f_b = \frac{150}{L} \quad (6.3.1-2)$$

where:

L ——main span length of cable-stayed bridge (m);

f_b ——fundamental frequency of symmetric vertical bending of cable-stayed bridge(Hz).

Commentary

There are many types of cable-stayed bridges, making it difficult to derive a precise and convenient formula for calculating the fundamental frequency. After statistically analyzing the fundamental frequencies of existing cable-stayed bridges, empirical formulas for the first vertical bending mode and the first symmetric torsional mode of a cable-stayed bridge with two towers are provided in the *Specifications*.

6.3.2 The fundamental frequency of symmetric torsion, f_t , for a double-tower cable-stayed bridge may be estimated using Eq. (6.3.2):

$$f_t = \frac{C}{\sqrt{L}} \quad (6.3.2)$$

where,

C ——empirical coefficient for the fundamental frequency of torsion, which may be taken from Table 6.3.2;

f_t ——fundamental frequency of symmetric torsion (Hz).

Table 6.3.2 Empirical coefficients for the fundamental frequency of torsion of cable-stayed bridges

Cross-section of main girder	Parallel cable planes		Inclined cable planes	
	Steel/composite main girder	Concrete main girder	Steel/composite main girder	Concrete main girder
Open section	10	9	12	11
Partially closed section	12	12	14	12
Closed section	17	14	21	17

Note: Open section refers to plate girder section; partially closed section refers to separated box girder section; and closed section refers to closed box girder section.

6.4 Estimation of Fundamental Frequencies of Suspension Bridges

6.4.1 The fundamental frequency of antisymmetric vertical bending, f_b^a , for a double-tower suspension bridge with a simply-supported central span may be calculated using Eq. (6.4.1):

$$f_b^a = \frac{1}{L} \sqrt{\frac{2H_g + EI_z (2\pi/L)^2}{m}} \quad (6.4.1)$$

where,

f_b^a ——fundamental frequency of antisymmetric vertical bending (Hz);

L ——main span length of suspension bridge (m);

E ——modulus of elasticity of main girder (MPa);

I_z ——moment of inertia for vertical bending of main girder (m^4);

H_g ——horizontal component of tension in an individual suspension cable under dead load (N);

m ——mass per unit length of deck system, suspension cables, and hangers (kg/m). For a suspension bridge with parallel double suspension cables, $m = m_d + 2m_c$;

m_d ——mass per unit length of deck system (kg/m);

m_c ——mass per unit length of suspension cable and hangers at one side (kg/m).

6. 4. 2 The fundamental frequency of antisymmetric vertical bending, f_b^a , for a double-tower suspension bridge with a main span longer than 500 m may be calculated using Eq. (6.4.2):

$$f_b^a = \frac{1.16}{\sqrt{f_{sg}}} \quad (6.4.2)$$

where,

f_b^a ——fundamental frequency of antisymmetric vertical bending (Hz);

f_{sg} ——rise of suspension cable (m).

Commentary

When the span exceeds 500 m, $EI_z \left(\frac{2\pi}{L}\right)^2$ is generally an order of magnitude smaller than $2H_g$. If

$$EI_z \left(\frac{2\pi}{L}\right)^2 = 0.2H_g, \text{ considering } H_g = \frac{mgL^2}{16f_{sg}}, \text{ then } f_b^a = \frac{1}{L} \sqrt{\frac{2 \cdot 2H_g}{m}} = \sqrt{\frac{2 \cdot 2g}{16f_{sg}}} = \frac{1.16}{\sqrt{f_{sg}}}.$$

6. 4. 3 The fundamental frequency of symmetric vertical bending, f_b^s , for a double-tower suspension bridge with a simply-supported central span may be calculated using Eq. (6.4.3):

$$f_b^s = \frac{0.1}{L} \sqrt{\frac{E_c A_c}{m}} \quad (6.4.3)$$

where,

f_b^s ——fundamental frequency of symmetric vertical bending (Hz);

E_c ——modulus of elasticity of suspension cable (N/m²);

A_c ——cross-sectional area of individual suspension cable (m²).

Commentary

Using the Rayleigh method, the formula for calculating the frequency of the first symmetric vertical bending mode of a suspension bridge can be obtained:

$$f_b^s = \frac{1}{2\pi} \sqrt{\frac{EI_z \left(\frac{120}{L^4}\right) + H_g \left(\frac{20}{L^2}\right) + \frac{E_c A_c 10}{L_E 6} \left(\frac{8f_{sg}}{L^2}\right)^2}{m}} \quad (6-8)$$

$$L_E = \int \frac{dx}{\cos^3 \alpha_c} \quad (6-9)$$

where,

α_c ——angle of inclination of suspension cable to the horizontal ($^\circ$).

The first and second terms in Eq. (6-8) are generally 1 ~ 2 orders of magnitude smaller than the last term, and can be neglected in the calculation. Considering $f_{sg}/L \approx 0.1$ and $L_E \approx 2L$, the formula in this clause can be obtained after simplification.

6.4.4 The fundamental frequency of antisymmetric torsion, f_t^a , for a double-tower suspension bridge with a simply-supported central span may be calculated using Eq. (6.4.4):

$$f_t^a = \frac{1}{L} \sqrt{\frac{\frac{H_g B_c^2}{2} + G I_d + E I_\omega \left(\frac{2\pi}{L}\right)^2}{m_d r^2 + m_c \frac{B_c^2}{2}}} \quad (6.4.4)$$

where,

f_t^a ——fundamental frequency of antisymmetric torsion (Hz);

H_g ——horizontal component of tension in an individual suspension cable under dead load (N);

I_ω ——warping torsional constant of main girder (m^6);

G ——shear modulus of main girder (MPa);

I_d ——St. Venant torsional constant of main girder (m^4);

r ——radius of gyration of main girder (m), which may be calculated using $r = \sqrt{I_m/m_d}$;

I_m ——mass moment of inertia per unit length of main girder ($\text{kg} \cdot \text{m}^2/\text{m}$);

B_c ——center-to-center distance between suspension cables (m).

Commentary

An analytical formula for the frequency of the first antisymmetric torsional mode of a suspension bridge is provided in this clause. If the main girder is a closed box girder, the term related to warping torsional stiffness can be ignored.

6.4.5 The fundamental frequency of symmetric torsion, f_t^s , for a double-tower suspension bridge with a simply-supported central span may be calculated using Eq. (6.4.5):

$$f_t^s = \frac{1}{2L} \sqrt{\frac{G I_d + 0.05256 E_c A_c (B_c/2)^2}{m_d r^2 + m_c \frac{B_c^2}{2}}} \quad (6.4.5)$$

where,

f_t^s —fundamental frequency of symmetric torsion (Hz).

6.5 Estimation Formulas for Frequencies of Stay Cables and Hangers

6.5.1 Frequencies, f_n , of flexible hangers may be calculated using Eq. (6.5.1):

$$f_n = \frac{n}{2l} \sqrt{\frac{F}{m}} \quad (6.5.1)$$

where,

f_n —the n th modal frequency of the hanger (Hz);

n —mode number (1, 2, 3, ...);

l —length of the hanger (m);

F —force of the hanger (N);

m —mass per unit length of the hanger (kg/m).

Similar to the vibration equation of a horizontal taut string, based on D'Alembert's principle, the spatial free-vibration equation of hangers (cables) can be derived:

$$F \frac{\partial^2 v(x,t)}{\partial x^2} - m \frac{\partial^2 v(x,t)}{\partial t^2} = 0 \quad (6-10)$$

where,

F —horizontal component of cable force (N);

$v(x,t)$ —vibration response of a horizontal taut string (m);

x —coordinate of horizontal taut string (m);

t —time (s).

Based on the separation of variables and mode shape functions satisfying the boundary conditions, the circular frequency, ω_n , and mode shape, \tilde{v}_n , of a hanger can be derived as shown in Eqs. (6-11) and (6-12).

$$\omega_n = \frac{n\pi}{l} \sqrt{\frac{F}{m}} \quad (6-11)$$

$$\tilde{v}_n = A_n \sin \frac{n\pi x}{l} \quad (6-12)$$

6.5.2 The fundamental frequency of a rigid H-section hanger fixed at both ends may be calculated using Eqs. (6.5.2-1) ~ (6.5.2-3).

Frequency of bending vibration about weak axis:

$$f_1 = \frac{3.56}{l^2} \sqrt{\frac{EI_1}{\rho_s A} + \frac{Pl^2}{4\pi^2 \rho_s A}} \quad (6.5.2-1)$$

Frequency of bending vibration about strong axis:

$$f_2 = \frac{3.56}{l^2} \sqrt{\frac{EI_2}{\rho_s A} + \frac{Pl^2}{4\pi^2 \rho_s A}} \quad (6.5.2-2)$$

Frequency of torsional vibration

$$f_t = \frac{3.56}{l^2} \sqrt{\frac{EI_\omega}{\rho_s I_p} + \frac{(GI_d A + PI_p) l^2}{4\pi^2 \rho_s A I_p}} \quad (6.5.2-3)$$

where,

- f_1 ——frequency of bending vibration about the weak axis of the hanger (Hz);
- f_2 ——frequency of bending vibration about the strong axis of the hanger (Hz);
- f_t ——frequency of torsional vibration of the hanger (Hz);
- E ——modulus of elasticity of the hanger (Pa);
- I_1 ——moment of inertia about the weak axis of section (m^4);
- I_2 ——moment of inertia about the strong axis of section (m^4);
- ρ_s ——density of structure (kg/m^3);
- A ——cross-sectional area (m^2);
- P ——initial tension force of the hanger (N);
- I_ω ——warping torsional constant of the section (m^6);
- I_p ——polar moment of inertia of the section (m^4);
- G ——shear modulus (Pa);
- I_d ——St. Venant torsional constant of section (m^4).

Figure 6.5.2 illustrates the cross-section of the rigid H-section hanger as well as its strong and weak axes.

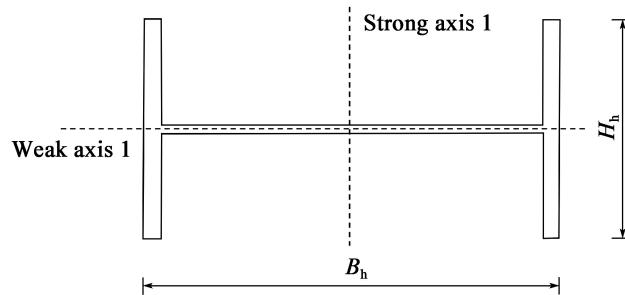


Figure 6.5.2 Schematic for cross-section of rigid H-section hanger and its strong and weak axes

6.5.3 Frequencies , f_n , of out-of-plane and in-plane vibrations of stay cables may be calculated using Eqs. (6.5.3-1) ~ (6.5.3-5) ;

1 Frequency of out-of-plane vibration of stay cables :

$$f_n = \frac{n}{2l} \sqrt{\frac{F}{m}} \quad (6.5.3-1)$$

where ,

f_n ——the n th out-of-plane modal frequency of a stay cable (Hz) ;

F ——cable force (N) ;

m ——mass per unit length of the stay cable (kg/m) ;

l ——effective length of the stay cable (m) ;

n ——mode number (may take 1 , 2 , 3 ,)

2 Frequency of in-plane antisymmetric vibration of stay cables :

$$f_n = \frac{n}{2l} \sqrt{\frac{F}{m}} \quad (6.5.3-2)$$

where ,

f_n ——the n th in-plane modal frequency of stay cable (Hz) , n is 2 , 4 , 6 , ...

3 Frequency of in-plane symmetric vibration of stay cables :

$$f_n = \frac{\eta}{2l\pi} \sqrt{\frac{F}{m}} \quad (6.5.3-3)$$

where ,

f_n ——the n th in-plane modal frequency of stay cable (Hz) , n is 1 , 3 , 5 , 7 , 9 , ... ;

η ——coefficient , calculated using Eq. (6.5.3-4) ;

$$\eta = \begin{cases} -0.0017\lambda^2 + 0.1254\lambda + 3.1444 & n = 1 \\ 0.0053\lambda + 9.4239 & n = 3 \\ n\pi & n \geq 5 \end{cases} \quad (6.5.3-4)$$

λ ——coefficient , calculated using Eq. (6.5.3-5) :

$$\lambda = EA (mgl \cos \alpha_c)^2 / F^3 \quad (6.5.3-5)$$

A ——cross-sectional area of stay cable (m^2) ;

α_c ——angle of inclination of stay cable ($^\circ$) ;

E ——modulus of elasticity of stay cable (Pa) .

Commentary

The equation of motion of the in-plane symmetric vibration of stay cables is different from that of the in-plane antisymmetric vibration and the out-of-plane vibration, and is given by:

$$\frac{\partial}{\partial s} \left\{ (F + h) \frac{\partial}{\partial s} (x + u) \right\} = m \frac{\partial^2 u}{\partial t^2} + c_0 \frac{\partial u}{\partial t} - mg \sin \alpha_c \quad (6-13)$$

$$\frac{\partial}{\partial s} \left\{ (F + h) \left(\frac{dy}{ds} + \frac{\partial v}{\partial s} \right) \right\} = m \frac{\partial^2 v}{\partial t^2} + c_1 \frac{\partial v}{\partial t} - mg \cos \alpha_c \quad (6-14)$$

$$\frac{\partial}{\partial s} \left\{ (F + h) \frac{\partial w}{\partial s} \right\} = m \frac{\partial^2 w}{\partial t^2} + c_2 \frac{\partial w}{\partial t} \quad (6-15)$$

where,

- h ——additional dynamic tension generated by the stretching of cable due to vibration (N);
- c_0, c_1, c_2 ——internal damping coefficients;
- u, v, w ——displacement components of stay cable (m);
- y ——sag in the direction of the cable self-weight;
- s ——arc-length coordinate.

Eq. (6.5.3-4) in this clause is derived through numerical methods by solving and fitting the relevant coefficients. The mode numbers of the stay cable in this clause are defined in Figure 6-3.

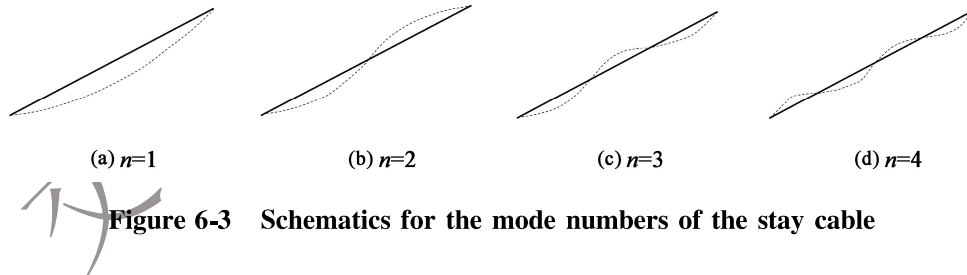


Figure 6-3 Schematics for the mode numbers of the stay cable

6.6 Damping Ratios of Bridges

6.6.1 The damping ratio, ζ_s , for mode shapes dominated by the vibration of the main girder may be taken from Table 6.6.1.

Table 6.6.1 Damping ratio for mode shape dominated by main girder vibration

Type of main girder	Damping ratio	Type of main girder	Damping ratio
Steel box girder	0.003	Steel-concrete composite girder	0.01
Steel truss girder	0.005	Concrete girder	0.02

6.6.2 The damping ratio, ζ_s , for mode shapes dominated by the vibration of the tower may be taken from Table 6.6.2.

Table 6.6.2 Damping ratio for mode shape dominated by tower vibration

Type of tower	Damping ratio	Type of tower	Damping ratio
Steel tower	0.005	teel-concrete composite tower	0.01
Concrete tower	0.02		

6.6.3 The damping ratio, ζ_s , of stay cables and hangers without supplemental damping devices may be taken as 0.001.

7 Wind-Resistant Ultimate Limit State Design

7.1 General

7.1.1 The ultimate limit state design and verification of bridge structures and members under wind actions shall be conducted considering the following aspects:

- 1 The structural strength, static stability, ultimate load-carrying capacity, and other performance under wind action W1 when it is combined with other loads such as vehicular loads;
- 2 The structural strength, static stability, ultimate load-carrying capacity, aerostatic stability, aerodynamic stability, and other performance under wind action W2;
- 3 The possibility of vortex resonance in bridge structures or members within the wind speed ranges corresponding to wind actions W1 and W2.

7.2 Aerostatic Stability

7.2.1 The aerostatic stability shall be checked for cable-stayed bridges with a main span larger than 400 m and suspension bridges with a main span larger than 600 m.

Commentary

Based on the research and analysis results on wind-induced stability of existing highway cable-stayed and suspension bridges, the aerostatic stability of bridges generally does not govern the design. Therefore, for safety considerations, span lengths of 400 m and 600 m are conservatively

used in the *Specifications* as the threshold conditions for initiating the aerostatic stability check for cable-stayed bridges and suspension bridges, respectively.

7.2.2 The critical wind speed for aerostatic lateral buckling of suspension bridges may be calculated using Eqs. (7.2.2-1) ~ (7.2.2-4) :

$$U_{lb} = K_{lb} \cdot f_t \cdot B \quad (7.2.2-1)$$

$$K_{lb} = \sqrt{\frac{\pi^3 \frac{B}{D} \mu \frac{r}{b}}{1.88 C_H \varepsilon \sqrt{4.54 + \frac{C_L' B_c}{C_H D}}}} \quad (7.2.2-2)$$

$$\mu = \frac{m}{\pi \rho b^2} \quad (7.2.2-3)$$

$$\varepsilon = \frac{f_t}{f_b} \quad (7.2.2-4)$$

where,

- U_{lb} ——critical wind speed for aerostatic lateral buckling (m/s) ;
- B ——characteristic width of main girder (m) ;
- b ——half of the characteristic width of the main girder (m), calculated as $B/2$;
- D ——characteristic depth of main girder (m) ;
- B_c ——center-to-center distance between suspension cables (m) ;
- m ——mass per unit length of deck system and suspension cables (kg/m) ;
- I_m ——mass moment of inertia per unit length of deck system and suspension cables ($\text{kg} \cdot \text{m}^2/\text{m}$) ;
- r ——radius of gyration of bridge (m), $r = \sqrt{I_m/m}$;
- μ ——ratio of the mass per unit length of bridge to the air density, calculated as $m/(\pi \rho b^2)$;
- f_t ——fundamental torsional frequency of main girder (Hz) ;
- f_b ——fundamental vertical bending frequency of main girder (Hz) ;
- ε ——ratio between torsional and bending frequencies, $\varepsilon = f_t/f_b$;
- C_H ——lateral force coefficient of main girder section ;
- C_L' ——slope of lift coefficient, C_L , of main girder when the wind attack angle $\alpha = 0^\circ$, which may be obtained through wind tunnel testing or virtual wind tunnel testing.

Commentary

Under static wind load, a suspension bridge may undergo static instability similar to lateral overturning of girders when the vertical flexural stiffness and torsional stiffness of the structure are relatively small, as shown in Figure 7-1.

For single-span suspension bridges, the lateral buckling often manifests in an antisymmetric mode. The calculation formula for the critical uniform horizontal wind load is given by:

$$q_{lb} = \frac{8\pi^3 \sqrt{EI \cdot \overline{GI}_d}}{L^3 \sqrt{K} \sqrt{K+1 + \frac{C'_L B_c}{C_H D}}} \quad (7-1)$$

$$\overline{EI} = EI + \frac{l}{2\pi^2} H_g \quad (7-2)$$

$$\overline{GI}_d = GI_d + EI_\omega \frac{4\pi^2}{L^2} + \frac{B_c^2}{2} H_g \quad (7-3)$$

$$K = \frac{1}{4} \left(\frac{4\pi^2}{3} + 1 \right) = 3.54 \quad (7-4)$$

where,

EI —flexural stiffness of main girder ($N \cdot m^2$);

GI_d —St. Venant torsional stiffness of main girder ($N \cdot m^2$);

EI_ω —warping torsional stiffness of main girder ($N \cdot m^4$);

H_g —horizontal component of tension in an individual cable under dead load (N).

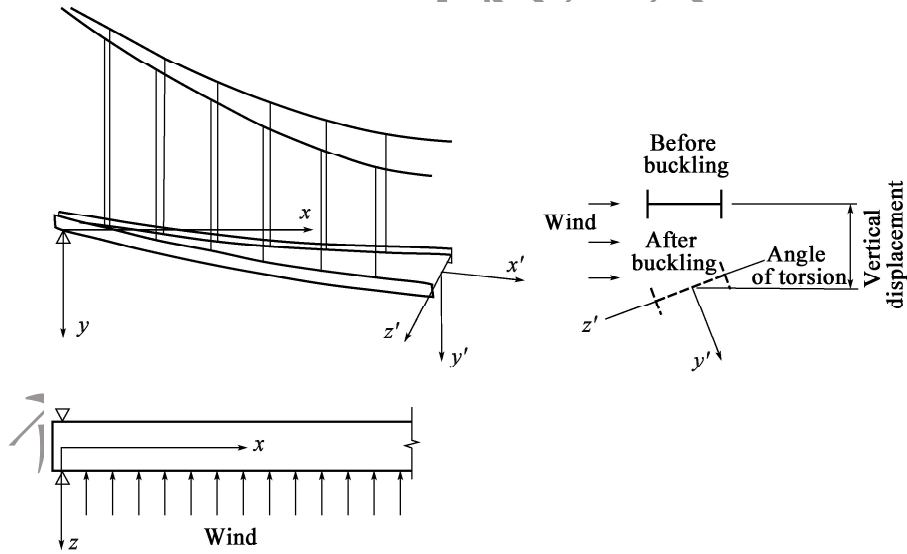


Figure 7-1 Schematic for mechanism of aerostatic lateral buckling

The critical wind speed can be written as:

$$U_{lb} = \sqrt{\frac{2q_{lb}}{\rho C_H D}} \quad (7-5)$$

Introducing the relationship between stiffness and frequency, for the first antisymmetric mode, we have:

$$2\pi f_b = \left(\frac{2\pi}{L} \right)^2 \sqrt{\frac{EI}{m}} \quad (7-6)$$

$$2\pi f_t = \frac{2\pi}{L} \sqrt{\frac{GI_d}{I_m}} \quad (7-7)$$

Accordingly, the equations in this clause are obtained.

7.2.3 The critical wind speed for aerostatic torsional divergence of suspension bridges and cable-stayed bridges may be calculated using Eqs. (7.2.3-1) and (7.2.3-2):

$$U_{td} = K_{td} f_t B \quad (7.2.3-1)$$

$$K_{td} = \sqrt{\frac{\pi^3}{2} \mu \left(\frac{r}{b}\right)^2 \cdot \frac{1}{C'_M}} \quad (7.2.3-2)$$

where,

U_{td} ——critical wind speed for aerostatic torsional divergence (m/s);

C'_M ——slope of torsional moment coefficient, C_M , of main girder, which may be obtained through wind tunnel testing or virtual wind tunnel test.

Commentary

Streamlined aircraft wings have experienced torsional failure incidents when reaching a certain critical flight speed. This is because the static torsional moment of the airflow causes the wing to develop an angle of twist, which in turn increases the effective wind attack angle and further enhances the aerodynamic torsional moment. When the increment of the aerodynamic torsional moment exceeds that of the structural resistance moment, unstable torsional divergence occurs. Similar phenomena may also appear in bridge cross-sections when the structural span is large.

A bridge is idealized as a single-degree-of-freedom structure, as shown in Figure 7-2 (a). The torsional moment coefficient, C_M , varies with the wind attack angle, as illustrated in Figure 7-2 (b).

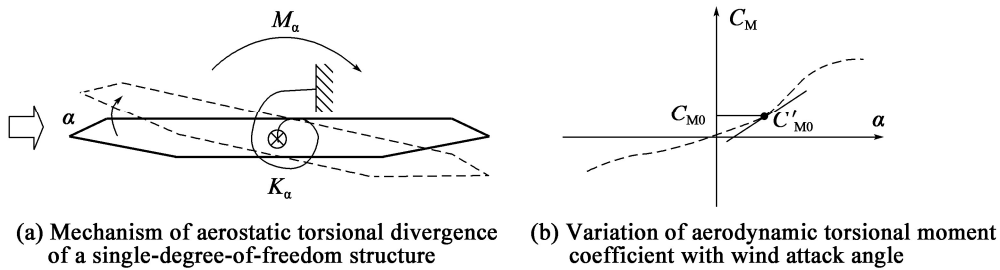


Figure 7-2 Schematics for the mechanism of aerostatic torsional divergence

Under the action of the mean wind at a certain wind attack angle, the aerodynamic moment per unit length of the bridge deck is:

$$M_{\alpha} = \frac{1}{2}\rho U^2 B^2 C_M(\alpha) = \frac{1}{2}\rho U^2 B^2 \left[C_{M0} + \frac{dC_M}{d\alpha} \Big|_{\alpha=0} \right] \quad (7-8)$$

From the condition that the aerodynamic moment equals the structural resistance moment $M_{\alpha} = K_{\alpha}\alpha$, it can be derived that:

$$(K_{\alpha} - \lambda C'_{M0})\alpha = \lambda C_{M0} \quad (7-9)$$

where

$$\lambda = \frac{1}{2}\rho U^2 B^2, \quad C'_{M0} = \frac{dC_{M0}}{d\alpha} \Big|_{\alpha=0}.$$

When $\lambda = K_{\alpha}/C'_{M0}$, will tend to infinity, thus the critical wind speed for torsional divergence is obtained to be:

$$U_{td} = \sqrt{\frac{2K_{\alpha}}{\rho B^2 C'_{M0}}} \quad (7-10)$$

As can be seen from the above equation, the smaller the torsional stiffness, K_{α} , of the structure and the larger the slope, C'_{M0} , of the aerodynamic moment coefficient of the cross-section, the lower the critical wind speed for torsional divergence. By introducing the relationship between structural torsional stiffness and torsional frequency $\omega_t = \sqrt{K_{\alpha}/I_m} = 2\pi f_t$, and taking into account $I_m = mr^2$, the equation in this clause can be obtained.

7.2.4 For cable-stayed bridges with a main span larger than 800 m and suspension bridges with a main span larger than 1200 m, in addition to calculating the critical wind speed for aerostatic stability in accordance with Clauses 7.2.2 and 7.2.3 of the *Specifications*, an aerostatic stability analysis shall also be conducted considering the effects of geometric nonlinearity and aerodynamic nonlinearity. Full-bridge aeroelastic model testing can be carried out for verification whenever necessary.

7.2.5 Aerostatic stability check of bridges shall conform to the requirements in Eqs. (7.2.5-1) and (7.2.5-2):

$$U_{lb} > \gamma_{ai} U_d \quad (7.2.5-1)$$

$$U_{td} > \gamma_{ai} U_d \quad (7.2.5-2)$$

where,

U_{lb} ——critical wind speed for aerostatic lateral buckling (m/s);

U_{td} ——critical wind speed for aerostatic torsional divergence (m/s);

U_d ——reference wind speed for bridge structure or member (m/s);

γ_{ai} ——partial factor for aerostatic stability, which is selected in accordance with Clause 7.2.6 in the *Specifications*.

7.2.6 The determination of the partial factor for aerostatic stability shall conform to the following provisions:

- 1 When calculating the critical wind speed for aerostatic instability using Clause 7.2.2 or 7.2.3 of the *Specifications*, it shall be taken as 2.0.
- 2 When analyzing the critical wind speed for aerostatic instability using the calculation method that only considers the aerodynamic nonlinearity and geometric nonlinearity, it shall be taken as 1.60.
- 3 When acquiring the critical wind speed for aerostatic instability through full-bridge aeroelastic model testing, it shall be taken as 1.40.
- 4 When analyzing the critical wind speed for aerostatic instability using the calculation method considering aerodynamic nonlinearity, geometric nonlinearity and material nonlinearity, it shall be taken as 1.30.

Commentary

When the partial factor for aerostatic stability is taken as 2.0, the corresponding safety factor for wind load is 4.0. Studies have shown that after considering geometric nonlinearity and aerodynamic nonlinearity, the critical wind speed obtained for aerostatic stability is generally 60%-70% of that obtained in accordance with Clause 7.2.3 in the *Specifications*. Taking into account various uncertainties with an uncertainty factor of 1.2, the partial factor for aerostatic stability is approximately in the range of 1.44-1.68, and hence 1.60 is adopted in the *Specifications*. When material nonlinearity is also considered, the safety factor for wind load is usually not smaller than 1.7, corresponding to a partial factor for aerostatic stability of 1.30. However, in actual wind tunnel testing, material nonlinearity cannot be considered, and both geometric nonlinearity and aerodynamic nonlinearity are automatically simulated. Therefore, the partial factor for aerostatic stability is taken as 1.40.

7.2.7 When the aerostatic stability fails to meet the verification requirements, it may be improved by modifying the basic aerodynamic shape of the members, increasing the structural stiffness, or supplementing aerodynamic countermeasures.

7.3 Galloping Stability

7.3.1 Galloping stability shall be checked for structures or members with the following features:

- 1 Steel main girders with a width-to-depth ratio $B/D < 4$;
- 2 Steel towers;
- 3 Steel members with a sectional galloping force coefficient $C_g < 0$;
- 4 Stay cables, hangers and steel main girders affected by ice or snow accretion.

7.3.2 When the galloping force coefficient $C_g < 0$, the critical wind speed for galloping stability may be calculated using Eq. (7.3.2):

$$U_{cg} = -\frac{4m\omega_{b1}\zeta_s}{\rho C_g D} \quad (7.3.2)$$

where,

U_{cg} ——galloping critical wind speed (m/s);

m ——mass per unit length of member (kg/m);

ω_{b1} ——circular frequency of the first bending mode of the structure (rad/s), $\omega_{b1} = 2\pi f_{b1}$;

ζ_s ——damping ratio of structure or member;

D ——characteristic height of structure cross-section (m);

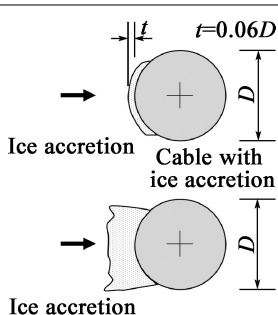
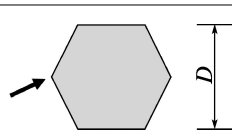
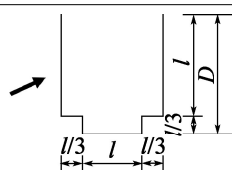
B ——characteristic width of structure cross-section (m);

C_g ——galloping force coefficient of structure cross-section, $C_g = \frac{B}{D}C'_L + C_D$, generally may be obtained through wind tunnel testing or virtual wind tunnel testing. Table 7.3.2 lists galloping force coefficients of typical sections;

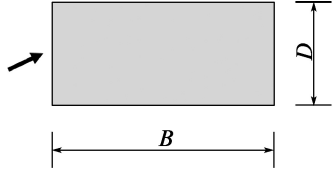
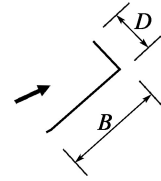
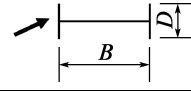
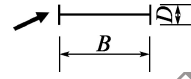
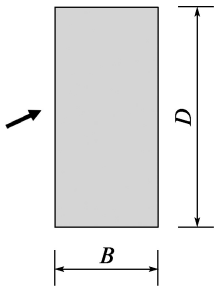
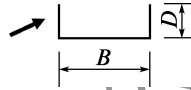
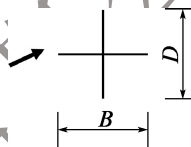
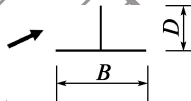
C'_L ——slope of lift coefficient of the structure section;

C_D ——drag coefficient of the structure section.

Table 7.3.2 Galloping force coefficients, C_g , of typical cross-sections

Cross-section	C_g	Cross-section	C_g
	-1.0		-1.0
			-4.0

continued

Cross-section		C_g	Cross-section		C_g
	$\frac{B}{D} = 2.0$	-2.0		$\frac{B}{D} = 2.0$	-0.7
	$\frac{B}{D} = 1.5$	-1.7		$\frac{B}{D} = 2.7$	-5.0
	$\frac{B}{D} = 1.0$	-1.2		$\frac{B}{D} = 5.0$	-7.0
	$\frac{B}{D} = \frac{2}{3}$	-1.0		$\frac{B}{D} = 3.0$	-7.5
	$\frac{B}{D} = \frac{1}{2}$	-0.7		$\frac{B}{D} = \frac{3}{4}$	-3.2
	$\frac{B}{D} = \frac{1}{3}$	-0.4		$\frac{B}{D} = 2.0$	-1.0

Commentary

Gallop- ing is an aerodynamic instability phenomenon with divergent vibrations due to negative damping generated by the motion of bluff bodies. It may occur in steel bridges and steel towers with bluff cross-sections. For the main girder and towers made of concrete, the damping is relatively high, and gallop- ing generally does not occur.

When structures undergo cross-wind vibration, the vibration in the z -direction generates a relative velocity, \dot{z} , which combines with the incoming wind speed, U , to produce an additional wind attack angle. Figure 7-3 illustrates the decomposition of the additional wind attack angle when gallop- ing occurs. Thus, the additional wind attack angle can be expressed as:

$$\Delta\alpha = -\dot{z}/U \quad (7-11)$$

where,

$\Delta\alpha$ ——additional wind attack angle induced by structural vibration relative to the incoming wind speed;

\dot{z} ——velocity of motion in the z -direction (m/s) ;
 U ——incoming wind speed (m/s).

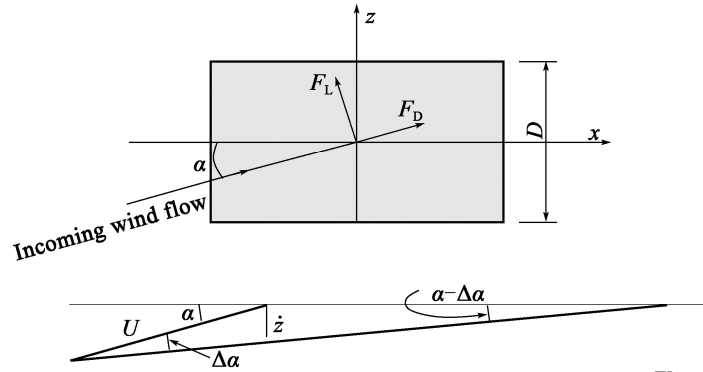


Figure 7-3 Schematic for decomposition of relative wind speed during galloping

Under incoming wind flow at the wind attack angle, α , the drag and lift forces acting on the structure can be respectively expressed as:

$$F_D(\alpha) = \frac{1}{2} \rho U^2 D C_D(\alpha) \quad (7-12)$$

$$F_L(\alpha) = \frac{1}{2} \rho U^2 B C_L(\alpha) \quad (7-13)$$

where,

C_D , C_L ——drag and lift coefficients of the member, respectively.

Then, the aerodynamic resultant force acting on the structure may be represented as:

$$F = F_D \sin \alpha + F_L \cos \alpha = \frac{1}{2} \rho U^2 D (C_D \sin \alpha + \frac{B}{D} C_L \cos \alpha) \quad (7-14)$$

From this, the rate of change of the aerodynamic force with respect to the wind attack angle, $\frac{dF}{d\alpha}$, can be obtained as:

$$\frac{dF}{d\alpha} = \frac{1}{2} \rho U^2 D (C_D \cos \alpha + \frac{dC_D}{d\alpha} \sin \alpha - \frac{B}{D} C_L \sin \alpha + \frac{B}{D} \frac{dC_L}{d\alpha} \cos \alpha) \quad (7-15)$$

When $\alpha = 0$, $\frac{dF}{d\alpha} = \frac{1}{2} \rho U^2 b C_g$, in which $C_g = C_D + \frac{B}{D} \frac{dC_L}{d\alpha}$, then $\Delta F \cong \frac{1}{2} \rho_a U^2 D C_g \Delta \alpha$.

Introducing $\Delta \alpha = -\dot{z}/U$ to obtain:

$$\Delta F \cong \frac{1}{2} \rho U^2 D C_g (-\frac{\dot{z}}{U}) = -\frac{1}{2} \rho U D C_g \dot{z} \quad (7-16)$$

When $C_g < 0$, the change in force is opposite to the direction of velocity, resulting in negative damping. However, for the galloping divergence of the structure to occur, the negative damping

caused by the aerodynamic force needs to be higher than the damping of the structure. Therefore, $C_g < 0$ is a necessary condition for galloping.

7.3.3 The galloping force coefficient for a continuous steel girder bridge with variable cross-sections may be calculated using Eq. (7.3.3-1). When $C_g < 0$, the galloping critical wind speed may be calculated using Eq. (7.3.3-2), and it shall be acquired through aeroelastic model testing whenever necessary.

$$C_g = \frac{\sum_{i=1}^n C_{gi} \varphi_{y,i}^2 \frac{\Delta L_i}{L}}{\sum_{i=1}^n \varphi_{y,i}^2 \frac{\Delta L_i}{L}} \quad (7.3.3-1)$$

$$U_{cg} = -\frac{4\tilde{m}\omega_{bl}\zeta_s}{\rho C_g B} \quad (7.3.3-2)$$

where,

U_{cg} ——galloping critical wind speed (m/s);

$C_{g,i}$ ——galloping force coefficient of the main girder section of the i th segment, $C_{g,i} = \frac{dC_{L,i}}{d\alpha} + C_{D,i}$, in which the corresponding coefficients $C_{L,i}$ and $C_{D,i}$ may be obtained through wind tunnel testing or virtual wind tunnel testing.

$\frac{dC_{L,i}}{d\alpha}$ ——slope of lift coefficient of the i th segment, where the lift coefficients $C_{L,i}$ of the continuous girder with variable cross-sections may be defined based on the girder width B ;

$C_{D,i}$ ——drag coefficient of the i th segment, where the drag coefficients of the continuous girder with variable cross-sections may be defined based on the girder width B ;

B ——characteristic width of the main girder (m);

\tilde{m} ——modal effective mass, $\tilde{m} = \left(\sum_{i=1}^n m_i \varphi_{y,i}^2 \frac{\Delta L_i}{L} \right) / \left(\sum_{i=1}^n \varphi_{y,i}^2 \frac{\Delta L_i}{L} \right)$;

m_i ——mass per unit length of the i th segment of the main girder (kg/m);

n ——number of segments of the main girder;

ΔL_i ——length of the i th segment of the main girder (m);

L ——total length of the main girder (m);

$\varphi_{y,i}$ ——modal displacement of the first vertical bending mode at the midpoint of the i th segment.

Commentary

For the galloping stability assessment of structures with variable cross-sections, it is necessary to consider the uneven distribution of aerodynamic forces along the span length. Based on the

consideration of modal characteristics, the negative damping effect of aerodynamic forces is comprehensively taken into account according to the lowest bending mode shape of the structure, thereby the galloping critical wind speed is obtained. Generally, the width of continuous girder bridges with variable cross-sections remains constant along the bridge axis. For convenience, the drag coefficient, C_D , mentioned in this clause is defined with reference to the bridge width B , namely, $F_D = \frac{1}{2}\rho U^2 C_D B$.

7.3.4 The galloping stability of steel towers and steel girder bridges with a span larger than 100 m shall be checked through aeroelastic model testing under the condition of a simulated structural damping ratio.

7.3.5 The galloping stability check of bridges and members shall meet the requirements of Eq. (7.3.5):

$$U_{cg} > \gamma_{cg} U_d \quad (7.3.5)$$

where,

U_{cg} —galloping critical wind speed of the bridge or member (m/s);

U_d —reference wind speed of the bridge or member (m/s);

γ_{cg} —partial factor for galloping stability, taken as 1.2.

7.3.6 When the galloping stability fails to meet the verification requirements, it may be improved by modifying the basic aerodynamic shape of members, supplementing aerodynamic countermeasures, or implementing damping measures.

7.4 Wake Galloping

7.4.1 For stay cables or hangers with center-to-center spacing in the range of 2 ~ 20 times their diameters, wake galloping should be checked.

Commentary

Wake galloping is a phenomenon that typically occurs between two or more cylinders, where one cylinder is located upstream of the other. If the downstream cylinder is positioned approximately 1/4 of the way outside the wake of the upstream cylinder, it enters a region of galloping instability, where galloping motion begins and its amplitude increases until it reaches a pronounced limit cycle. This motion is a large-amplitude vibration around an elliptical orbit, with the major axis of the ellipse approximately aligned with the direction of the main flow. Figure 7-4 illustrates the

conditions under which wake galloping occurs, and Figure 7-5 shows a typical trajectory of wake galloping motion.

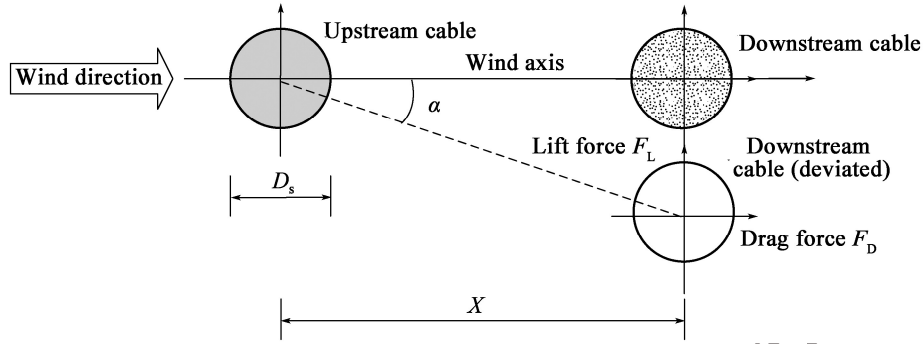


Figure 7-4 Schematic for the condition of the occurrence of wake galloping

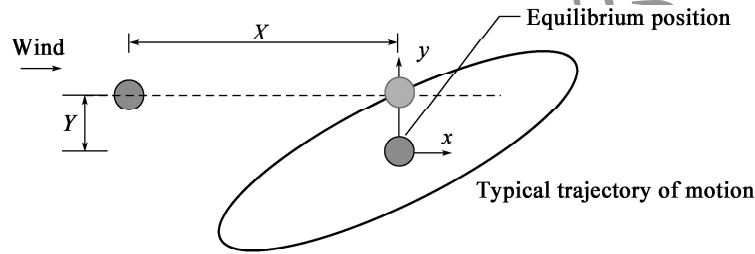


Figure 7-5 Typical trajectory of wake galloping motion

7.4.2 The critical wind speed for wake galloping of stay cables and hangers may be calculated using Eq. (7.4.2), or it may be directly obtained through sectional model vibration testing or aeroelastic model testing under simulated damping conditions.

$$U_{wg} = C_{wg} f_i D_c \sqrt{\frac{m \zeta_s}{\rho D_c^2}} \quad (7.4.2)$$

where,

U_{wg} —critical wind speed for wake galloping (m/s) ;

C_{wg} —constant, which may be taken as 25 when the center-to-center spacing between upstream and downstream cables along the wind direction is 2 ~ 6 times the cable diameter, 40 for 6 ~ 10 times the cable diameter, and 80 for 10 ~ 20 times the cable diameter;

f_i —vibration frequency of the i th mode of the stay cable or hanger;

m —mass per unit length of member (kg/m) ;

ζ_s —damping ratio of structure or member;

ρ —air density (kg/m³) , which is usually taken as 1.25 kg/m³ ;

D_c —diameter of the stay cable and hanger (m) .

Commentary

In recent years, the phenomenon of wake galloping of stay cables or hangers with different amplitudes has been observed during the operation of multiple bridges, and in some cases, stay cables or hangers have even clashed with each other. When the frequencies of stay cables or hangers with close spacings are relatively low, significant wake galloping can occur even at relatively low wind speeds. Increasing the damping ratio or frequency of the stay cables or hangers can raise the critical wind speed for wake galloping, and increasing the structural frequency is more effective.

Taking hangers of a suspension bridge or an arch bridge as an example, the spacing between the hangers is often less than 6 times their diameter. If $(m\zeta_s)/(\rho D_c^2) = 10$, the diameter of the hanger $D_c = 0.1$ m, and the natural frequency of the hanger is 1 Hz, then $U_{wg} = 7.9$ m/s. When the spacing between hangers exceeds 10 times their diameter, $U_{wg} = 25.3$ m/s. It can be seen that the likelihood of wake galloping is higher when the spacing between hangers is relatively close. The longitudinal spacing of stay cables in a cable-stayed bridge is generally larger, but if the outer stay cables are spaced closely, there is still a risk of wake galloping due to the close cable spacing.

7.4.3 The wake galloping stability check shall comply with the requirements of Eq. (7.4.3):

$$U_{wg} > \gamma_{wg} U_d \quad (7.4.3)$$

where,

U_{wg} — critical wind speed for wake galloping of member (m/s);

U_d — reference wind speed of member (m/s);

γ_{wg} — partial factor for wake galloping stability, taken as 1.2.

7.4.4 When the wake galloping stability fails to meet the requirements, proper vibration control measures may be selected in accordance with Clause 9.4.7 in the *Specifications*.

7.5 Flutter Stability

7.5.1 The flutter stability index, I_f , of bridges shall be calculated using Eq. (7.5.1):

$$I_f = \frac{K_s}{\sqrt{\mu}} \cdot \frac{U_d}{f_l B} \quad (7.5.1)$$

where,

- U_d ——reference wind speed of bridge or member (m/s) ;
- K_s ——coefficient related to cross-sectional shape, which is taken as 12 for closed-box sections, 15 for partially closed sections, and 22 for open or truss sections ;
- μ ——ratio of bridge structure density to air density, $\mu = m/(\pi \rho b^2)$;
- b ——half of the section width of the main girder (m) ;
- m ——mass per unit length of bridge (kg/m) , which includes the masses of suspension cables and hangers for suspension bridges, and the masses of stay cables in cable-stayed bridges ;
- f_t ——fundamental torsional frequency of the main girder (Hz) .

Commentary

The flutter stability index is a comprehensive index used to assess the flutter performance of bridges, proposed by Prof. Xiang Haifan from Tongji University. This index represents the relationship between the requirements for flutter stability performance and the actual flutter stability of the bridge, and can comprehensively reflect the relationship between the wind environment at the bridge site, the stiffness and mass of the structure, and the aerodynamic shape performance of the main girder. The detailed derivation is as follows:

$$I_f = \frac{\gamma_f \gamma_t \gamma_\alpha U_d}{U_f} = \frac{\gamma_f \gamma_t \gamma_\alpha U_d}{\eta_s \eta_\alpha \cdot 2.5 \sqrt{\mu \frac{r}{b} f_t B}} = \frac{\gamma_f \gamma_t \gamma_\alpha}{\eta_s \eta_\alpha \cdot 2.5 \sqrt{\mu \frac{r}{b}}} \cdot \frac{U_d}{f_t B} = \frac{K_s}{\sqrt{\mu}} \cdot \frac{U_d}{f_t B} \quad (7-17)$$

Considering that the value ranges of most parameters in this equation are relatively limited, but the value ranges of η_s and μ are relatively large, the values of η_s are classified into three categories: closed box section, partially closed section, as well as open and truss sections. A coefficient, K_s , is introduced to represent the relationship with the cross-sectional shape. Figure 7-6 presents the relationship between I_f and the main span length, using examples of a cable-stayed bridge with inclined cable planes and a closed steel box girder as well as a cable-stayed bridge with an open-section girder.

7.5.2 For a double-tower cable-stayed bridge in its completed state, the flutter stability may be checked based on the fundamental frequency of symmetric torsion. For a double-tower suspension bridge in its completed state, the flutter stability may be checked using the lower value between the fundamental frequencies of symmetric torsion and antisymmetric torsion. When the structure is complex or the torsional mode shape is difficult to identify, the torsional mode shape and its frequency should be determined through modal analysis and then the flutter stability should be checked.

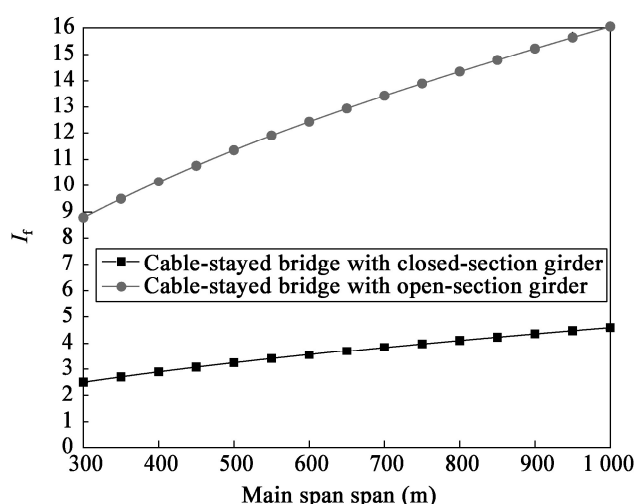


Figure 7-6 Relationship between I_f of cable-stayed bridges with open- and closed-section girders and main span length

7.5.3 The flutter stability check of bridges is conducted according to the following principles:

- 1 When the flutter stability index $I_f < 2$, the flutter critical wind speed of the bridge may be calculated in accordance with Clause 7.5.4 of the *Specifications*.
- 2 When the flutter stability index $2 \leq I_f < 4$, the flutter critical wind speed of the bridge may be calculated in accordance with Clause 7.5.4 of the *Specifications*, or it may be verified through wind tunnel testing or virtual wind tunnel testing on sectional models.
- 3 When the flutter stability index $4 \leq I_f < 10$, the aerodynamic shape of the main girder shall be selected through wind tunnel testing or virtual wind tunnel testing on sectional models, and verified through wind tunnel testing on sectional models or full-bridge aeroelastic model testing.
- 4 When the flutter stability index $I_f \geq 10$, the aerodynamic shape of the main girder shall be selected through wind tunnel testing or virtual wind tunnel testing on sectional models, and verified through wind tunnel testing on sectional models or full-bridge aeroelastic model testing as well as detailed flutter stability analysis.

Commentary

The larger the flutter stability index, the higher the requirement for flutter stability. Table 7-1 gives the flutter stability index for some bridges.

Table 7-1 Flutter stability index for representative bridges in China

Bridge	Bridge type	Main span (m)	U_d (m/s)	K_s	m (ton/m)	f_i (Hz)	I_f
Sutong Yangtze River Bridge	Cable-stayed bridge	1088	49.7	12	32.17	0.53	6.2
Jiujiang Yangtze River Bridge	Cable-stayed bridge	818	34.6	12	33.1	0.610	3.7
Yangpu Bridge in Shanghai	Cable-stayed bridge	602	43.6	22	44	0.510	8.9
Zhoushan Xihoumen Bridge	Suspension bridge	1650	55.1	12	27.5	0.215	18.4
Runyang Yangtze River Suspension Bridge	Suspension bridge	1490	37.4	12	30.63	0.231	11.0
Taizhou Yangtze Bridge	Suspension bridge	1080	39.4	12	29.5	0.266	10.3
Aizhai Bridge	Suspension bridge	1000	34.9	22	27	0.303	15.3
Lupu Bridge in Shanghai	Arch bridge	550	39.4	12	38.9	1.315	1.8
Ningbo Mingzhou Bridge	Arch bridge	450	37.6	12	47.2	1.264	1.6

Note: In the table, m includes the contributions of suspension cables, hangers, and stay cables.

7.5.4 When the flutter stability index of a bridge $I_f < 4$, the flutter critical wind speed may be calculated using Eqs. (7.5.4-1) and (7.5.4-2):

$$U_f = \eta_s \eta_\alpha U_{co} \quad (7.5.4-1)$$

$$U_{co} = 2.5 \sqrt{\mu \frac{r}{b} f_i B} \quad (7.5.4-2)$$

where,

U_f ——flutter critical wind speed of the bridge (m/s) ;

U_{co} ——flutter critical wind speed of an ideal flat plate with the same width as the main girder (m/s) ;

η_s ——shape factor, namely, a dimensionless correction factor for the flutter critical wind speed under a nonzero wind attack angle relative to zero wind attack angle, which may be taken from Table 7.5.4;

η_α ——factor for attack angle effect, namely, a dimensionless shape correction factor for the flutter critical wind speed of a non-flat plate girder cross-section, which may be taken from Table 7.5.4.

Table 7.5.4 Shape factor, η_s , and factor for attack angle effect, η_α



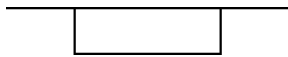
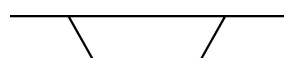
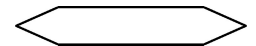
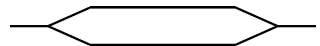
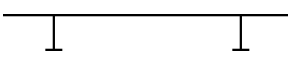
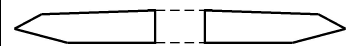
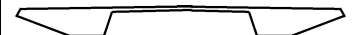
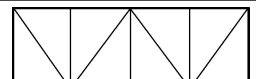
Cross-sectional shape		Shape factor, η_s			Factor for attack angle effect, η_α
		Material of main span			
		Steel	Composite structure	Concrete	
	Ideal flat plate	1	1	1	/
	Rectangular cross-section	0.5	0.55	0.60	0.80

Table 7.5.4 Shape factor, η_s , and factor for attack angle effect, η_α

Cross-sectional shape		Shapefactor, η_s			Factor for attack angle effect, η_a
		Material of main span			
		Steel	Composite structure	Concrete	
	Box girder with overhangs	0.65	0.70	0.75	0.70
	Box girder with inclined webs	0.60	0.70	0.90	0.70
	Streamlined box girder	0.70	0.70	0.80	0.80
	Streamlined box girder with separators	0.80	0.80	0.80	0.80
	Open-section plate girder	0.35	0.40	0.50	0.85
	Separated double-box girder	1.0	/	/	0.80
	P-K girder	0.7	/	/	0.70
	Truss girder	0.35	/	/	0.70

Commentary

For the data in Table 7.5.4, the flutter critical wind speed, U_{co} , of a flat plate was first calculated based on the flat plate flutter theory, and then the flutter critical wind speeds at different wind attack angles were directly measured through sectional model testing. The ratio of the flutter critical wind speed at a wind attack angle of 0 to the flutter critical wind speed, U_{co} , of the flat plate is defined as the cross-section shape factor, η_s , while the ratio of the minimum flutter critical wind speed at the wind attack angle within $+3^\circ$ and -3° to the flutter critical wind speed at a wind attack angle of 0° is defined as the factor for attack angle effect.

1 Van der Put's formula

Based on the exact expression of Theodorsen's aerodynamic force on a flat plate, Klppel et al. calculated the nomogram of dimensionless parameters (conservatively neglecting the structural damping ratio). Van der Put fitted the curves in the nomogram into approximate straight lines and expressed them as:

$$U_{co} = \left[1 + (\varepsilon - 0.5) \sqrt{\left(\frac{r}{b} \right) \cdot 0.72\mu} \right] \omega_b \cdot b \quad (7-18)$$

where,

ε ——ratio of torsional frequency to bending frequency, $\varepsilon = \frac{\omega_t}{\omega_b} = \frac{f_t}{f_b}$;

μ ——ratio of mass per unit length of bridge deck to air density, $\mu = \frac{m}{\pi \rho b^2}$;

b ——half of the characteristic width of the main girder (m), calculated by $B/2$;

r ——radius of gyration of bridge (m), $r = \sqrt{\frac{I_m}{m}}$.

2 Selberg's formula

Based on Theodorsen's formula for the aerodynamic force on a flat plate, Selberg derived an approximate formula from Bleich's flutter solution:

$$U_{co} = 0.44 B \omega_t \sqrt{\left(1 - \frac{\omega_t^2}{\omega_b^2} \right) \frac{\sqrt{\bar{\nu}}}{\bar{\mu}}} \quad (7-19)$$

where,

$\bar{\mu}$ ——ratio of air density to mass per unit length of bridge deck, $\bar{\mu} = \frac{\pi \rho B^4}{4m} = \frac{1}{\mu}$; $\bar{\nu} = 8 \left(\frac{r}{B} \right)^2 = 2 \left(\frac{r}{b} \right)^2$.

The results calculated using Selberg's formula are slightly higher than those using Van der Put's formula because it takes into account the beneficial effect of damping.

3 Xiang Haifan's formula

Professor Xiang Haifan from Tongji University approximately fitted Klppel's nomogram into a straight line passing through the origin and made appropriate adjustments to the slope, thereby eliminating the parameter ε with relatively minor influence and obtaining a simplified calculation formula:

$$U_{co} = 2.5 \sqrt{\mu \frac{r}{b}} B f_t \quad (7-20)$$

Figure 7-7 compares the differences between three different methods for calculating the flutter critical wind speed of a flat plate. For the common torsion-to-bending frequency ratios of bridges ranging from 1.5 to 3, the results of Van der Put's formula and Xiang Haifan's formula are relatively close. However, Selberg's formula is significantly influenced by the torsion-to-bending

frequency ratio, and its results are generally higher. When the torsion-to-bending frequency ratio is less than 1.5, the results from the Selberg's formula are lower than those from the other two methods.

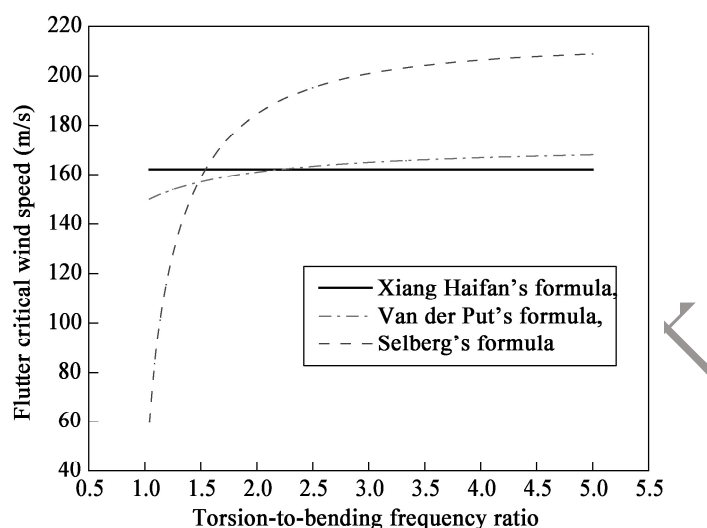


Figure 7-7 Comparison of three calculation methods for flutter critical wind speed of a flat plate

Xiang Haifan's formula is simple in form and convenient for calculation. The parameters in Table 7.5.4 of the *Specifications* are also based on this formula.

7.5.5 Flutter stability shall be verified in the uniform flow fields with wind attack angles of -3° , 0° and $+3^\circ$. For areas such as mountainous regions where the attack angle effect is more pronounced, additional conditions with the wind attack angle of -5° and $+5^\circ$ should be checked. For some special topographic areas, additional conditions with the wind attack angle of -7° and $+7^\circ$ may be checked.

Commentary

Generally, the average wind attack angle for bridges under strong wind conditions ranges from -3° to $+3^\circ$. To account for the effects of unfavorable wind attack angle, flutter stability is typically checked at three conditions with the wind attack angle of -3° , 0° and $+3^\circ$. For bridges located in mountainous regions, it has been found from existing research reports that due to the influence of the local terrain of the mountainous regions, the bridge site may experience a larger wind attack angle. Therefore, flutter stability for mountainous bridges can be checked for additional wind attack angles of -5° and $+5^\circ$. For some bridges in special topographic areas, such as curved bridges or bridges parallel to hillsides, where the wind attack angle effects are more pronounced due to the spatial orientation of structural members or airflow over the hillsides, the conditions with the wind attack angle of -7° and $+7^\circ$ may be considered.

7.5.6 When the flutter stability is verified through sectional model testing, if no obvious flutter divergence phenomenon is observed, the test wind speed corresponding to a standard deviation of torsional displacement of 0.5° under simulated damping ratio may be taken and converted as the flutter critical wind speed.

Commentary

For bridges with bluff cross-sectional shapes, during wind tunnel tests on sectional models, when a significant divergence in torsional displacement occurs at a certain wind speed, as shown in Figure 7-8 (a), it is referred to as a “hard flutter” phenomenon. However, in some tests, no obvious flutter divergence point may be observed, but the vibration amplitude of the model gradually increases with increasing wind speed. Under simulated damping ratio conditions, when the standard deviation of torsional displacement reaches 0.5° , it is also considered as flutter instability and termed “soft flutter”, as shown in Figure 7-8(b).

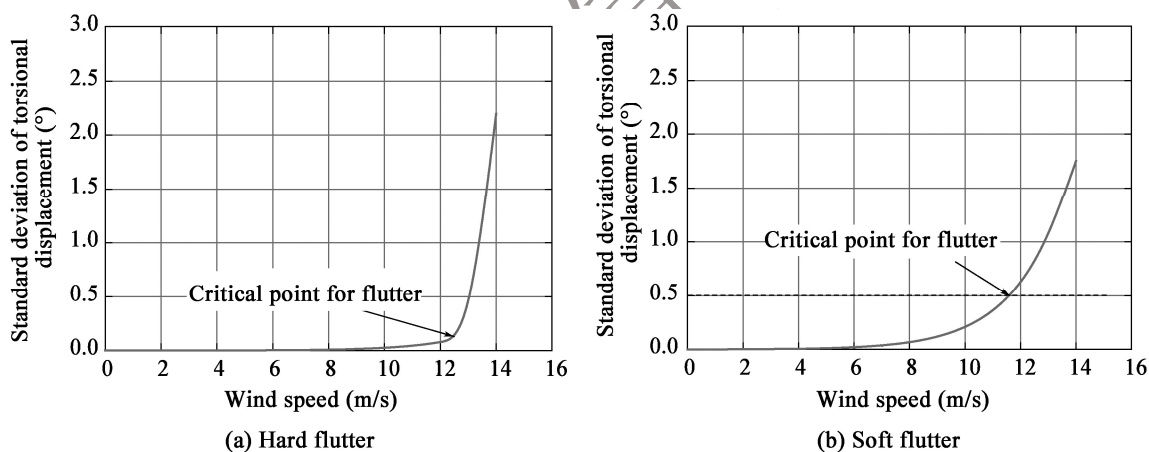


Figure 7-8 Variation of the amplitude of hard flutter and soft flutter with wind speed

7.5.7 Solid-web rigid H-section hangers should not be used. When solid-web rigid H-section hangers are used, the flutter critical wind speed may be approximately calculated using Eq. (7.5.7):

$$U_f = 7.5 f_t B_h \quad (7.5.7)$$

where,

U_f —flutter critical wind speed of H-section hanger (m/s);

B_h —cross-sectional width of H-section hanger (m), which may be determined according to Figure 6.5.2 in the *Specifications*;

f_t —fundamental torsional frequency of H-section hanger (Hz).

Commentary

The solid-web rigid H-section hanger is fabricated by welding steel plates, commonly in H- or box-shaped configurations. It has the advantages of high stiffness, simple structure, and equivalent service life to the main structure. However, its poor aerodynamic performance has led to multiple incidents of damage to hangers due to wind-induced vibration worldwide. Early research suggested that wind-induced vibration in such slender members is mainly due to vortex resonance and galloping. From July to August 2006, severe wind-induced torsional vibrations occurred successively in the H-section hangers of two long-span steel arch bridges constructed in China, with the flange plates at the upper and lower connections of the 30 m to 40 m long hangers almost completely fractured. This type of vibration was confirmed to be flutter. Table 7-2 presents the experimental results of flutter critical wind speed of solid-web H-section hangers with different width-to-height ratios.

Table 7-2 Experimental results of flutter critical wind speed of solid-web H-section hangers

Width-to-height ratio, B_h/H_h	0.75	1.0	1.6	2.4
$U_f/(f_t B_h)$	9.1	8.9	12.2	7.6

7.5.8 Flutter stability of bridges or members shall be checked using Eq. (7.5.8) :

$$U_f > \gamma_f \gamma_t \gamma_\alpha U_d \quad (7.5.8)$$

where,

U_f ——flutter critical wind speed of bridge or member (m/s) ;

U_d ——reference wind speed of bridge or member (m/s) ;

γ_f ——partial factor for flutter stability, which shall be taken as 1.4 when the flutter critical wind speed is calculated according to Clauses 7.5.4 and 7.5.7, 1.15 when the flutter critical wind speed is obtained through wind tunnel testing, and 1.25 when virtual wind tunnel testing is used;

γ_t ——partial factor for spatial influence of wind speed fluctuation, which may be selected from Table 7.5.8, and is taken as 1.0 for H-section hangers;

γ_α ——partial factor for attack angle effect. It shall be taken as 1.0 when the wind attack angle α is $+3^\circ$, 0° and -3° ; it may be taken as 0.7 when the wind attack angle α is $+5^\circ$ and -5° ; it may be taken as 0.5 when the wind attack angle α is $+7^\circ$ and -7° ; it shall be taken as 1.0 for the wind attack angle effect on H-section hangers.

Table 7.5.8 Partial factor, γ_t , for spatial influence of wind speed fluctuation

Mainspan length (m)	Terrain category			
	A	B	C	D
100	1.30	1.36	1.43	1.49
200	1.27	1.33	1.39	1.44
300	1.25	1.30	1.37	1.42
400	1.24	1.29	1.35	1.40
500	1.23	1.28	1.33	1.38
650	1.22	1.27	1.31	1.36
800	1.21	1.26	1.30	1.35
1000	1.20	1.25	1.28	1.33
1200	1.20	1.24	1.27	1.31
1500	1.19	1.22	1.25	1.29
1800	1.18	1.20	1.23	1.27
2000	1.17	1.19	1.22	1.26

Commentary

Since the flutter critical wind speed is generally obtained in uniform flow fields, the influence of turbulence shall be considered for the wind speed in the verification for flutter. A partial factor, γ_t , for the spatial influence of wind speed fluctuation is introduced in this clause, and its calculation principle is as follows:

For the structure in the horizontal direction shown in Figure 7-9, at location x and time t , the wind pressure per unit length is:

$$p(x, t) = \frac{1}{2} \rho C_H D (U + u)^2 \approx \bar{p} + \frac{2\bar{p}}{U} u(x, t) \quad (7-21)$$

where,

ρ ——air density (kg/m^3), generally taken as 1.25 kg/m^3 ;

C_H ——lateral force coefficient of main girder;

D ——characteristic depth of main girder (m);

U ——mean wind speed at the height of Z (m/s);

u ——horizontal fluctuating component of wind (m/s);

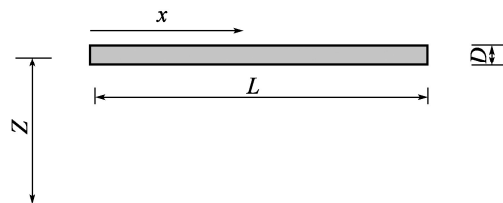


Figure 7-9 Illustration of a structure in the horizontal direction

Thus, the total pressure on the main girder of a bridge is:

$$P_{to}(t) = \int_0^L p(x,t) dx = \bar{P} + \int_0^L \frac{2\bar{p}}{U} u(x,t) dx = \bar{P} + P(t) \quad (7-22)$$

where,

L ——main span length of main girder (m);

\bar{P} —— $\bar{P} = \bar{p}L$.

Fourier transform is performed on the fluctuating pressure part in the above equation, and the following mapping is established:

$$\begin{aligned} P^T(t) &= 0 & t < -T \text{ or } t > T \\ P^T(t) &= P(t) & -T \leq t \leq T \end{aligned}$$

Thus, the Fourier transform of the fluctuating pressure can be written as:

$$F_p(f) = \int_{-\infty}^{+\infty} P^T(t) e^{-i2\pi ft} dt = \int_{-\infty}^{+\infty} \int_0^L \frac{2\bar{p}}{U} u^T(x,t) e^{-i2\pi ft} dt dx = \int_0^L \frac{2\bar{p}}{U} F_u(x,f) dx \quad (7-23)$$

where

$F_u(x,f) = \int_{-\infty}^{+\infty} u^T(x,t) e^{-i2\pi ft} dt$ is the Fourier transform of the fluctuating wind speed $u^T(x,t)$.

The complex conjugate of $F_p(f)$ is:

$$F_p^*(f) = \int_{-T}^T P^T(t) e^{i2\pi ft} dt = \frac{2\bar{p}}{U} \int_{-T}^T F_u^*(x,f) dx \quad (7-24)$$

where $F_u^*(x,f)$ is the complex conjugate of $F_u(x,f)$. The power spectral density function of $P(t)$ is:

$$\begin{aligned} S_p(f) &= \lim_{T \rightarrow \infty} \frac{1}{2T} E[F_p(f) F_p^*(f)] \\ &= \lim_{T \rightarrow \infty} \frac{1}{2T} \left(\frac{2\bar{p}}{U} \right)^2 \int_0^L \int_0^L E[F_u(x_1,f) F_u^*(x_2,f)] dx_1 dx_2 \\ &= \left(\frac{2\bar{p}}{U} \right)^2 \int_0^L \int_0^L \lim_{T \rightarrow \infty} \frac{1}{2T} E[F_u(x_1,f) F_u^*(x_2,f)] dx_1 dx_2 \\ &= \left(\frac{2\bar{p}}{U} \right)^2 \int_0^L \int_0^L S_u(x_1, x_2, f) dx_1 dx_2 \end{aligned} \quad (7-25)$$

where

$S_u(x_1, x_2, f)$ is the spectral density at the locations of x_1 and x_2 of the bridge span. According to the relationship given by Davenport, we have:

$$S_u(x_1, x_2, f) = e^{\frac{-K_1 U}{\nu} |x_1 - x_2|} S_u(f) \quad (7-26)$$

where $S_u(f)$ is the autospectrum of the horizontal fluctuating component of wind speed. Thus, Eq. (7-25) can be written as

$$S_p(f) = \left(\frac{2\bar{p}}{U}\right)^2 S_u(f) \int_0^L \int_0^L e^{\frac{-K_1 U}{\nu} |x_1 - x_2|} dx_1 dx_2 = \left(\frac{2\bar{p}}{U}\right)^2 S_u(f) |\chi_u(f)|^2 \quad (7-27)$$

where $|\chi_u(f)|^2$ represents the spatial effect of fluctuating wind speed along the bridge axis, and has the significance of an aerodynamic admittance;

$$|\chi_u(f)|^2 = \frac{1}{L^2} \int_0^L \int_0^L e^{\frac{-K_1 U}{\nu} |x_1 - x_2|} dx_1 dx_2 = \frac{2}{\gamma^2} (\gamma - 1 + e^{-\gamma}) \quad (7-28)$$

where $\gamma = \frac{K_1 L n}{U}$. K_1 is the correlation coefficient of fluctuating wind. Thus, the root-mean-square deviation of fluctuating wind pressure is:

$$\sigma_p = \left[\int_0^\infty S_p(f) df \right]^{1/2} \quad (7-29)$$

Based on Davenport's theory, the expectation of the maximum wind pressure is:

$$E[P_{tmax}] = \bar{p} + g\sigma_p \quad (7-30)$$

$$g = \frac{0.5772}{\sqrt{2 \ln(n_0 T)}} + \frac{0.5772}{\sqrt{2 \ln(n_0 T)}} \quad (7-31)$$

$$n_0 = \left[\int_0^\infty f^2 S_p(f) df \right]^{1/2} / \sigma_p \quad (7-32)$$

Hence, the partial factor γ_t for spatial influence of wind speed fluctuation is obtained:

$$\gamma_t = \sqrt{\frac{E[P_{tmax}]}{\bar{p}}} = \sqrt{1 - g \frac{\sigma_p}{\bar{p}}} \quad (7-33)$$

The calculation of the partial factor, γ_t , for spatial influence of wind speed fluctuation indicates that for similar terrain categories, γ_t varies little with the basic wind speed and is relatively insensitive to changes in deck elevation, although some variation exists. It also shows little change with variations in the horizontal correlation coefficient but is significantly affected by changes in the terrain category. For long-span bridges, with a typical deck elevation within 30 ~ 70 m and reference wind speeds generally between 20 ~ 50 m/s, it is recommended to use the calculation results based on a reference wind speed of 40 m/s, a deck elevation of 40 m, and a horizontal correlation coefficient of 7. By analyzing these results, the partial factor, γ_t , for the spatial

influence of wind speed fluctuation mentioned in this clause can be obtained. Additionally, since using the Kaimal horizontal wind spectrum for terrain categories C and D would overestimate the structural response by approximately 5%, the results presented in the table have been correspondingly reduced.

7.5.9 When the verification for flutter stability of structures or members fails to meet the requirements, it may be improved by modifying the basic aerodynamic shape of the members, supplementing aerodynamic countermeasures, or changing the structural system.

7.6 Vortex Resonance

7.6.1 Within the wind speed ranges corresponding to wind actions W1 and W2, vortex resonance in structures and members shall be prevented and shall be checked in accordance with Clauses 8.2.1 ~ 8.2.5 of the *Specifications*.

7.7 Wind-induced Stability Verification during Construction

7.7.1 For cable-stayed bridges, the aerostatic stability, galloping stability, and flutter stability should be checked for critical construction stages such as the maximum double-cantilever and maximum single-cantilever stages.

7.7.2 Catwalks for the construction of suspension cables in suspension bridges should be checked for aerostatic stability, galloping stability, and flutter stability.

7.7.3 When the main girder of a suspension bridge is erected through segmental assembly, the aerostatic stability, galloping stability, and flutter stability throughout the entire erection process of the main girder shall be checked.

Commentary

During the erection of the main girder of a suspension bridge, there is a trough in flutter stability. The impact of this factor on the construction schedule shall be considered in the construction organization design, mainly taking into account changes in structural stiffness and wind-resistant performance during the construction process, and reasonably arranging the schedule based on the seasonal changes of strong winds at the bridge site. Figure 7-10 shows the variation curve of the

flutter critical wind speed of the Runyang Yangtze River Suspension Bridge with the assembly rate of the main girder, where the assembly rate of the main girder refers to the ratio of the length of the main girder that has been assembled in the main span to the total length of the main girder in the main span.

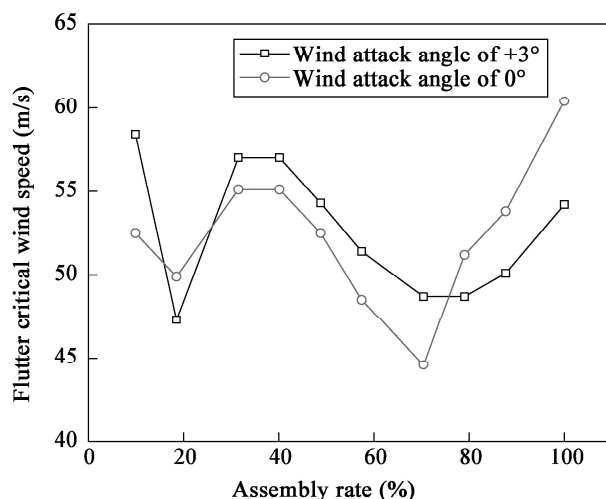


Figure 7-10 Variation of flutter critical wind speed during the construction of Runyang Yangtze River Suspension Bridge with the assembly process

7.7.4 Galloping stability check for steel towers and steel continuous girders during construction shall meet the requirement of Eq. (7.7.4):

$$U_{cg} > \gamma_{cg} U_{sd} \quad (7.7.4)$$

where,

U_{cg} — galloping critical wind speed during the construction of the bridge and member (m/s);

U_{sd} — design wind speed at reference height during the construction of the bridge or member (m/s);

γ_{cg} — partial factor for galloping stability, taken as 1.2.

7.7.5 Flutter stability of structures or members during construction shall be checked in accordance with Eq. (7.7.5):

$$U_f > \gamma_f \gamma_i \gamma_\alpha U_{sd} \quad (7.7.5)$$

where,

U_f — flutter critical wind speed during the construction of the bridge or member (m/s);

γ_f — partial factor for flutter stability, determined in accordance with Clause 7.5.8 of the *Specifications*;

γ_i — partial factor for spatial influence of wind speed fluctuation, determined in accordance with Clause 7.5.8 of the *Specifications*;

γ_α — partial factor for attack angle effect, determined in accordance with Clause 7.5.8 of the *Specifications*.

8 Wind-Resistant Serviceability Limit State Design

8.1 General

8.1.1 Serviceability limit state design and verification of bridge structures and members under wind actions shall be conducted considering the following aspects:

- 1 The structural stiffness and durability, as well as safety and ride comfort of moving vehicles or pedestrians under wind action W1 when it is combined with other loads such as vehicular loads;
- 2 The fatigue resistance of fatigue-prone members under wind action W2 or below.

8.2 Vortex Resonance

8.2.1 For concrete bridge structures or members and steel bridges with a fundamental frequency higher than 5 Hz, vortex resonance may not be checked.

Commentary

Due to the relatively large damping in concrete bridge structures or members, the aerodynamic negative damping is insufficient to overcome the structural damping. Thus vortex resonance generally does not occur, and the check for vortex resonance is not required. When the fundamental frequency of structures is larger than 5 Hz, the Strouhal number, S_r , for relatively bluff cross-sections is generally about 0.2. Because $S_r = fD/U$, the onset wind speed for vortex resonance is $U = fD/S_r = 5D/S_r$. Assuming that the depth of the main girder is 2 m, the onset wind speed for

vortex resonance is $U = 10/S_v = 10/0.2 = 50 \text{ m/s}$.

8.2.2 Vortex resonance shall be checked for bridge structures or members with the following characteristics:

- 1 Steel members with a frequency lower than 5 Hz;
- 2 Steel bridges with a main span larger than 100 m;
- 3 Steel-concrete composite bridges with a main span larger than 100 m;
- 4 Steel towers or steel-concrete hybrid towers.

8.2.3 Vortex resonance shall be checked according to the following principles:

- 1 For steel girder bridges with a main span $L < 100 \text{ m}$, it may be checked in accordance with Clauses 8.2.6 ~ 8.2.8.
- 2 For steel girder bridges with a main span $L \leq 100 \text{ m}$, full-bridge aeroelastic model testing shall be conducted to check the vortex resonance.
- 3 For cable-stayed bridges or suspension bridges with a main span $100 \leq L < 400 \text{ m}$, wind tunnel testing or virtual wind tunnel testing on sectional models should be conducted to check the vortex resonance.
- 4 For cable-stayed bridges with a main span $400 \leq L < 800 \text{ m}$ or suspension bridges with a main span $400 \leq L < 1200 \text{ m}$, wind tunnel testing on sectional models shall be conducted to check the vortex resonance.
- 5 For cable-stayed bridges with a main span $L \geq 800 \text{ m}$ or suspension bridges with a main span $L \geq 1200 \text{ m}$, wind tunnel testing on sectional models shall be conducted to check the vortex resonance, and wind tunnel testing on sectional models with a scale no less than 1:30 may be conducted for further verification whenever necessary.

8.2.4 The vortex resonance should be verified in a uniform flow field, a flow field with 0.25 times the design turbulence intensity, and a flow field with the design turbulence intensity at the bridge site. The onset wind speed, lock-in region, and amplitude of vortex resonance should be measured. The flow field with 0.25 times the design turbulence intensity should be used as the basis for the final evaluation of vortex resonance.

8.2.5 Wind tunnel test models for vortex resonance shall accurately simulate the aerodynamic shapes of structural members, appurtenances, and facilities.

Commentary

The appurtenances and facilities of a bridge, such as construction cranes, ladders, maintenance vehicle tracks, railings, wind barriers, sound barriers, and curbs, all have an impact on vortex resonance due to their shapes and locations.

8.2.6 The onset wind speeds for vertical and torsional vortex resonances of solid-web bridges with spans less than 200 m may be calculated using Eqs. (8.2.6-1) and (8.2.6-2), respectively.

$$U_{vh} = 2.0 f_b B \quad (8.2.6-1)$$

$$U_{vt} = 1.33 f_t B \quad (8.2.6-2)$$

where, U_{vh} ——onset wind speed for vertical vortex resonance (m/s);

U_{vt} ——onset wind speed for torsional vortex resonance (m/s);

B ——characteristic width of main girder (m), as shown in Figure 8.2.7;

f_b ——frequency of vertical bending vibration (Hz);

f_t ——frequency of torsional vibration (Hz).

8.2.7 The amplitude of vertical vortex resonance of solid-web bridges with spans less than 200 m may be estimated using Eqs. (8.2.7-1) ~ (8.2.7-4):

$$h_v = \frac{E_h E_{th} B}{2\pi m_s \zeta_s} \quad (8.2.7-1)$$

$$m_r = \frac{m}{(\rho B^2)} \quad (8.2.7-2)$$

$$E_h = 0.065 \beta_{ds} \left(\frac{B}{D} \right)^{-1} \quad (8.2.7-3)$$

$$E_{th} = 1 - 15 \beta_t \left(\frac{B}{D} \right)^{1/2} I_u^2 \geq 0 \quad (8.2.7-4)$$

where, h_v ——amplitude of vertical vortex resonance (m);

m ——mass per unit length of bridge (kg/m). For bridges with variable cross-sections, it may be taken as the average value at 1/4 of the span; for cable-stayed bridges, half of the masses of stay cables shall be included; for suspension bridges, the masses of suspension cables shall be included;

ζ_s ——damping ratio of the bridge structure;

β_{ds} ——shape correction factor. It may be taken as 2 for bluff cross-sections with the width

less than 1/4 of the effective height or with vertical webs, and 1 for hexagonal cross-sections or bluff cross-sections with a width larger than 1/4 of the effective height or with inclined webs;

D ——characteristic depth of the main girder (m), as shown in 8.2.7;

β_t ——coefficient, which is 0 for hexagonal cross-sections and 1 for other cross-sections;

I_u ——design longitudinal turbulence intensity, which may be selected from Table 4.3.1 of the *Specifications*, or may be determined using $I_u = 1/\ln(Z/z_0)$;

Z ——reference height of bridge deck (m);

z_0 ——terrain roughness height of the bridge site (m), which may be selected from Table 4.2.1.

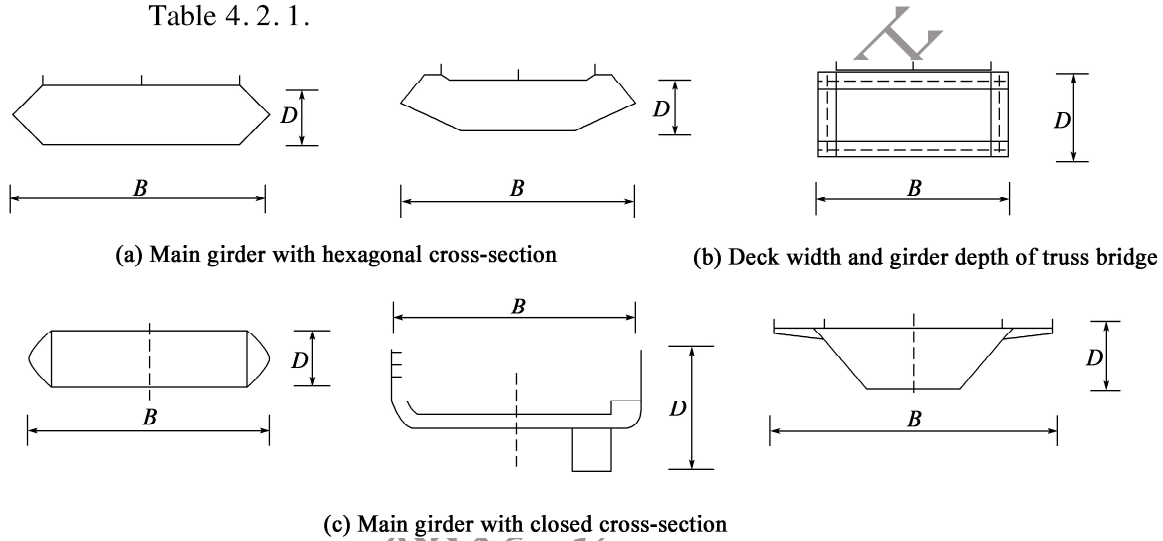


Figure 8.2.7 Width and depth of bridge deck

8.2.8 The amplitude of torsional vortex resonance of solid-web bridges with spans less than 200 m may be estimated using Eqs. (8.2.8-1) ~ (8.2.8-4):

$$\theta_t = \frac{E_\theta E_{t\theta}}{2\pi I_{pr} \zeta_s} \quad (8.2.8-1)$$

$$I_{pr} = \frac{I_m}{\rho B^4} \quad (8.2.8-2)$$

$$E_\theta = 17.16 \beta_{ds} \left(\frac{B}{D} \right)^{-3} \quad (8.2.8-3)$$

$$E_{t\theta} = 1 - 20 \beta_t \left(\frac{B}{D} \right)^{1/2} I_u^2 \geq 0 \quad (8.2.8-4)$$

where, θ_t ——amplitude of torsional vortex resonance ($^\circ$);

I_m ——mass moment of inertia per unit length of bridge ($\text{kg} \cdot \text{m}^2/\text{m}$). For bridges with variable cross-sections, it shall be taken as the average value at 1/4 of the span; for cable-stayed bridges, half of the mass of stay cables shall be included; for suspension bridges, the total mass of suspension cables shall be included;

ζ_s ——structural damping ratio.

8.2.9 For bridges with spans less than 200 m, the amplitude of vortex resonance within the wind speed range corresponding to wind action W1 or below may be verified by Eqs. (8.2.9-1) and (8.2.9-2) :

1 The amplitude of vertical vortex resonance shall meet the requirement of Eq. (8.2.9-1) :

$$h_v < \gamma_v \frac{0.04}{f_v} \quad (8.2.9-1)$$

where,

h_v ——amplitude of vertical vortex resonance (m) ;

f_v ——frequency of vertical vibration (Hz) ;

γ_v ——partial factor for vortex resonance. It shall be taken as 1.0 when h_v is obtained through wind tunnel testing, and 0.8 when h_v is calculated in accordance with Clause 8.2.7 of the *Specifications* or obtained through virtual wind tunnel testing.

2 The amplitude of torsional vortex resonance shall be checked to meet the following requirement :

$$\theta_t < \gamma_v \frac{4.56}{B f_t} \quad (8.2.9-2)$$

where,

θ_t ——amplitude of torsional vortex resonance (°) ;

f_t ——frequency of torsional vibration (Hz) ;

B ——characteristic width of main girder (m) ;

γ_v ——partial factor for vortex resonance. It is taken as 1.0 when θ_t is obtained through wind tunnel testing, and 0.8 when θ_t is calculated in accordance with Clause 8.2.8 of the *Specifications* or obtained through virtual wind tunnel testing.

Commentary

The allowable displacement amplitude specified in the *Specifications* is determined based on the allowable acceleration of 1 m/s^2 for a bridge with a span less than 200 m. Assuming that the displacement of the structure varies sinusoidally with time when vortex resonance occurs, the vibrational acceleration is $a = 4\pi^2 f^2 A$, with an allowable value of 1 m/s^2 . Given the approximation $4\pi^2 \approx 40$, the allowable amplitude can be obtained to be $A = 1/(40f^2)$. Considering that the approximate formula for the vertical fundamental frequency of a bridge with a span less than 200 m is $f = 100/L$, remaining one f , and taking $L = 160$, then the allowable amplitude is $A = 0.04/f$. Therefore, Eq. (8.2.9-1) is only applicable to bridges with spans less than 200 m.

If the acceleration amplitude is used as the basis for evaluating vortex resonance, then $A = 1/(40f^2) = 0.025/f^2$. Considering that the vertical bending frequencies of some large-span bridges are relatively low, and assuming a vertical bending frequency of 0.1 Hz, the allowable amplitude can reach $A = 2.5$ m, which is relatively large. It can be seen that using only the acceleration amplitude as the criterion for evaluating vortex resonance has limitations.

Professor Chen Zhengqing from Hunan University has proposed that the allowable amplitude of vortex resonance should be determined by comprehensively considering factors such as pedestrian and driver comfort, structural fatigue, and the sight distance for vehicles on the bridge. To avoid the impact of vertical vortex resonance of the bridge on the line of sight of drivers, for high-order modal vortex resonance with three or more half-waves, the allowable amplitude shall be limited to at least 0.35 m. In this case, the sight distance for vehicles may become the controlling factor in determining the amplitude limit of vortex resonance.

8.2.10 When the vortex resonance in structures or members fails to meet the check requirements, it may be improved by modifying the basic aerodynamic shape and supplementing aerodynamic or damping measures.

8.3 Buffeting

8.3.1 The buffeting displacement and acceleration responses of bridges may be obtained through time-domain analysis, frequency-domain analysis, wind tunnel testing, or virtual wind tunnel testing.

8.3.2 Buffeting response testing of bridges shall be conducted using full-bridge aeroelastic models under conditions that simulate turbulent flow fields, structural dynamic characteristics, geometries of structures and members, and structural damping ratios.

8.3.3 When the buffeting effects on structures produced under wind action W1 are determined to be significant, studies on the effects of wind-vehicle-bridge coupled vibration should be conducted.

8.4 Stay Cables and Hangers

8.4.1 Potential wind-induced vibrations, such as parametric vibration, linear internal resonance, vortex resonance, and wind-rain-induced vibration, shall be checked for stay cables and hangers. Whenever necessary, corresponding control measures shall be taken.

8.4.2 The amplitude of vortex resonance of stay cables may be approximately calculated using Eq. (8.4.2) :

$$y_{\max} = \frac{0.008\sigma_{c_t} D_c}{S_t^2 S_c} \quad (8.4.2)$$

where ,

y_{\max} —amplitude of vortex resonance (m) ;

S_t —Strouhal number, $S_t = fD_c/U$, which is generally taken as 0.2 for cylindrical members ;

S_c —Scruton number, $S_c = m\zeta_s/(\rho D_c^2)$;

D_c —diameter of stay cable (m) ;

σ_{c_t} —standard deviation of lift coefficient, which is generally taken as 0.45 for cylindrical members ;

ζ_s —damping ratio of stay cable ;

ρ —air density (kg/m^3) , which is generally taken as 1.25 kg/m^3 .

8.4.3 When the excitation frequency at the end of a stay cable is close to or coincides with the natural frequency of the stay cable , the linear internal resonance response of the stay cable shall be checked.

Commentary

Assuming the relative motion of one end of a stay cable perpendicular to the chord length direction ; $y_B(t) = y_B \sin \omega t$, the transverse vibration of the stay cable due to the change in the cable tension under the external excitation is shown in Figure 8-1.

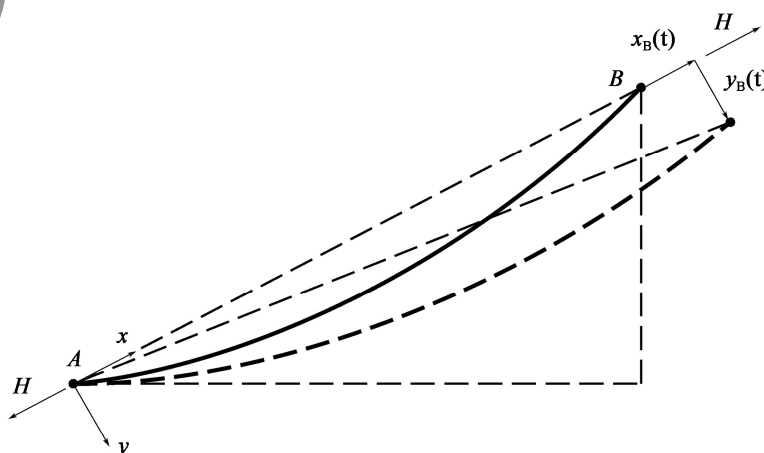


Figure 8-1 Linear internal resonance caused by the displacement at the end of stay cable

According to the principle of forced vibration, when the ratio of the excitation frequency to the in-plane vibration frequency of the stay cable is close to 1, the predominant component of its maximum vibration response is the corresponding in-plane vibration. Taking the first in-plane vibration mode as an example, the maximum amplitude is:.

$$y_{1\max} = \frac{y_B}{\pi\zeta_s} \quad (8-1)$$

where,

$y_{1\max}$ ——maximum amplitude of the first in-plane vibration mode (m);

y_B ——amplitude of relative motion of the cable end perpendicular to the chord length direction;

ζ_s ——damping ratio of stay cable.

This formula is derived on the basis of the small-amplitude linear model. When the excitation amplitude at the cable end is relatively large, the sag effect of stay cables becomes pronounced, which leads to significantly overestimated results calculated from the aforementioned formula, thereby losing validity. In such cases, numerical analysis methods can be employed to obtain the maximum amplitude of the linear internal resonance response in stay cables.

8.4.4 When the excitation frequency at the end of a stay cable is twice its natural frequency, the parametric resonance response of the stay cable shall be checked.

Commentary

When the bridge undergoes harmonic vibration at its fundamental bending frequency f_b , the stay cables will exhibit transverse vibration at a frequency of $f_c = f_b/2$, and parametric resonance of the stay cables is likely to occur. When the relative motion of the cable end along the chord length direction satisfies $x_B(t) = x_B \sin(2\omega t)$, and the change in cable tension, frequencies, and excitation displacement satisfy Eqs. (8-2) ~ (8-4), the parametric resonance will occur in the stay cables:

$$\frac{\Delta F_{\max}}{F} > 2 \sqrt{(1 - \beta_1^2)^2 + (2\zeta_s \beta_1)^2} \quad (8-2)$$

$$\beta_1 = \frac{f_b}{2f_c} \approx 1 \quad (8-3)$$

$$x_B \geq 4X_0\beta_1\zeta_s \quad (8-4)$$

where,

ΔF_{\max} ——amplitude of change in cable tension (N);

F ——tension in stay cable (N);

β_1 ——frequency ratio;

f_b ——excitation frequency (Hz);

f_c ——natural vibration frequency of stay cable (Hz);

X_0 ——linear elastic elongation of stay cable under constant load tension (m), which may be calculated by $X_0 = Fl/EA$;

l ——effective length of stay cable (m);

E ——modulus of elasticity of stay cable (Pa);

A ——cross-sectional area of stay cable (m²).

At this point, the maximum amplitude of steady-state response at the first resonant mode of the stay cable can be approximately calculated using Eq. (8-5):

$$A_{1\max} = \frac{4}{\pi} \cdot \sqrt{\frac{X_0 l}{3}} \cdot \beta_1 \cdot \sqrt{1 - \frac{1}{\beta_1^2} \pm \sqrt{\frac{1}{\beta_1^4} \left(\frac{x_B}{2X_0} \right)^2 - \frac{4\zeta_s^2}{\beta_1^2}}} \quad (8-5)$$

where,

$A_{1\max}$ ——maximum amplitude of steady-state response at the first resonant mode of the stay cable (m);

x_B ——excitation amplitude (m), and the direction of excitation is shown in Figure 8-1.

Figure 8-2 shows the relationship between the maximum amplitude of steady-state response at the first resonant mode of a 400 m-long stay cable in a cable-stayed bridge, the damping ratio, and the excitation amplitude, x_B . Since the excitation at the end of the stay cable in a cable-stayed bridge generally has both x_B and y_B components, the applicability of the above formula is limited. To obtain a more accurate maximum amplitude of the parametric resonant steady-state response of the stay cable, numerical analysis methods can be used.

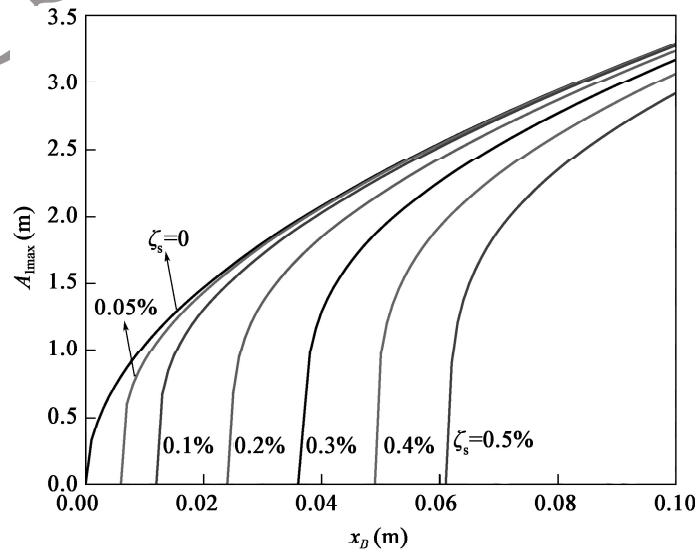


Figure 8-2 Relationship between maximum amplitude of steady-state response at the first resonant mode of stay cable, the damping ratio, and the excitation amplitude

8.4.5 Potential wind-rain-induced vibration of stay cables shall be checked, and aerodynamic countermeasures or additional damping measures may be employed for vibration control whenever necessary.

Commentary

The aerodynamic damping measures for stay cables mainly involve altering the cross-sectional shapes of the cables and preventing the formation of water rivulets, thereby improving their aerodynamic performance. To improve the dynamic behaviors of stay cables under wind or combined wind and rain conditions, the surface treatments for stay cables mainly include: (a) creating grooves or projections along the axial direction on the surface of the PE pipe of the stay cable; (b) applying a dimpled surface treatment to the stay cable; (c) helically adding strip structures or wrapping strips at intervals on the surface of the stay cable along the axial direction.

8.4.6 In the absence of experimental conditions, the criteria for preventing wind-rain-induced vibration in stay cables may be assessed using Eqs. (8.4.6-1) ~ (8.4.6-2).

For stay cables with smooth surfaces

$$S_c > 10 \quad (8.4.6-1)$$

For stay cables with effective surface treatment

$$S_c > 5 \quad (8.4.6-2)$$

where,

S_c —Scruton number, $S_c = m\zeta_s/(\rho D_c^2)$;

m —mass per unit length of stay cable (kg/m);

ζ_s —damping ratio of stay cable;

ρ —air density (kg/m³), which is generally taken as 1.25 kg/m³;

D_c —outer diameter of stay cable (m).

8.4.7 The maximum amplitude of wind-induced vibration of stay cables and hangers should be smaller than 1/1700 of their lengths.

8.4.8 Solid-web H-section hangers should not be used. When using solid-web H-section hangers, the onset wind speed for vortex resonance may be obtained using Eqs. (8.4.8-1) ~ (8.4.8-3). Whenever necessary, the vortex resonance shall be verified through wind tunnel testing

or virtual wind tunnel testing. If the verification for vortex-induced resonance fails to meet the requirements, corresponding vibration control measures shall be taken.

$$U_{vh}/(f_1 B_h) = 1.5 \quad (8.4.8-1)$$

$$U_{vh}/(f_2 B_h) = 5.5 \quad (8.4.8-2)$$

$$U_{vt}/(f_t B_h) = 2.5 \quad (8.4.8-3)$$

where,

U_{vh} ——onset wind speed for vertical vortex resonance (m/s);

U_{vt} ——onset wind speed for torsional vortex resonance (m/s);

f_1 ——fundamental frequency of bending about the weak axis (Hz);

f_2 ——fundamental frequency of bending about the strong axis (Hz);

f_t ——fundamental frequency of torsion (Hz);

B_h ——cross-sectional width of H-section hanger (m), which may be determined according to Figure 6.5.2 in the *Specifications*.

Commentary

Studies have shown that solid-web H-section hangers are prone to large-amplitude vortex resonance at relatively low wind speeds. Table 8-1 gives experimental results on vortex resonance of solid-web H-section hangers with various width-to-depth ratios. When the width-to-depth ratio is 1, the amplitude of vortex resonance about the weak axis may reach 0.347 times the width, B_h . When the width-to-depth ratio is 1.6, the onset wind speed is only 1.5 times $f_1 B_h$. Due to the larger stiffness, the onset wind speed for vortex resonance about the strong axis is higher than that about the weak axis. Significant vortex-induced resonance can also occur in the torsional direction, with a maximum amplitude reaching 5.26°.

Table 8-1 Experimental results on vortex resonance of solid-web H-section hangers

Width-to-height ratio, B_h/H_h	Onset wind speed for vortex resonance			Maximum amplitude of vortex resonance		
	Weak axis $U_{vh}/(f_1 B_h)$	Strong axis $U_{vh}/(f_2 B_h)$	Torsion $U_{vt}/(f_t B_h)$	Weak axis h_v/B_h	Strong axis h_v/B_h	Torsional amplitude, θ_t (°)
0.75	6.2	12.2	6.0	0.150	0.062	3.40
1	7.9	/	9.2	0.347	/	3.10
1.6	1.5	5.7	2.5	0.016	0.012	0.50
2.4	1.7	/	3.3	0.132	/	5.26

8.5 Wind-induced Vibration Serviceability Criteria

8.5.1 Within the wind speed range corresponding to wind action W1 or below, the peak vertical acceleration caused by buffeting or vortex resonance on bridges with pedestrian access should not exceed 1.1 m/s^2 , and the peak transverse acceleration should not exceed 0.5 m/s^2 .

Commentary

Studies have shown that excessive vertical vibration can also cause discomfort to pedestrians. Figure 8-3 presents the simulation test results on pedestrian comfort, which are categorized into five levels: Very good, Good, Average, Poor and Unacceptable. It can be observed that pedestrian comfort is not only related to peak acceleration but also exhibits a certain correlation with vibration frequency. These test results are in good agreement with similar research findings in the world. For ease of use, the average peak acceleration corresponding to the minimum frequency for the Average comfort level is adopted as the limit value in this clause, with a criterion of 1.1 m/s^2 for peak vertical acceleration and 0.5 m/s^2 for peak transverse acceleration.

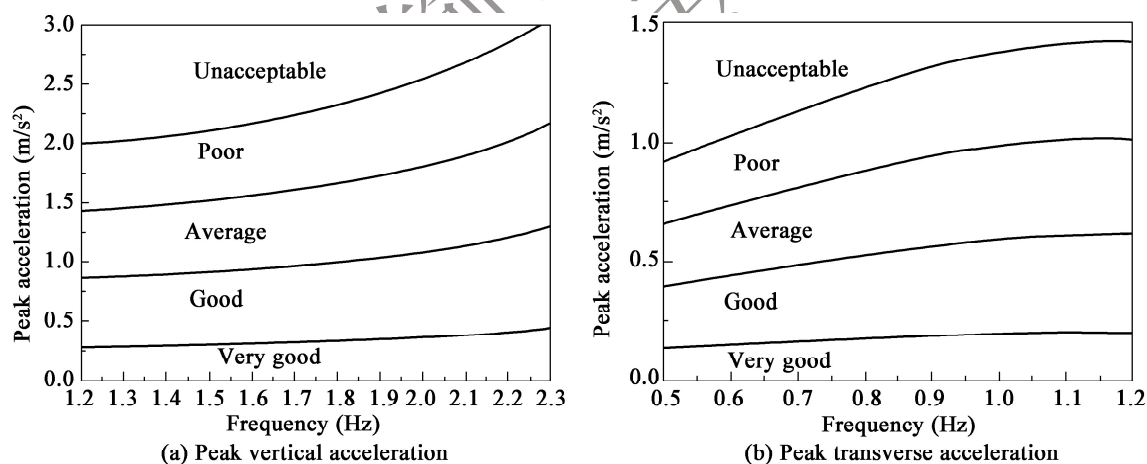


Figure 8-3 Statistical results of measurements on pedestrian comfort levels

If torsional vortex resonance occurs in the main girder, the peak acceleration due to the torsional vortex resonance can be converted to the peak vertical acceleration at the pedestrian locations based on the relative positions between the pedestrian locations and the central axis of the main girder. Then, the verification is performed in accordance with this clause.

8.5.2 Within the wind speed range corresponding to wind action W1 or below, the dynamic

response at the locations of vehicle occupants should meet the following comfort criteria:

- 1 Peak vertical acceleration should not exceed 3.6 m/s^2 ;
- 2 Peak transverse acceleration should not exceed 2.4 m/s^2 .

Commentary

The dynamic response at the locations of vehicle occupants on the bridge deck can be obtained through the analysis of wind-vehicle-bridge coupled vibration. The limits for acceleration in this clause refer to the international standard *ISO 2631 Mechanical Vibration and Shock — Evaluation of Human Exposure to Whole-body Vibration*.

交通运输部信息公告
浏览专用

9 Wind-induced Vibration Control

9.1 General

9.1.1 When the wind-resistant performance of structures fails to meet the design requirements for the ultimate limit state or serviceability limit state, measures shall be taken to meet the requirements by optimizing aerodynamic shapes of members, adding aerodynamic countermeasures, attaching damping devices, or changing the structural system or its stiffness.

Commentary

The aerodynamic performance of the main girder of a bridge can be optimized through adjusting the angle of inclination of webs, the shape of fairings, and modifying the basic cross-sections. It can also be improved through additional aerodynamic countermeasures such as guide vanes, spoilers, and central stabilizers. Supplementary damping devices enhance the damping of members or structural systems by installing dampers to reduce or suppress vibrations. Structural stiffness can be adjusted by altering the structural system, such as changing the connection method between the tower and the girder, the arrangement of cable planes, support conditions, and equipping central buckles in suspension bridges. Modifying member dimensions and materials can also improve structural stiffness and damping ratio to some extent.

9.1.2 When aerodynamic countermeasures are used to improve or enhance the wind-resistant performance of structures or members, their effectiveness shall be verified through wind tunnel testing or virtual wind tunnel testing.

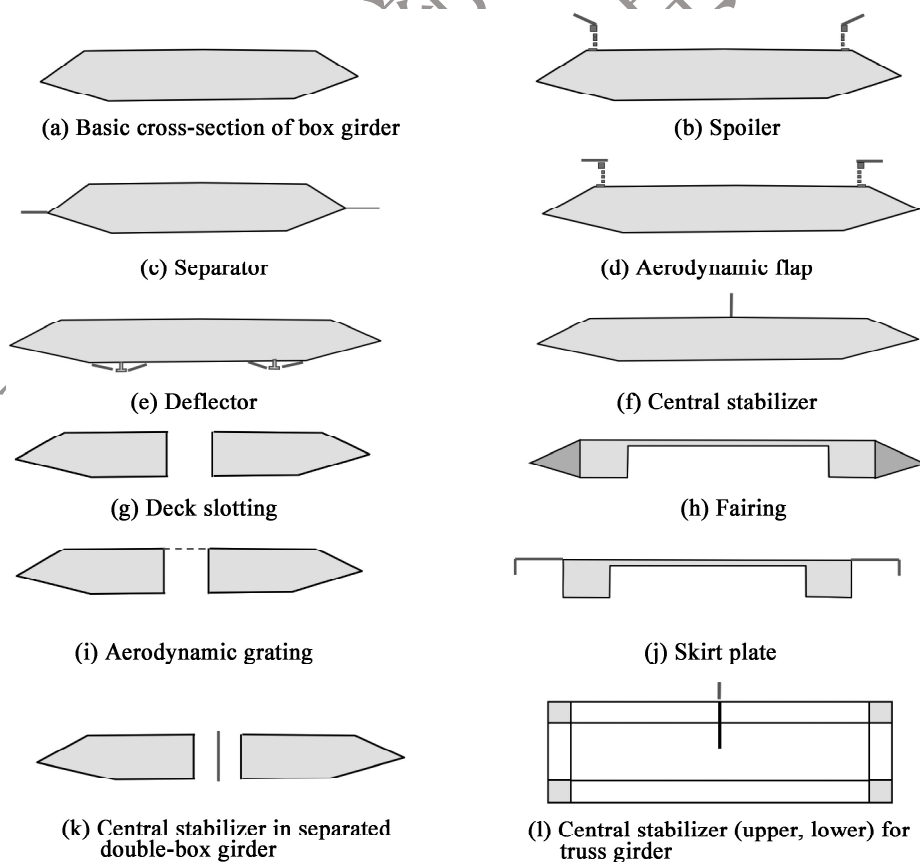
9.1.3 Control measures for wind-induced vibration should be selected by comprehensively considering the requirements for wind-resistant performance, economy, and durability throughout the lifecycle of bridges.

9.2 Girders

9.2.1 The wind-resistant performance of the main girder section may be improved or enhanced by adding aerodynamic countermeasures.

Commentary

Commonly used aerodynamic countermeasures for main girders include: additional deflectors, spoilers, fairings, separators, central stabilizers, aerodynamic flaps, deck slotting, aerodynamic gratings, and wind fins, as shown in Figure 9-1. The flutter stability and the performance of vortex resonance suppression of several bridges in China have been improved by adopting aerodynamic countermeasures in their wind-resistant design. Central stabilizers have been used in the Runyang Yangtze River Suspension Bridge, the Beipanjiang Bridge (Zhensheng Expressway), the Aizhai Bridge, and the Sidu River Bridge to enhance their flutter performance. Measures such as spoilers, deflectors, and aerodynamic gratings can effectively suppress vortex resonance in bridges.



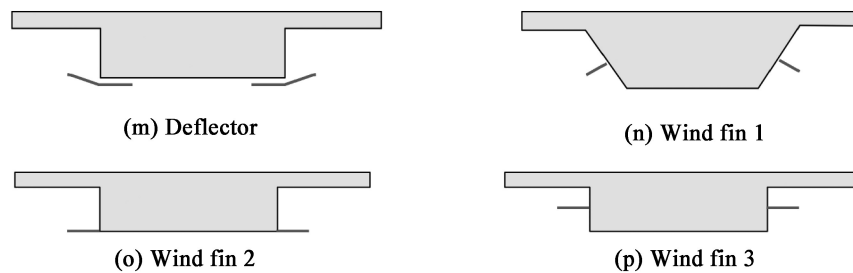


Figure 9-1 Examples of aerodynamic countermeasures for the main girder

9.2.2 The shape and position of appurtenances for steel main girders, such as maintenance vehicle tracks, wind barriers, and railings on bridge decks, shall be determined to meet the requirements for wind-resistant performance of the bridges.

Commentary

In the wind-resistant design of bridges, the shape and position of appurtenances such as maintenance vehicle tracks and wind barriers have a significant influence on the aerodynamic performance of the main girder. The Sutong Yangtze River Bridge has avoided the vortex resonance by reasonably positioning the maintenance vehicle tracks and adding deflectors. Recent research has shown that the wind barriers can not only improve traffic safety and ride comfort, but also enhance the flutter critical wind speed and the suppression of vortex resonance of the bridges.

9.2.3 On the premise that the check requirements for the ultimate limit state of wind resistance are satisfied, additional damping devices may be employed to suppress vortex resonance or reduce buffeting response.

Commentary

The additional damping measures include: 1) tuned damping devices, such as tuned mass damper (TMD), tuned liquid damper (TLD), tuned liquid column damper (TLCD), etc.; 2) untuned damping devices, such as viscous shear damper and oil damper. In terms of control methods, they can be classified into passive control, semiactive control, active control, and hybrid control. For the control of vortex resonance or buffeting response, tuned dampers have good applicability. In terms of control methods, considering the complexity of maintenance for actual bridges, passive control methods offer significant advantages. For the control of vortex resonance or buffeting response in the world, the TMD method has been widely used. During the wind resistance study of the Chongqi Bridge, the phenomenon of vortex resonance was discovered, and the study proposed

the installation of a TMD as a vibration control measure. After the occurrence of vortex resonance during the construction process, the TMD was installed to effectively suppress the vortex resonance. Figure 9-2 shows the schematic structure of a commonly used TMD.

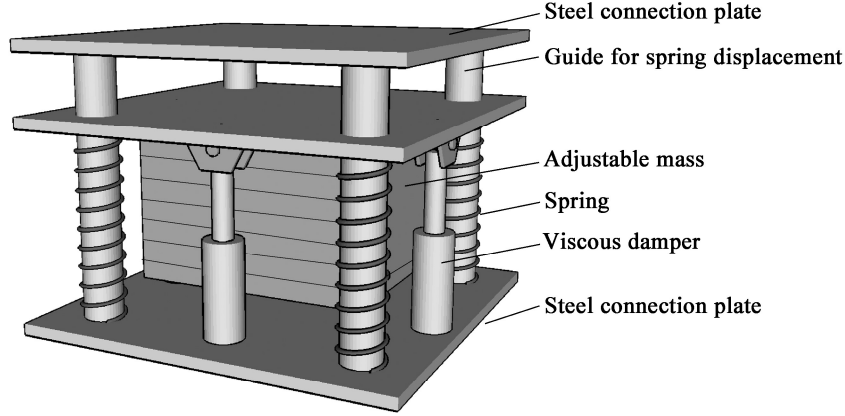


Figure 9-2 Schematic structure of the commonly used TMD

9.2.4 When tuned dampers are utilized to control wind-induced vibration of the main girder, the optimal frequency ratio and optimal damping ratio of the tuned dampers may be calculated using Eqs. (9.2.4-1) and (9.2.4-3).

$$\frac{f_0}{f_s} = \frac{1}{1 + \mu_m} \quad (9.2.4-1)$$

$$\zeta_0 = \sqrt{\frac{3\mu_m}{8(1 + \mu_m)}} \quad (9.2.4-2)$$

$$\mu_m = \frac{m_0 \varphi_i^2(x_0)}{\int_0^L m(x) \varphi_i^2(x) dx} \quad (9.2.4-3)$$

where,

f_0 ——frequency of the damper (Hz);

ζ_0 ——damping ratio provided by the damper (Hz);

f_s ——frequency of controlled mode of the bridge (Hz);

μ_m ——ratio of the mass of the damper to the generalized mass of the controlled mode of the structure;

L ——total length of the bridge (m);

m_0 ——mass of the damper (kg);

$m(x)$ ——mass per unit length of the bridge (kg/m);

$\varphi_i(x)$ ——controlled mode shape;

x_0 ——installation location of the damper (m);

$\varphi_i(x_0)$ ——mode shape value corresponding to the installation location of damper.

9.2.5 When multiple-tuned mass dampers are arranged, the range of frequency and damping of the multiple-tuned mass dampers shall be optimized.

Commentary

At a specific frequency, TMD can effectively control the structural vibration, but it is sensitive to changes in the parameters of the main structure. To improve its robustness, multiple-tuned mass dampers (MTMD) can be used. Figure 9-3 illustrates the working principle of MTMD.

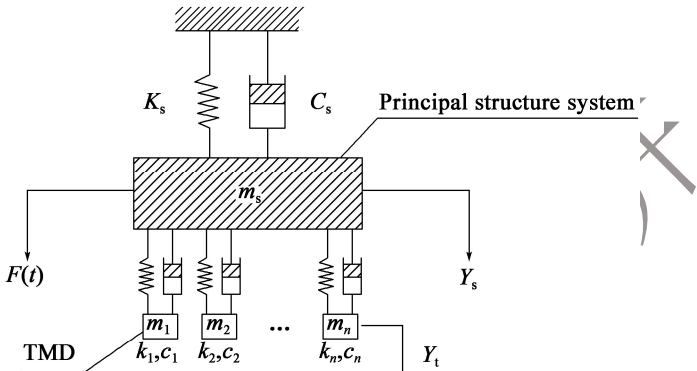


Figure 9-3 Principle of multiple tuned mass dampers (MTMD)

9.3 Towers and High Piers

9.3.1 The wind load and wind-induced vibration response of towers and high piers may be reduced by optimizing their cross-sectional shapes, and damping devices may be added to steel towers whenever necessary.

Commentary

For bridge towers or high piers, the wind load can be reduced by optimizing the cross-sectional shape. Taking the basic rectangular cross-section as an example, the drag coefficient can be lowered by using fillets, semicircles, chamfers, and inset corners, etc. , as shown in Figure 9-4. For steel towers, the wind-induced vibration can be reduced by optimizing the shape and dimensions of the chamfers.

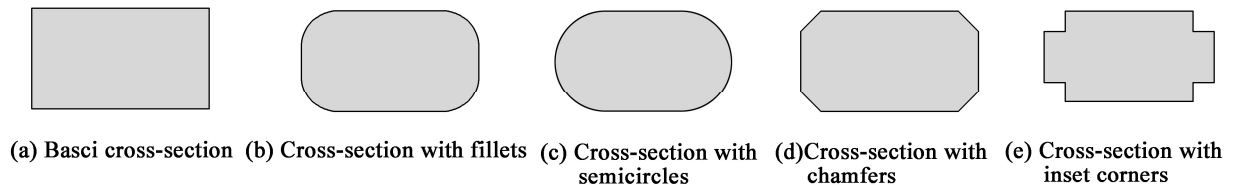


Figure 9-4 Optimization of the cross-sectional shape of the bridge tower

9.4 Stay Cables and Hangers

9.4.1 When stay cables and hangers fail to meet the requirements for wind-resistant performance, damping devices may be supplemented for control.

Commentary

With the increasing length of stay cables and hangers, the stiffness and damping ratio of the members rapidly decrease. Additional damping devices can effectively increase the system damping ratio of the members and reduce the amplitude of wind-induced vibration. Both internal and external damping measures can be used for stay cables to provide the systems damping ratio. Internal damping involves placing damping material in the annular space between the stay cable and the steel sleeve at the anchorage of the main girder or tower. External damping is achieved by installing damping devices on the main girder or tower to provide additional damping. Commonly used additional damping devices include oil dampers, rubber dampers, MR (magnetorheological) dampers, frictional dampers and shear dampers. Figure 9-5 schematically shows the damper installation on a cable-stayed bridge.

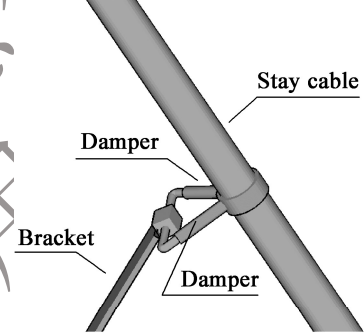


Figure 9-5 Schematic of stay cable attached with dampers

9.4.2 The design of supplemental dampers for stay cables should comprehensively consider the influences of the installation location of the damper, the stiffness of the damper, the nonlinearity of the damper, cable sag, and inclination angle, etc. When hydraulic viscous dampers are used, the damping coefficient, c , may be determined using Eqs. (9.4.2-1) and (9.4.2-2):

$$\frac{\zeta_n}{x_c/l} \cong \frac{\pi^2 \kappa}{(\pi^2 \kappa)^2 + 1} \quad (9.4.2-1)$$

$$\kappa \cong \frac{c}{ml\omega_{01}} n \frac{x_c}{l} \quad (9.4.2-2)$$

where,

κ ——dimensionless damping parameter of the damper;

ζ_n ——the n th modal damping ratio provided by the damper;

ω_{01} ——the first modal circular frequency of the cable (rad/s);

x_c ——distance from the damper location to the nearer cable end (m), as shown in Figure 9.4.2;

n ——mode number of the cable;
 c ——damping coefficient of the damper.

For a linear damper, the optimal damping coefficient that maximizes the additional modal damping ratio of the cable may be determined using Eq. (9.4.2-3) :

$$c_{opt} = 0.10ml\omega_{01} / \left(n \frac{x_c}{l} \right) \quad (9.4.2-3)$$

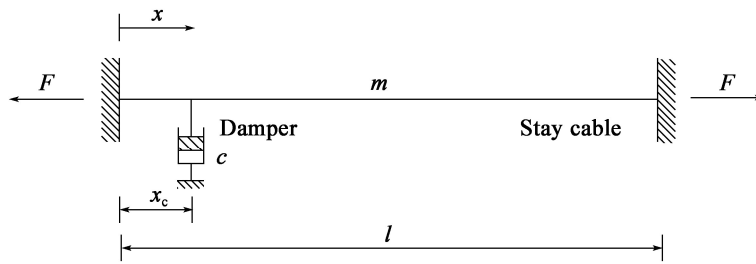


Figure 9.4.2 Illustration of an external damper for a cable

Commentary

Main factors affecting the efficiency of dampers include the installation location of the damper, the stiffness of the damper, the nonlinearity of the damper, cable sag, and inclination angle. A universal design curve for dampers derived from Eq. (9.4.2-1) is plotted in Figure 9-6.

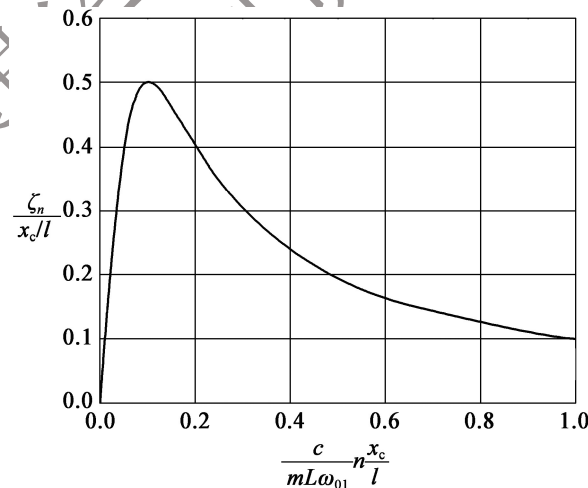


Figure 9-6 Universal design curve for damper

Since the factors such as the stiffness of the damper, the nonlinearity of the damper, cable sag, and inclination angle are not considered in this equation, the actual modal damping ratio achievable by the damper is usually lower than the calculated value. Therefore, when this equation is used to

determine the damper parameters in practice, the modal damping ratio achievable by the damper is considered to be 50% of the calculated value.

9.4.3 Additional helical fillets or surface treatment for stay cables may be implemented to avoid or mitigate wind-rain-induced vibration.

Commentary

Current research on wind-rain-induced vibration of cables has shown that the wind-rain-induced vibration occurs when wind causes rainwater to form water films or rivulets on the cable surface, which alter the aerodynamic shape of the cable or oscillate on the cable surface, thereby inducing large-amplitude vibrations in the cable. The water films or rivulets are the fundamental causes of the wind-rain-induced vibration. To disrupt the formation of water rivulets, numerous experiments and practical engineering projects worldwide have demonstrated that surface treatment on the cable, such as creating axial grooves or projected ribs on the surface of the PE sheath, producing indented holes or dimples on the cable surface, or helically adding strip structures or wrapping strips at intervals on the cable surface along the axial direction, can effectively suppress the wind-rain-induced vibration. However, inappropriate aerodynamic control measures for the wind-rain-induced vibration may lead to unfavorable vibrations such as galloping of the cable. Therefore, it is essential to validate special aerodynamic countermeasures through wind tunnel testing. Figure 9-7 shows examples of aerodynamic countermeasures of additional helical fillet and dimpled surfaces.

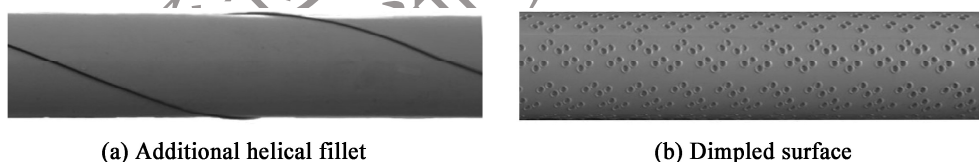


Figure 9-7 Examples of aerodynamic countermeasures on the cable surface

9.4.4 Relevant design parameters of additional helical fillets and surface treatment shall be verified through wind tunnel testing.

Commentary

Helical fillets are arranged on the surface of the cable, and relevant design parameters such as the geometric shape and pitch of the helix have a significant impact on the drag coefficient of the cable. Figure 9-8 illustrates the arrangement of the additional helical fillet.

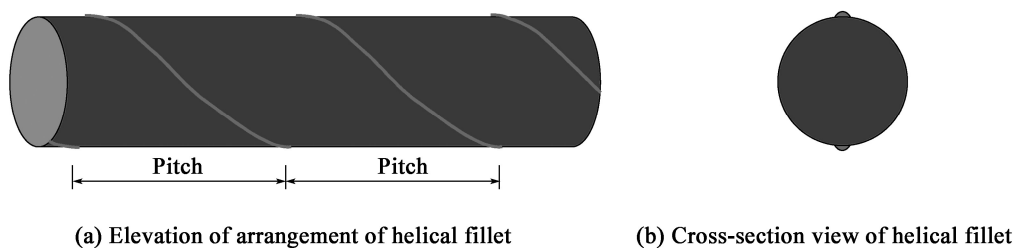


Figure 9-8 Schematic for arrangement of additional helical fillet

9.4.5 Cross-ties may be added to control the vibrations of stay cables.

9.4.6 Rigid H-section hangers shall be avoided. When rigid hangers fail to meet the requirements for wind-resistant performance, measures such as adding transverse cables or damping devices may be implemented to achieve the requirements.

Commentary

Rigid H-section hangers are prone to flutter, galloping, and vortex resonance, etc. Neither web openings nor flange openings can improve the flutter critical wind speed; instead, they may reduce the flutter stability. However, increasing the height-to-width ratio can somewhat enhance the flutter stability. Moderate openings in the webs and flanges can improve galloping performance, with significant improvement mainly observed in the weak axis, while an increase in the height-to-width ratio can notably enhance the galloping stability of H-section hangers. Neither web openings nor flange openings can suppress vortex-induced resonance, but a moderate increase in the height-to-width ratio can reduce the range of wind yaw angle where vortex resonance occurs or decrease its amplitude. Connecting H-section hangers with cross-bracings can increase their stiffness. Figure 9-9 schematically shows the arrangement of wind bracings for connecting H-section hangers.

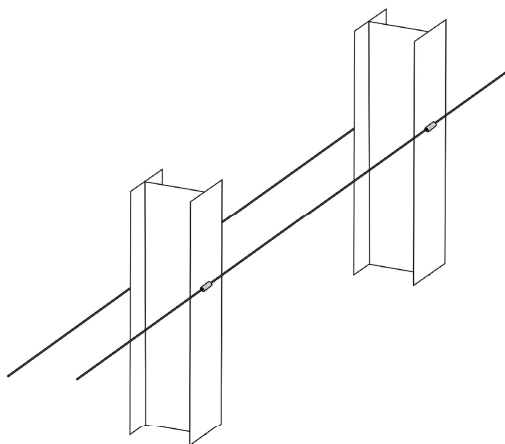


Figure 9-9 Schematic for arrangement of wind bracings as a structural vibration control measure for rigid H-section hangers

9.4.7 When it is determined that significant wind-induced vibrations are likely to occur in horizontally parallel stay cables or hangers, transverse connectors may be installed for vibration control.

Commentary

Transverse connectors link the parallel hangers of arch bridges or suspension bridges to form a unit and prevent individual cables or hangers from undergoing low-frequency vibrations. Figure 9-10 shows common types of connections. For suspension bridges with longer hangers, installing dampers at the lower ends of the hangers also has a certain damping effect.

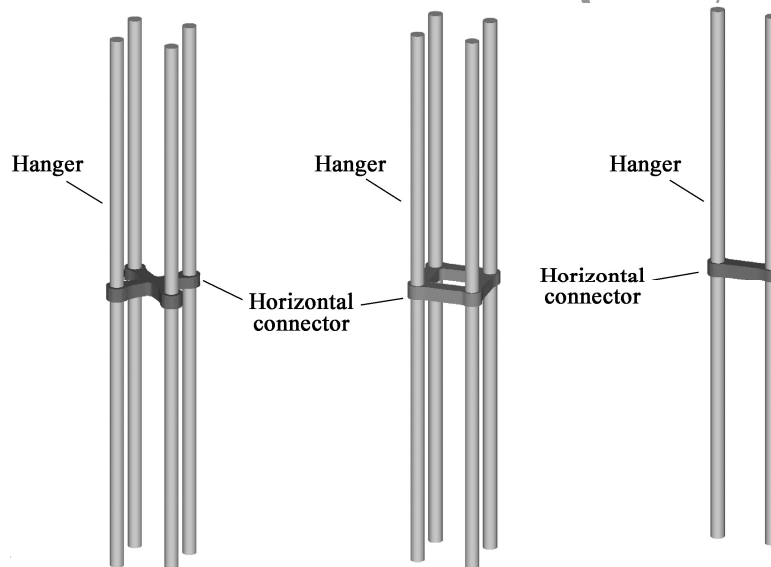


Figure 9-10 Transverse connectors for parallel hangers

10 Wind-induced Traffic Safety

10.1 General

10.1.1 Wind-induced traffic safety should be assessed for bridges in the following situations:

- 1 Bridges located in the wind risk region R1;
- 2 Bridges with abrupt changes in wind speed on the deck or those spanning gorges;
- 3 Bridges that have a significant impact on lifeline engineering or where the consequences of wind-induced traffic accidents are severe.

10.1.2 The assessment of wind-induced traffic safety of bridges shall determine the extent of impact of wind on traffic safety, control objectives, and safeguard measures.

10.2 Assessment of Wind-induced Traffic Safety

10.2.1 The impact of wind on traffic safety shall be comprehensively considered based on factors such as the category of wind risk region for bridges, the characteristics of wind environment on the bridge deck, other meteorological conditions at the bridge site, the types of vehicles, their design speeds and load conditions, as well as the severity of the consequences of vehicle accidents.

Commentary

The wind risk region where the bridge is located reflects, to some extent, the degree to which the traffic safety on the bridge is affected by crosswinds in that region.

The distribution of wind speeds of different scales at the deck elevation is one of the important

indicators for evaluating the impact of wind on traffic safety. This can generally be obtained through a comprehensive analysis with the aid of meteorological data at the bridge site, taking into account the influences of deck elevation and topographic features. Generally speaking, it is also necessary to analyze the annual number of days with wind speeds reaching or exceeding Wind Scale 8 at the deck elevation to determine the necessity of assessing the impact of wind on traffic safety.

After the wind flowing along the outer side of the main girder at the deck elevation passes the girder, a new wind speed profile distribution is generated within the roadway clearance, reflecting the influence of the form of the main girder and appurtenances such as railings on the wind environment on the bridge deck. Meanwhile, local structures such as bridge towers at the height of the main girder cause abrupt changes in the crosswind speed at different locations along the bridge deck. In addition, local special terrain and structures may also contribute to abrupt changes in the wind speed on the deck. These characteristics of the wind environment on the deck can be obtained through wind tunnel testing or virtual wind tunnel testing. Appurtenances on the bridge deck, such as railings and wind barriers, can alter the flow characteristics around the cross-section of the main girder, thereby changing the crosswind speed within the vertical clearance for moving vehicles on the bridge deck. The environmental wind speed within the vertical clearance for moving vehicles is typically evaluated using the equivalent wind speed on the deck. The equivalent wind speed on the deck is a representative value of the crosswind speed within a certain clearance for vehicular traffic on the deck, which is determined based on the principle of equivalent lateral aerodynamic force acting on vehicles. It is the square root of the integral of the square of the crosswind speed over a certain vertical clearance, as presented in Eq. (10-1).

$$U_{eq} = \sqrt{\left(\frac{1}{z_r}\right) \int_0^z \tilde{U}^2(z) dz} \quad (10-1)$$

where,

z_r ——vertical clearance for vehicular traffic. According to the provisions of *Limits of Dimensions, Axle Load and Masses for Motor Vehicles, Trailers and Combination Vehicles* (GB 1589-2016), the height limit for motor vehicles, combination vehicles, trucks, and trailers is generally 4.0 m, and the height limit for double-deck buses operating on fixed routes in cities is 4.2 m. Generally, the height of medium-sized and smaller passenger vehicles, as well as medium-sized and smaller cargo vehicles, does not exceed 3 m.

$\tilde{U}(z)$ ——crosswind speed at the height z above the deck (m/s).

An influence factor λ_s for wind speed on the deck is used to represent the proportional relationship between the equivalent wind speed on the deck and the incoming wind speed outside the deck, as shown in Eq. (10-2):

$$\lambda_s = \frac{U_{eq}}{U_{\infty}} \quad (10-2)$$

where,

U_{∞} ——incoming wind speed at deck level (m/s).

Taking the concrete double-box girder of the approach bridge of the Hangzhou Bay Bridge as an example, the characteristics of the wind environment on the deck level were extracted through virtual wind tunnel testing. Figure 10-1 illustrates the centerline positions of the traffic lanes, and Figure 10-2 presents the crosswind speed profile distributions at the corresponding positions. Table 10-1 gives the influence factors for wind speed on the deck for different positions and vertical clearances.

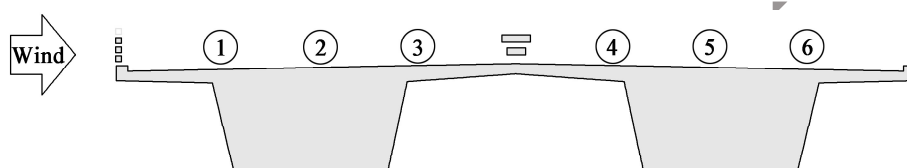


Figure 10-1 Schematic for centerline positions of traffic lanes

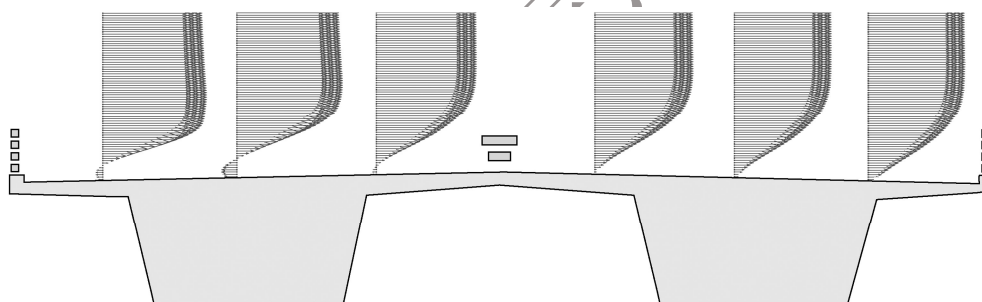


Figure 10-2 Crosswind speed profile distributions at different positions of the bridge deck

Table 10-1 Influence factors for wind speed on deck for various positions of traffic lanes and vertical clearances for traffic

Vertical clearance	Position of traffic lane					
	①	②	③	④	⑤	⑥
3 m	0.84	0.73	0.70	0.71	0.73	0.76
4 m	0.94	0.87	0.85	0.84	0.84	0.86

The difference in cross wind stability among vehicles of different types and under various load conditions is significant. Studies have shown that small passenger cars are prone to deviation in driving direction under crosswind conditions, leading to side impact accidents. Large empty box-type container trucks are more susceptible to rollover accidents under crosswinds. Most vehicles are more likely to experience side-slip accidents caused by crosswinds when the road is wet and slippery due to rain or snow.

For the impact of wind on traffic safety on bridge decks, both the risk probability of vehicle accidents for different vehicle types and the severity of the consequences of such accidents are considered. The consequences of wind on traffic safety extend beyond the accidents themselves and also involve the impact on the capacity of the route. For example, a vehicle accident on a narrow bridge may lead to a disruption of traffic. For bridges spanning water source protection areas, fish farming zones and others, it is necessary to strictly control the risk probability of wind-induced vehicle accidents to prevent chemical leaks caused by accidents. For bridges crossing over gorges, it is essential to thoroughly assess the impact of crosswinds on traffic safety and strictly avoid the occurrence of vehicles plunging off the bridge.

10.2.2 The influence of bridge towers, abutment structures, arch springings or arch ribs, bridge-tunnel transition zones, and local topographic features on the wind environment characteristics for moving vehicles on bridge decks should be determined through wind tunnel testing or virtual wind tunnel testing.

Commentary

Bridge towers, abutment structures, arch springs or arch ribs, bridge-tunnel transition zones, and local topographic features can affect the wind environment characteristics for moving vehicles on bridge decks. Figure 10-3 illustrates the distribution of crosswind speed in the vicinity of the bridge towers along the longitudinal axis of the bridge.

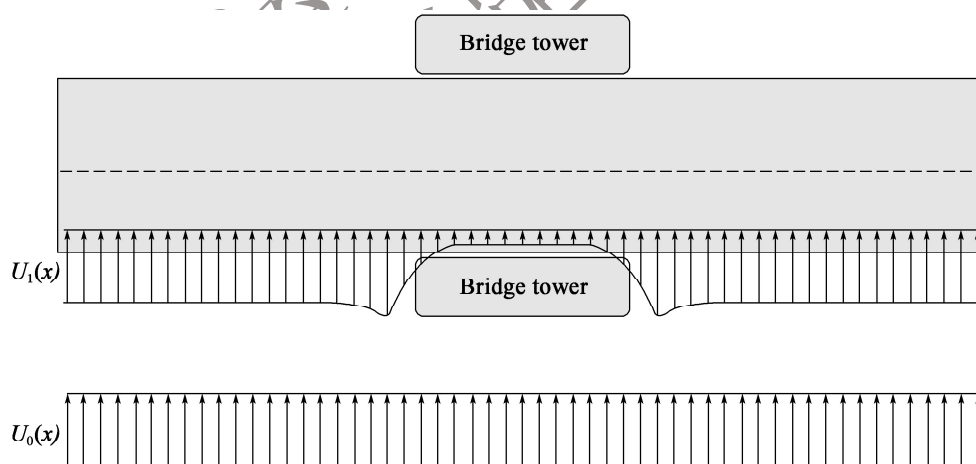


Figure 10-3 Schematic for the distribution of crosswind speed in the vicinity of the bridge tower along the longitudinal axis of the bridge

10.2.3 The control objectives for wind-induced traffic safety on bridge decks should be determined by comprehensively considering the design speed, vehicle types, traffic capacity requirements, traffic safety and ride comfort requirements, as well as the implementable traffic management measures and engineering structural measures.

Commentary

Taking the Hangzhou Bay Bridge as an example, the bridge crosses over the waters of Hangzhou Bay with a design speed of 100 km/h and is accessible to all compliant vehicles, mainly including basic passenger cars, crossover passenger cars, medium-sized commercial buses, large commercial buses, and large commercial van-type trucks. Studies on wind-induced traffic safety have shown that under the original design plan, the entire bridge would need to be closed when the wind reaches Wind Scale 8 at the ground surface. As an important land route connecting Ningbo to Shanghai, the Hangzhou Bay Bridge has high requirements for traffic capacity during windy days. Its traffic control objective is set as: the entire bridge remains open when the wind reaches Wind Scale 10, and it will be closed when the wind reaches Wind Scale 11.

10.2.4 The control objectives for wind-induced traffic safety may be ensured by selecting appropriate types of railing or installing wind barriers.

Commentary

When the control objectives of wind-induced traffic safety cannot be achieved only through traffic management measures, engineering solutions such as appropriate types of railing or wind barrier are often employed. Taking the Hangzhou Bay Bridge as an example, in order to achieve the control objective that the bridge is still accessible during the occurrence of Wind Scale 10, besides traffic management measures to restrict the speed to 40 km/h when the wind reaches Wind Scale 10, engineering measures including increasing the height of the railings along the entire bridge from 1.06 m to 1.5 m and installing wind barriers on the traffic barriers of the south and north navigation channel bridges and the approach bridges in the high-pier areas have also been implemented on the bridge.

A wind barrier is a device installed on the main girder to reduce the impact of lateral wind speed on the bridge deck, thereby enhancing the traffic safety and ride comfort on the bridge deck. It typically consists of posts, barrier strips, as well as anchoring and damping components. Figure 10-4 presents three different methods of connecting wind barriers to the bridge deck.

In recent years, wind barriers have been employed in several bridges around the world after research. Taking the north navigation channel bridge of the Hangzhou Bay Bridge as an example, virtual wind tunnel testing was conducted on the wind environment on the deck with a typical closed steel box girder section shown in Figure 10-5, in which different types of railings and wind barriers were considered, as illustrated in Figure 10-6. The extracted influence factors for wind speed of different positions and typical vertical clearances on the bridge deck are listed in Table 10-2. A

comparison of the data in the table reveals that the influence factors for wind speed on the deck decrease somewhat with the increasing height of the railings, and significantly decrease after the installation of wind barriers. Taking the finally adopted scheme S5 as an example, the influence factor for wind speed on the deck within the vertical clearance of 3 m and 4 m at the position of Lane ① is reduced by 63% and 62%, respectively, when compared with the corresponding cases of S1. By installing wind barriers, optimizing the design of railings and implementing relevant management measures, a consistent level of wind-induced traffic safety was maintained between the main bridge and its connecting lines.

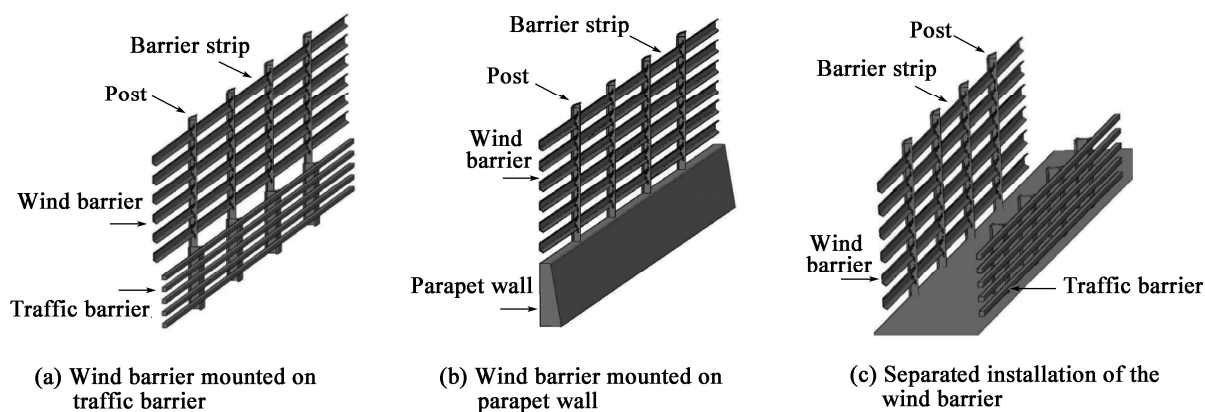


Figure 10-4 Composition of wind barrier and its connection to the bridge deck

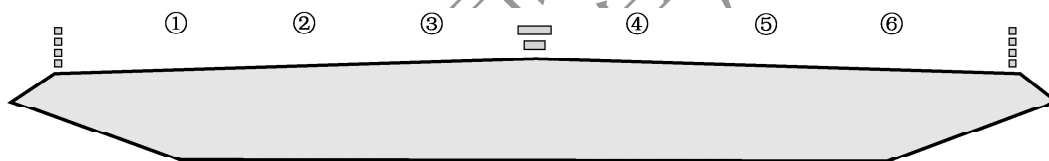


Figure 10-5 Schematic for positions to extract the wind speed profile on the deck of the north navigation channel bridge of the Hangzhou Bay Bridge

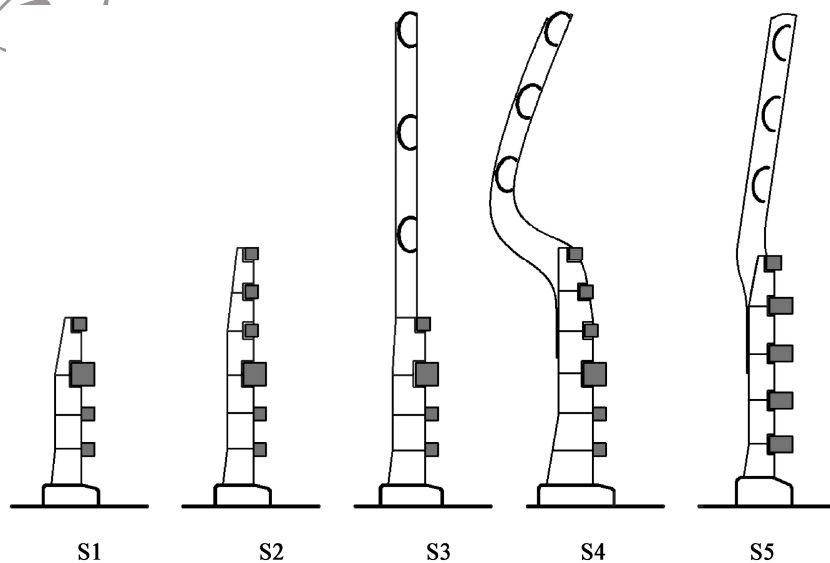


Figure 10-6 Schemes of railings and wind barriers for the main navigation channel bridge

Table 10-2 Influence factor, λ_s , for wind speed on bridge deck at different traffic lanes and typical vertical clearances

Position of traffic lane	Vertical clearance									
	S1		S2		S3		S4		S5	
	3 m	4 m	3 m	4 m	3 m	4 m	3 m	4 m	3 m	4 m
①	0.95	0.98	0.90	0.92	0.70	0.74	0.68	0.66	0.60	0.61
②	0.88	0.93	0.84	0.88	0.63	0.67	0.63	0.60	0.55	0.54
③	0.85	0.90	0.83	0.87	0.60	0.64	0.59	0.57	0.53	0.51
④	0.81	0.88	0.79	0.85	0.57	0.62	0.53	0.52	0.48	0.47
⑤	0.79	0.87	0.77	0.83	0.54	0.59	0.50	0.49	0.46	0.46
⑥	0.79	0.87	0.74	0.80	0.51	0.57	0.46	0.47	0.44	0.44

10.3 Design of Wind Barriers

10.3.1 The design life of posts of a wind barrier shall not be less than 50 years, and the design life of the barrier strips shall not be less than 20 years.

10.3.2 The wind load for structural design of wind barriers shall be selected based on the wind action W2.

10.3.3 The selection of type and materials for wind barriers should be comprehensively determined according to the vehicle collision condition, fire resistance, durability and landscape requirements.

10.3.4 Types and sheltering efficiency of wind barriers should be determined through wind tunnel testing or virtual wind tunnel testing, and the sheltering efficiency should be in the range of 0.35 ~ 0.70.

10.3.5 Wind barriers may be connected to the bridge by mounting on traffic barriers or parapet walls, or may be separately connected to the main girder and placed outside the traffic barriers or parapet walls.

10.3.6 The distance between the top of the wind barrier and the bridge deck should not exceed 4 m, and should not exceed 5 m in areas with abrupt changes in wind speed. A height transition section should be provided in the area where the height of the wind barrier changes.

Commentary

The height transition sections are set at both ends of the wind barrier to reduce abrupt changes in wind speed and mitigate the impact of crosswinds on vehicle driving.

10.3.7 If wind barriers are installed only at the sections with sudden changes in wind speed including bridge towers, abutment structures, arch springs or arch ribs, bridge-tunnel connections and others, the range and form of their arrangement should be determined based on wind tunnel testing or virtual wind tunnel testing, or they may be arranged according to Figure 10.3.7. The arrangement range at one side should not be less than 5 times the longitudinal dimension of the bridge towers, abutment structures, arch springs or arch ribs at the deck elevation, and the overlap section at one side should not be less than 0.25 times their longitudinal dimensions.

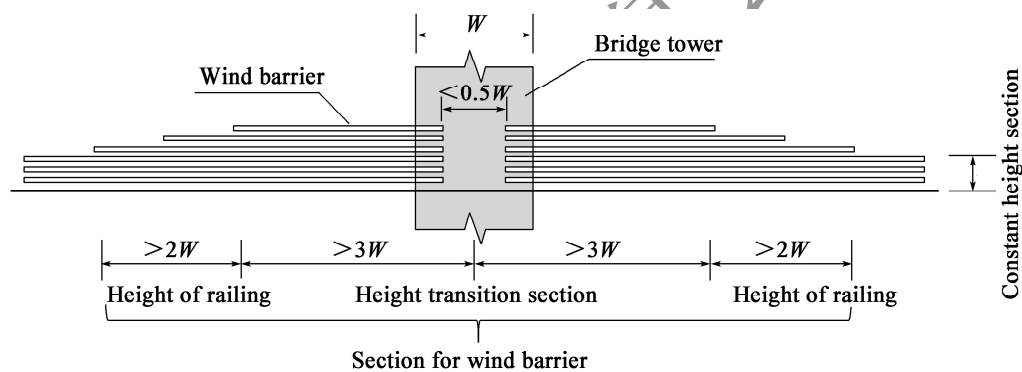


Figure 10.3.7 Schematic for arrangement of wind barrier at bridge tower
(W is the longitudinal width of the tower at the deck elevation)

Commentary

Wind barriers are installed only at the section of the bridge tower in the Taizhou Yangtze River Bridge, as shown in Figure 10-7.

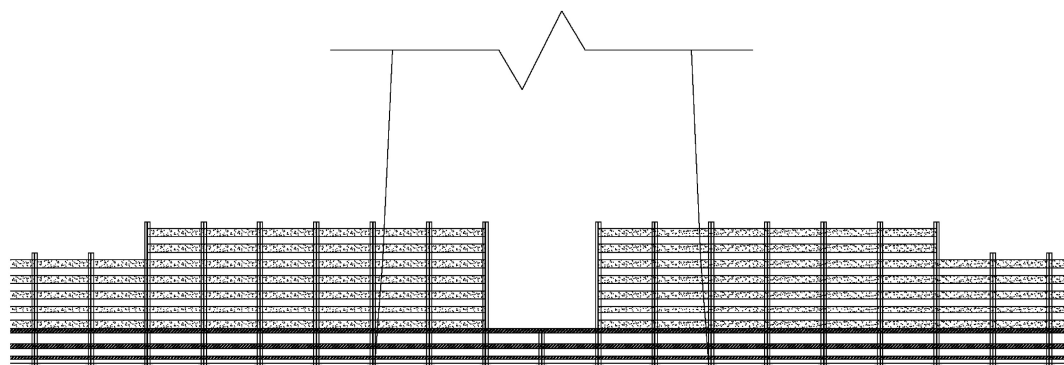


Figure 10-7 Arrangement of wind barriers at the tower section of Taizhou Yangtze River Bridge

11

Wind Tunnel Testing and Virtual Wind Tunnel Testing

11.0.1 The wind-resistant performance and relevant parameters of bridge structures or members may be verified and acquired through wind tunnel testing and virtual wind tunnel testing.

11.0.2 Flutter, galloping, and aerostatic stability testing should be conducted in a uniform flow field. Vortex resonance testing should be performed in either a uniform flow field or a turbulent flow field. Buffeting testing should be conducted in a wind tunnel or virtual wind tunnel that simulates the atmospheric boundary layer, and the simulated atmospheric boundary layer shall reflect the mean wind speed profile, turbulence intensity profile, and power spectrum of fluctuating wind at the bridge site.

11.0.3 Wind tunnel test models of bridge structures or members shall simulate their shapes, mass distributions, constraint conditions, principal modes, frequencies, and damping ratios according to the principle of similarity.

11.0.4 The turbulence characteristics, wind attack angle, and wind yaw angle considered in wind tunnel testing for the wind-resistant performance of bridge structures or members shall be consistent with the wind environment at the bridge site.

11.0.5 The scale of sectional models for stay cables and hangers should be 1:1, and the damping ratio of models should be lower than 0.15%. The simulated rainfall, wind yaw angle, inclination angle of cable, and other factors in wind-rain-induced vibration testing of stay cables should be consistent with the actual situations.

11.0.6 The coverage radius of topographic wind environment test models should not be less than 2 km. The approach flow may be selected as a turbulent flow field corresponding to Terrain Category B at the same scale. The scale of the test model should be larger than 1:1000.

Commentary

In the design of topographic wind environment testing, a larger simulation scope can better reflect the influence of the surrounding terrain on the wind field at the bridge site, but the simulation accuracy may be compromised. For cable-stayed or suspension bridges, the bridge tower can be selected as the reference component, with a coverage radius of 10 times its height for the design of the terrain model. For arch bridges or continuous girder bridges, the rise of the arch rib or the maximum pier height can be chosen as the reference component. Figure 11-1 illustrates the arrangement of a wind tunnel test for topographic wind environment, where roughness elements and spires are turbulence simulation devices used to simulate Terrain Category B at the same scale as the terrain model.

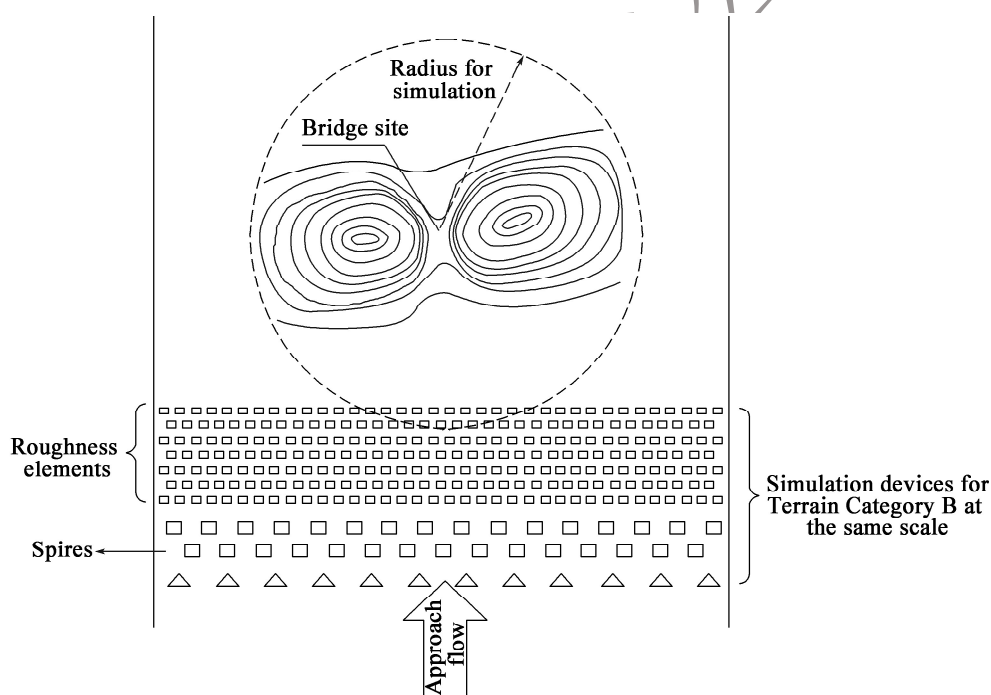


Figure 11-1 Schematic for the arrangement of the wind tunnel test model for the topographic wind environment

11.0.7 The requirements for wind tunnel testing and virtual wind tunnel testing may be found in Appendix B and Appendix C of the *Specifications*, respectively.

Appendix A

Wind Risk Region Map and Wind Speed Distribution Map for Bridges in China *

A.1 Wind Risk Region Map for Bridges in China

A.2 Basic Wind Speed Distribution in China

A.3 Wind Speeds for Different Return Periods in Major Regions of China

A.4 Probabilistic Distribution Models and Parameter Values of Wind Speed at Meteorological Stations across China

* Editor's note: Relevant data in Appendix A may refer to the corresponding Chinese version of the Specifications.

Appendix B

Basic Requirements for Wind Observation at Bridge Site in China

B.1 General Rules

B.1.1 For important bridges that are sensitive to wind actions, when the bridge site has complex terrain or lacks usable wind speed records, wind parameters at the bridge site may be obtained by establishing an observation station there.

B.1.2 Necessary measures shall be taken to ensure the normal operation of the instruments and equipment during the observation period.

Commentary

Wind observation instruments and equipment generally require a long-term power supply. Due to the harsh field working environment, these instruments and equipment are exposed to adverse conditions such as corrosion, lightning strikes, and strong winds. Therefore, during the observation period, measures for lightning protection, durability assurance, and continuous power supply for the instruments and equipment are of great importance.

B.1.3 The connection structure for wind observation towers and anemometers shall demonstrate adequate structural stiffness.

Commentary

Wind observation instruments and equipment are connected to the wind observation tower or

associated fix devices. If the stiffness of the wind observation tower itself or the fixing devices is not sufficient, the measured wind speed data will involve spurious data due to the displacement and vibration of the wind observation tower or the fixing devices.

B.1.4 The wind observation at the bridge site shall conform to the relevant requirements or provisions in *Specifications for Surface Meteorological Observation – Wind Direction and Wind Speed* (GB/T 35227).

B.1.5 The selection of locations for wind observation towers and the height for wind observation should be determined considering the topographic features of the bridge site, the deck elevation of the main bridge, and other factors.

B.1.6 The placement of anemometers shall avoid the interference from the observation tower itself or other structures under prevailing wind directions.

B.2 Wind Observation Period, Measurement Points and Parameters

B.2.1 The wind observation period at the bridge site shall not be less than two years.

B.2.2 The installation locations and heights of wind observation instruments and equipment should be determined based on the observation purposes, and the measurement layers for wind speed profile observation should not be fewer than four.

Commentary

A wind observation tower of 75 m height on the south bank of the Sutong Yangtze River Bridge was constructed with measurement points at heights of 10 m, 30 m, 50 m, and 70 m. An observation tower of 60 m in height was erected at the site of the Taizhou Yangtze River Bridge with measurement points at 10 m, 30 m, 50 m, and 60 m. An observation tower of 80 m in height was erected at the site of the Shanxi Linyi Yellow River Bridge with measurement points at 10 m, 30 m, 50 m, and 80 m.

B.2.3 Wind observation parameters shall include wind speed and wind direction. Anemometers for measuring mean wind speed and direction shall have a sampling frequency of no less than 1 Hz. Anemometers for observing fluctuating wind characteristics shall have a sampling frequency of no less than 10 Hz.

B.3 Wind Observation Data Analysis

B.3.1 The validity rate of wind observation data should not be less than 95% , and the data completeness rate should not be less than 98% . In the event of missing data, data interpolation and correction may be performed based on correlation analysis using data collected by other observation instruments during the same period.

Commentary

If Anemometer A has missing data while Anemometer B has collected valid data during the same period, a correlation analysis can be performed on their measured daily mean or maximum wind speed data. After passing the correlation test, a data ratio relationship between Anemometer A and Anemometer B can be established. Subsequently, the missing data from Anemometer A can be interpolated using the synchronized measurements from Anemometer B as a reference.

B.3.2 Wind observation data analysis shall primarily encompass wind speed, wind direction, wind attack angle, terrain roughness factor, turbulence intensity, gust factor, and wind speed spectra. Results of statistical analyses under high wind conditions shall serve as the basis for design parameter selection.

Commentary

The statistical analysis of wind speed includes mean wind speed, extreme wind speed, and 10-minute average maximum wind speed. Wind direction is primarily presented in the form of a wind rose diagram, as illustrated in Figure B-1. The number of high-wind days, which is a statistical parameter indicating the frequent occurrence of high winds at the bridge site, and is typically represented by the number of days with wind speeds exceeding a specified threshold within a specified period (e. g. , one year). Table B-1 presents a statistical summary of high-wind days above Wind Scale 7 from an observation report. The terrain roughness factor is obtained by fitting the mean wind speeds measured at multiple elevations and is derived from the statistics of data collected under high-wind conditions. Table B-2 presents the measurement analysis results of the terrain roughness factor for a river-crossing bridge. Turbulence intensity and gust factor exhibit significant variability and are obtained by fitting the asymptotic trend of turbulence intensity under strong wind conditions. Figure B-2 illustrates the relationship between turbulence intensity and mean wind speed.

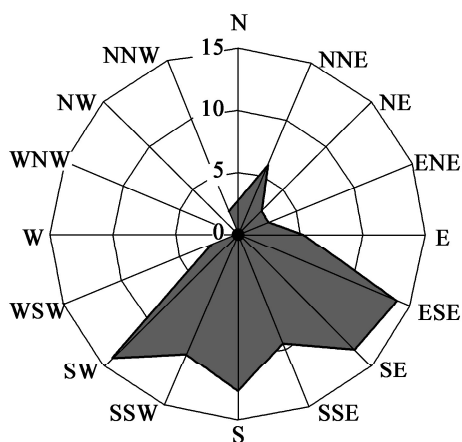


Figure B-1 Example of a wind rose diagram

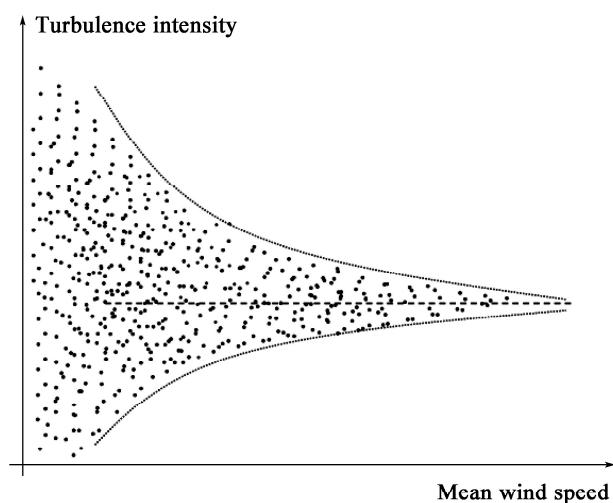


Figure B-2 Example of the relationship between turbulence intensity and mean wind speed

Table B-1 Number of high-wind days above Wind Scale 7 from an observation station

Measurement point	Elevation (m)	Month												Annual	Maximum consecutive days
		4	5	6	7	8	9	10	11	12	1	2	3		
A	10	6	7	6	2	7	4	4	9	6	12	9	8	77	5
	20	5	4	6	3	9	5	5	12	6	13	10	9	87	5
	40	7	5	9	5	10	6	6	12	6	13	11	11	101	6
	60	7	4	6	5	9	5	5	11	6	12	10	9	89	5
B	20	2	3	3	1	4	1	2	1	0	0	1	1	19	6

Table B-2 Statistical results of terrain roughness factor, α_0 , for a bridge site

Wind yaw angle		Northward	Southward	Eastward	Westward
All samples	Mean value	0.093	0.192	0.141	0.169
	Regression value	0.088	0.171	0.134	0.155
≥ 5 m/s	Mean value	0.092	0.182	0.129	0.166
	Regression value	0.082	0.166	0.134	0.158

B.3.3 The basic wind speed at the bridge site U_{s10} may be estimated based on the correlation between wind observation data at the bridge site and concurrent wind speed data from nearby meteorological stations, utilizing long-term wind speed records from these stations.

Commentary

Given the limited duration of wind observation records, short-term data alone are insufficient to reflect the regional long-term wind characteristics. Therefore, correlation analysis between the wind speed data from the observation station and those from nearby meteorological stations becomes particularly critical. In determining the design wind speed for the Sutong Yangtze River Bridge, a correlation analysis was conducted between wind observation data at the bridge site and concurrent data from Changshu and Nantong meteorological stations, demonstrating a strong correlation between the two datasets. Table B-3 presents the correlation analysis results and the finalized correlation estimation formula adopted for the Sutong Yangtze River Bridge, which incorporates a 99.7% confidence level. Based on the obtained correlation formula, the observation station data were adjusted and extrapolated with the data from the meteorological stations, resulting in an annual maximum wind speed sequence for the bridge site. Finally, statistical analysis was performed on this sequence to obtain the basic wind speed at the bridge site.

Table B-3 Correlation analysis results between daily maximum wind speed (5 m/s) from various observation stations for the Sutong Yangtze River Bridge

Item	Correlation formula	Correlation coefficient	Residual variance	Sample size
Correlation between river surface observation station (Y) and Nantong meteorological station (X)	$Y = 3.763 + 1.173X$	0.609	1.982	446
Correlation between river surface observation station (Y) and Changshu meteorological station (X)	$Y = 3.662 + 1.186X$	0.598	2.030	436
Correlation between river surface observation Station (Y) and Nantong (X_1), Changshu (X_2) meteorological stations	$Y = 2.805 + 0.701X_1 + 0.632X_2$	0.645	1.912	376
Finalized correlation formula	$Y = 8.540 + 0.701X_1 + 0.632X_2$	Based on the 3 σ principle		

Appendix C

Requirements for Wind Tunnel Testing

C.1 General

C.1.1 Aerostatic force testing, sectional model vibration testing, bridge tower model testing, full-bridge aeroelastic model testing, topographic wind environment model testing, and wind environment testing for traffic safety on bridge decks may be conducted in wind tunnels for bridge structures or members to verify their wind-resistant performance and acquire relevant aerodynamic parameters and wind parameters.

C.1.2 Wind tunnel testing should be conducted in wind tunnels capable of simulating the atmospheric boundary layer.

C.1.3 The test model shall be placed within the effective test section of the wind tunnel. Measurements shall be conducted at the mid-span cross-section of the model along the longitudinal axis of the wind tunnel. The unoccupied wind tunnel shall satisfy the following flow field characteristics:

- 1 At commonly used test wind speeds, the deviation of the wind speed distribution from the mean wind speed should be less than 2% .
- 2 The pitch angle, $|\alpha|$, between the direction of the approach flow and the axis of the wind tunnel should be less than 0.5, and the wind yaw angle, $|\beta|$, should be less than 1.0.
- 3 At commonly used test wind speeds, the turbulence intensity should be less than 2% .
- 4 Within 1 m zones of the entrance and exit of the wind tunnel test section, the axial static

pressure gradient of the wind speed should be less than 0.01 m.

C.1.4 When conducting wind tunnel testing simulating natural wind characteristics, if wind observation data from the bridge site is available, the wind field shall be simulated based on the wind parameters derived from such wind speed data, including wind speed profile, power spectral density functions, turbulence intensity profiles, and turbulent length scales. In the absence of wind observation data from the bridge site, the wind field simulation may adhere to the following principles:

- 1 The wind speed profile may be adopted in accordance with Clause 4.2.6 of the *Specifications*. The allowable tolerance for the terrain roughness factor, α_0 , may be 0.01.
- 2 The power spectral density functions of fluctuating wind speed in the horizontal along-wind and vertical directions may be determined using Eqs. (C.1.4-1) and (C.1.4-2), respectively:

$$\frac{nS_u(n)}{u_*^2} = \frac{200f}{(1+50f)^{5/3}} \quad (\text{C.1.4-1})$$

$$\frac{nS_w(n)}{u_*^2} = \frac{6f}{(1+4f)^2} \quad (\text{C.1.4-2})$$

$$f = \frac{nZ}{U(Z)} \quad (\text{C.1.4-3})$$

$$u_* = \frac{KU(Z)}{\ln \frac{Z-z_d}{z_0}} \quad (\text{C.1.4-4})$$

$$z_d = \bar{H} - z_0/K \quad (\text{C.1.4-5})$$

where,

$S_u(n)$ ——power spectral density function of fluctuating wind in the horizontal along-wind direction;

$S_w(n)$ ——power spectral density function of fluctuating wind in the vertical direction;

n ——frequency of wind fluctuation (Hz);

u_* ——frictional velocity of wind, also known as the shear velocity (m/s);

K ——dimensionless constant, $K \approx 0.4$;

Z ——height above the ground or water surface (m);

$U(Z)$ ——mean wind speed at height Z (m/s);

\bar{H} ——average height of surrounding buildings (m);

z_0 ——terrain roughness height (m), see Table 4.2.1.

- 3 The average design turbulence intensity, I_u , for the fluctuating along-wind speed

component u of the approach flow may be determined in accordance with Clause 4.3.1. The variation range of turbulence intensity should be within 30%. The turbulent length scales, L_x^u and L_y^u , in the cross wind and vertical directions for the turbulent component u may be selected from Table C.1.4.

Table C.1.4 Benchmark values of turbulent length scales for turbulent component u in the cross wind and vertical directions

Height (m)	Turbulent length scale (m)	
	L_x^u	L_y^u
$Z \leq 10$	50	20
$10 < Z \leq 20$	70	30
$20 < Z \leq 30$	90	40
$30 < Z \leq 40$	100	50
$40 < Z \leq 50$	110	50
$50 < Z \leq 70$	120	60
$70 < Z \leq 100$	140	70
$100 < Z \leq 150$	160	80
$150 < Z \leq 200$	180	90

Commentary

The integral length scales of turbulence represent the average size of eddies in the airflow. Corresponding to the three directions of eddies associated with fluctuating wind speed components in the along-wind, cross-wind, and vertical directions (u , v , and w), there are a total of nine turbulent integral length scales. For example, L_x^u , L_y^u , and L_z^u represent the longitudinal, transverse, and vertical average sizes of eddies associated with the along-wind fluctuating wind speed of the approach flow, respectively. L_x^u is mathematically defined as:

$$L_x^u = \frac{1}{\sigma_u^2} \int_0^\infty R_{u,u_1}(x) dx \quad (\text{C-1})$$

where,

$R_{u,u_1}(x)$ ——cross-covariance function of two longitudinal fluctuating wind speed components

$u_1 \equiv u(x_1, y_1, z_1, t)$ and $u_2 \equiv u(x_2, y_2, z_2, t)$;

σ_u ——root mean square of u_1 (and u_2).

C.1.5 Wind tunnel test models for bridges should conform to the provisions in Table C.1.5.

Table C.1.5 Requirements for wind tunnel test models of bridges

Model requirement	Type of testing			
	Sectional model testing		Bridge tower model testing	Full-bridge aeroelastic model testing
	Aerostatic testing	Sectional model vibration testing		
Modelscales	$\geq 1/80$		$\geq 1/200$	$\geq 1/300$
Model width/height of the effective test section	For closed circuit: ≤ 0.4 For open circuit: ≤ 0.2		≤ 0.2 (Model width is the spacing between tower columns)	/
Model length/model width	For closed circuit: > 2 For open circuit: > 3		/	/
Blockage ratio	$\leq 5\%$			

C.2 Aerostatic Force Testing

C.2.1 The model for aerostatic force testing shall maintain geometric similarity to the prototype bridge, and end plates or compensation models shall be equipped at both ends of the model. When end plates are used, aerodynamic corrections for forces acting on the end plates and the model support devices shall be considered. When compensation models are employed, the gap between the compensation model and the force measurement model should be less than 1 mm, the compensation model shall be of sufficient length, and aerodynamic corrections for the support devices of the force measurement model shall be performed.

C.2.2 The wind attack angle for the aerostatic force testing of the main girder should vary in a range of $-10^\circ \sim +10^\circ$, and the step size of the variation shall be 1° .

C.2.3 Two different wind speeds shall be selected for the aerostatic force testing of the main girder.

C.2.4 The aerostatic force testing for members with variable cross-sections should be conducted in segments, and the compensation segment model shall have sufficient length. For parallel members, the mutual influence of upstream and downstream members should be considered.

Commentary

For the force measurement testing of members with variable cross-sections, it is necessary to consider the aerodynamic effects of the upstream and downstream members, as well as adjacent members on the tested segment. This is typically achieved by conducting simultaneous tests on the

tested segment and the compensation segment. The role of the compensation segment is to account for the aerodynamic influence of adjacent members on the tested member. The model of the tested segment is connected to a force balance, while the model of the compensation segment is independent of the tested segment model. Figure C-1 illustrates the principle of the segmented force measurement testing.

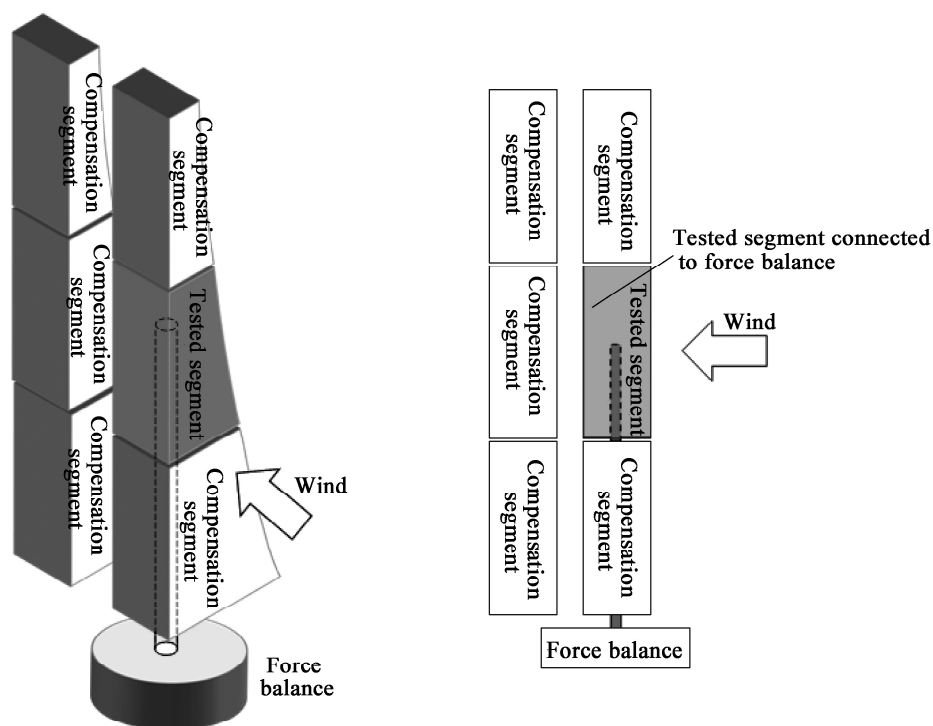


Figure C-1 Schematic for the principle of the segmented force measurement testing

C.2.5 The influence of wind yaw angle shall be considered in the aerostatic force testing for bridge tower members. The wind yaw angle should vary in a range of $0^{\circ} \sim 180^{\circ}$, the step size of the variation should not be larger than 15° , and it should not exceed 5° within the 30° range near the transverse and longitudinal directions of the bridge.

C.3 Sectional Model Vibration Testing

C.3.1 Sectional model vibration testing shall ensure the two-dimensional flow characteristics of members, employing a spring-suspended sectional model setup or a forced vibration model setup.

Commentary

In the sectional model vibration testing, it is crucial to ensure two-dimensional flow characteristics. Figure C-2 illustrates the schematics of three-dimensional flow around the ends and two-dimensional

flow across the cross-section. Generally, when the length-to-width ratio of the model is 4 or greater, the aerodynamic forces induced by three-dimensional flow around the ends have minimal impact on the overall aerodynamic forces on the model, and end plates may not be necessary. When the length-to-width ratio is less than 4, end plates can be installed to maintain the two-dimensional flow characteristics of the sectional model.

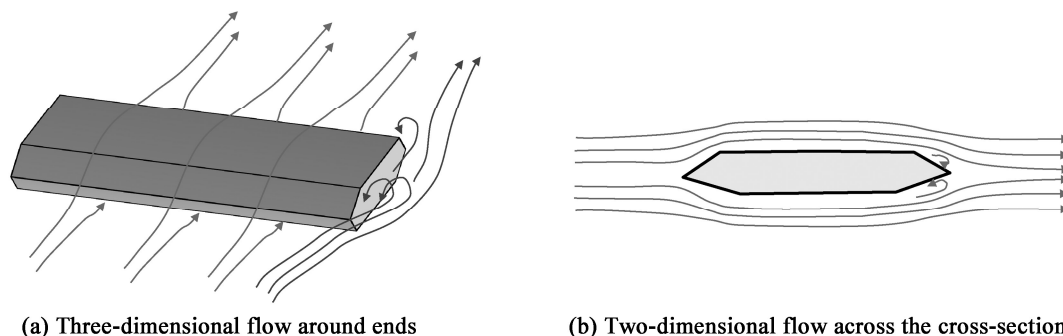


Figure C-2 Schematics for three-dimensional flow around ends and two-dimensional flow across cross-section

Sectional model vibration testing can determine flutter critical wind speed, onset wind speed for vortex resonance and vibration amplitudes. Sectional model vibration testing conducted in turbulent flow fields can measure the buffeting response of the model. Sectional models typically simulate two degrees of freedom: vertical vibration and torsional vibration. Horizontal springs may also be added to simulate the degree of freedom of lateral vibration. Figure C-3 schematically shows a spring-suspended sectional model, while Figure C-4 illustrates the sectional model testing with a forced vibration method.

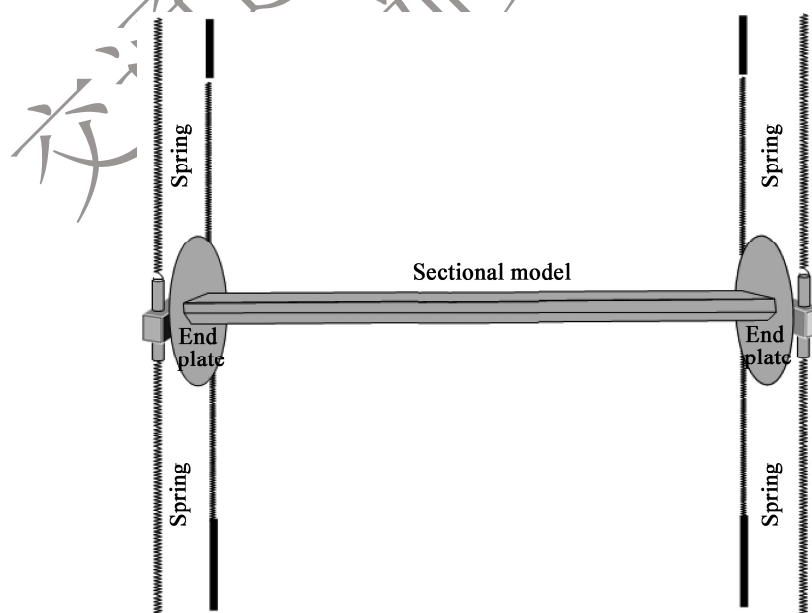


Figure C-3 Schematic for a spring-suspended sectional model

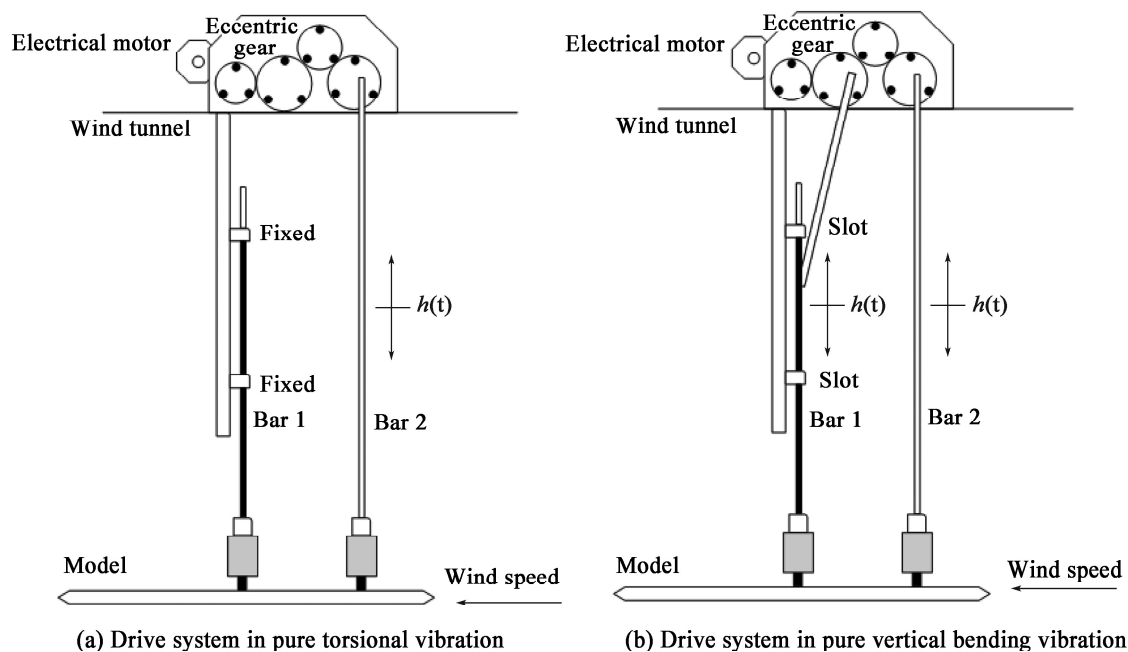


Figure C-4 Schematics for sectional model testing with forced vibration method

C.3.2 The model shall maintain geometric similarity to the prototype bridge, while its elastic parameters, $m/\rho b^2$ and $I_m/\rho b^4$, inertial parameters, $U/f_b b$ and $U/f_t b$, as well as the damping parameter, ζ_s , shall satisfy the similarity condition. Specifically, for suspension bridges and cable-stayed bridges, the mass, m , and mass moment of inertia, I_m , shall be the equivalent mass and equivalent mass moment of inertia that account for the global bridge interaction.

C.3.3 Tests shall be conducted in both uniform flow field and turbulent flow field according to the testing objectives. For the tests in the turbulent flow field, the similarity condition of turbulence intensity should be satisfied.

C.3.4 Sectional model vibration test conditions shall comply with the requirements in Table C.3.4.

Table C.3.4 Allowable tolerances of sectional model parameters

Parameter	Mass	Mass moment of inertia	Frequency	Damping ratio
Allowable tolerance	$\pm 3\%$	$\pm 3\%$	$\pm 3\%$	$\pm 10\%$

C.3.5 Tests with the forced vibration method shall comply with the requirements in Table C.3.5.

Table C.3.5 Allowable tolerances of sectional model parameters for tests with forced vibration method

Parameter	Mass	Mass moment of inertia	Drive amplitude		Frequency of forced vibration
			Vertical vibration amplitude	Torsional amplitude	
Allowable tolerance	$\pm 3\%$	$\pm 3\%$	$(0.01 \sim 0.02) B$	$1^\circ \sim 5^\circ$	$\pm 3\%$

Commentary

The forced vibration method is a test method that drives a sectional model to perform pure torsional, pure vertical or pure lateral motions and obtains flutter derivatives by directly measuring the self-excited flutter forces. Typically, eight flutter derivatives are used to describe the self-excited lift force and moment resulting from the interaction between the airflow and the structural motion, as shown in Eq. (C-2):

$$\begin{aligned} L_{se} &= \rho U^2 B \left[KH_1^* \frac{\dot{h}}{U} + KH_2^* \frac{B\dot{\alpha}}{U} + K^2 H_3^* \alpha + K^2 H_4^* \frac{h}{B} \right] \\ M_{se} &= \rho U^2 B^2 \left[KA_1^* \frac{\dot{h}}{U} + KA_2^* \frac{B\dot{\alpha}}{U} + K^2 A_3^* \alpha + K^2 A_4^* \frac{h}{B} \right] \end{aligned} \quad (C-2)$$

where,

L_{se} ——self-excited lift force (N/m);

M_{se} ——self-excited moment (N·m²/m);

B ——characteristic width of main girder (m);

α ——torsional vibration displacement (rad);

h ——vertical vibration displacement (m);

K ——reduced frequency, taken as $B\omega/U$, in which ω is the circular frequency of modal vibration (rad/s);

H_i^*, A_i^* ——flutter derivatives, which are functions of reduced frequency U/fB .

Self-excited flutter forces are generally obtained by directly measuring aerodynamic forces or by integrating the measured surface pressure. Figure C-5 illustrates the principle of two-degree-of-freedom vibration for a sectional model using the forced vibration method.

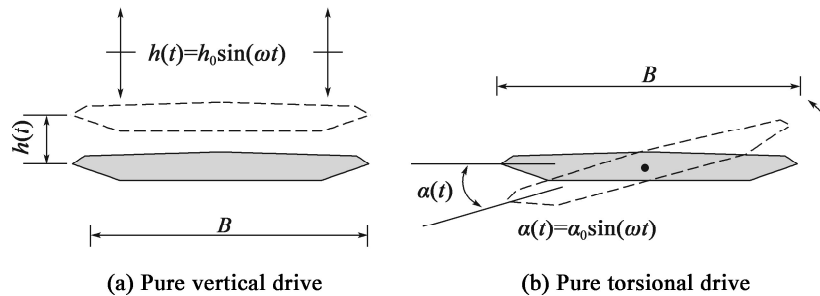


Figure C-5 Schematics for the principle of the sectional model testing with forced vibration method

C.4 Bridge Tower Model Testing

C.4.1 For free-standing bridge towers, either a full elastic model of the tower or an elastically supported rigid-body model of the tower may be employed for vibration or force measurement testing. When using an elastically supported rigid-body model, the test results shall be corrected based on the actual mode shapes.

Commentary

The wind-induced vibration response of bridge tower structures is primarily dominated by the contribution of low-order mode shapes. When the wind-induced vibration of the tower is determined to be dominated by the first bending mode shape, an elastically supported rigid-body tower model can be used for testing. In this case, the vibration displacement of the tower is linear, and the vibration response needs to be corrected based on the first bending mode shape. If multiple mode shapes participate in the wind-induced vibration, a full elastic model of the tower needs to be employed for testing.

C.4.2 The model shall maintain geometric similarity to the prototype bridge, and its elastic parameters, inertial parameters, and damping parameters, ζ_s , shall satisfy the similarity condition.

Commentary

When a full elastic model is used, the dimensionless parameters include $\frac{\rho_s}{\rho}$, $\frac{EI}{\rho U^2 D^4}$, and ζ_s .

When an elastically supported rigid-body model is used, the dimensionless parameters include $\frac{I_m}{\rho D^5}$,

$\frac{U}{fD}$, and ζ_s .

Where,

I_m ——mass moment of inertia of structure or member ($\text{kg} \cdot \text{m}^2$);

D ——characteristic dimension of structure or member (m);

ρ_s ——density of structure or member (kg/m^3).

C.4.3 The model shall maintain geometric similarity to the prototype bridge, and the dimensionless parameters of a full elastic model or an elastically supported rigid-body model and the damping parameter, ζ_s , shall meet the consistency requirements.

C.4.4 Bridge tower model testing shall be conducted in both uniform flow field and turbulent flow field according to the testing objectives. For the tests in the turbulent flow field, the similarity condition of turbulence intensity should be satisfied.

C.4.5 Bridge tower model test conditions shall meet the requirements in Table C.4.5.

Table C.4.5 Allowable tolerances of bridge tower model parameters

Parameter	Mass	Mass moment of inertia	Frequency	Damping ratio
Allowable tolerance	$\pm 3\%$	$\pm 3\%$	$\pm 3\%$	$\pm 10\%$

C.5 Full-bridge Aeroelastic Model Testing

C.5.1 The aeroelastic model shall maintain geometric similarity to the prototype bridge, and the similarity parameters, the model scale, $1/n$, and the test wind speed scale, $1/m$, shall be selected from Table C.5.1. If the bridge structure or members have near-streamlined or circular cross-sections, the geometric shape shall be determined based on the principle of aerodynamic equivalence by considering the Reynolds number effects.

Table C.5.1 Similarity factors of the full-bridge aeroelastic model

Parameter	Similarity factor	Scale ratio	
		Suspension bridge and cable-stayed bridge ^b	Beam bridge, arch bridge
Length	$C_L = L_m/L_p^a$	$1/n$	$1/n$
Time	$C_t = t_m/t_p$	$1/\sqrt{n}$	m/n
Wind speed	$C_U = U_m/U_p$	$1/\sqrt{n}$	$1/m^c$
Frequency	$C_f = f_m/f_p$	\sqrt{n}	n/m
Density	$C_\rho = \rho_m/\rho_p$	1	1
Mass per unit length	$C_M = M_m/M_p$	$1/n^2$	$1/n^2$
Mass moment of inertia per unit length	$C_I = I_{mm}/I_{mp}$	$1/n^4$	$1/n^4$
Tension force	$C_H = H_m/H_p$	$1/n^3$	$1/n^3$
Tensile stiffness	$C_{EA} = (EA)_m/(EA)_p$	$1/n^3$	$1/m^2 n^2$
Flexural stiffness	$C_{EI} = (EI)_m/(EI)_p$	$1/n^5$	$1/m^2 n^4$

continued

Parameter	Similarity factor	Scale ratio	
		Suspension bridge and cable-stayed bridge ⁽²⁾	Beam bridge, arch bridge
St. Venant torsional stiffness	$C_{GI_d} = (GI_d)_m / (GI_d)_p$	$1/n^5$	$1/m^2 n^4$
Warping torsional stiffness	$C_{EI_\omega} = (EI_\omega)_m / (EI_\omega)_p$	$1/n^7$	$1/m^2 n^6$
Structural damping (logarithmic decrement)	$C_\delta = \delta_m / \delta_p$	1	1

Notes: a The subscripts m and p of similarity factors denote the model and prototype bridge.

b The values in the right column may be adopted if the influences of stay cable vibration characteristics are not considered.

c The test wind speed scale, $1/m$, may be selected from the possible range that meets wind tunnel test conditions.

C.5.2 Full-bridge aeroelastic model testing shall be conducted in both a uniform flow field and a turbulent flow field according to the testing objectives. The turbulent flow field shall comply with the provisions in Clause C.1.4 of the *Specifications*, and the topographic effects shall be considered or topographic modelling shall be performed for the bridge sites surrounded by complex topography.

C.5.3 Full-bridge aeroelastic model test conditions shall comply with the requirements in Table C.5.3.

Table C.5.3 Allowable tolerances of full-bridge aeroelastic model parameters

Parameter	Mass	Mass moment of inertia	Stiffness	Frequency	Damping ratio
Allowable tolerance	$\pm 3\%$	$\pm 3\%$	$\pm 4\%$	$\pm 5\%$	$\pm 30\%$

Note: The frequency and damping ratio in the table refer to those corresponding to the low-order modes.

C.5.4 The full-bridge aeroelastic model should undergo vibration measurement tests at three wind attack angles of -3° , 0° and $+3^\circ$ in a uniform flow field.

C.6 Sectional Model Testing for Wind-rain-induced Vibration of Stay Cables

C.6.1 The stay cable sectional model shall maintain geometric similarity to the full-scale stay cable, and the scales for geometric dimensions of the model and wind speed shall be selected as 1:1. The scales for other parameters shall be selected in accordance with Table C.5.1. Testing parameters include a wind speed range of 1 m/s ~ 25 m/s, rainfall intensity range of 0 ~ 120 mm/h, and the wind yaw angle varying between 0° ~ 90° . Figure D.6.1 illustrates the definitions of the cable inclination angle, α , and wind yaw angle, β .

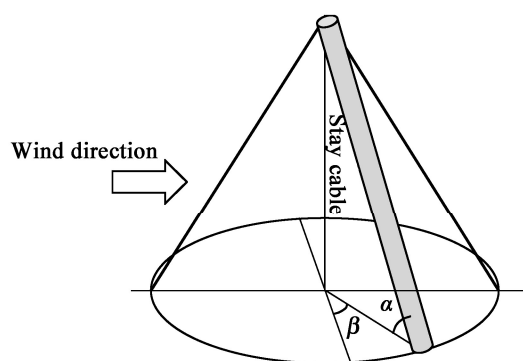


Figure C.6.1 Definition schematic for inclination angle of stay cable and wind yaw angle

C.6.2 Sectional model testing for wind-rain-induced vibration of stay cables shall be conducted in both uniform flow field and turbulent flow field according to the testing objectives, and the turbulent flow field shall comply with the provisions in Clause C.1.4 of the *Specifications*.

C.6.3 Sectional model test conditions for wind-rain-induced vibration of stay cables shall comply with the requirements in Table C.6.3.

Table C.6.3 Allowable tolerances of sectional model parameters for wind-rain-induced vibration of stay cable

Parameter	Mass	Frequency	Damping ratio
Allowable tolerance	$\pm 3\%$	$\pm 5\%$	$\pm 10\%$

C.7 Bridge Site Topographic Wind Environment Model Testing

C.7.1 Topographic wind environment models shall simulate the key topographic features of the area surrounding the bridge site.

C.7.2 The primary wind direction for the test shall consider the spatial arrangement of the bridge axis and main members, as well as the prevailing wind direction at the bridge site. The step size for changes in wind yaw angle should not exceed 15° .

C.8 Wind Environment Testing for Traffic Safety on Bridge Deck

C.8.1 The wind environment model for moving vehicles on the bridge deck shall simulate members such as bridge towers, abutment structures, arch ribs and trusses, as well as appurtenances on the bridge deck such as railings and wind barriers, that affect the flow within the vertical clearance for vehicular traffic on the bridge deck. Besides, it shall account for other

topographic features or structures that influence the wind environment on the bridge deck.

C.8.2 The primary wind direction in the test shall be determined by considering the approach flow perpendicular to the bridge axis, the prevailing wind direction at the bridge site, as well as the influences of the shapes of bridge towers, abutment structures, arch ribs, and trusses.

交通运输部信息公开
浏览专用

Appendix D

Requirements for Virtual Wind Tunnel Testing

D.1 General

D.1.1 Aerostatic force testing, sectional model vibration testing, bridge tower model testing, full-bridge aeroelastic model testing, topographic wind environment model testing, and wind environment testing for moving vehicles on bridge decks may be conducted in virtual wind tunnels for bridge structures or members to verify their wind-resistant performance and acquire relevant aerodynamic parameters and wind parameters.

Commentary

Virtual wind tunnel testing is a simulation established using high-performance computing platforms based on the fundamental principles of computational fluid dynamics. It achieves wind-resistant performance verification and parameter acquisition by numerically solving the flow field around models of topography, structures or members.

D.1.2 An appropriate numerical simulation method shall be selected for the virtual wind tunnel testing based on the requirements for the wind-resistant performance testing of the bridge.

Commentary

Virtual wind tunnel testing generally involves selecting a solution method and a turbulence model, as well as setting relevant parameters. The solution methods for virtual wind tunnel testing studying the wind-resistant performance of bridge structures or members include the finite element method, finite difference method, finite volume method, meshless method, and others. Researchers can

select an appropriate solution method based on factors such as test requirements and their own capabilities in practical applications.

The simulation of turbulent flow remains a relatively complex and challenging aspect of virtual wind tunnel testing, especially since bridge structures or members are often bluff bodies with complex turbulent flow structures around them, including flow separation and reattachment. Solution methods and turbulence models usually contain multiple parameters, and different parameter values can lead to different numerical solution results. Therefore, during the test process, it is necessary to select the turbulence model and its relevant parameters reasonably with reference to relevant research data and based on the simulated object, research purpose, and adopted calculation method. It is recommended that personnel conducting virtual wind tunnel tests not only possess professional knowledge related to the wind resistance of bridges, but also have extensive experience in both physical and virtual wind tunnel tests, enabling them to professionally evaluate the reasonability of the test results.

D.1.3 The numerical simulation method used in the virtual wind tunnel testing shall be validated against the completed wind tunnel test results. The relative error in the drag coefficient should not exceed 15%, that in the flutter critical wind speed should not exceed 20%, and that in the wind speed distribution should not exceed 10%.

Commentary

By selecting appropriate numerical methods, turbulence models, and relevant parameter settings, the relative errors between virtual and physical wind tunnel test results have generally reached an acceptable range for engineering applications. Among these, the wind speed distribution shows the highest accuracy in test results. The drag coefficient among the aerostatic coefficients exhibits relatively lower accuracy, while the lift coefficient and torsional moment coefficient may show significant deviations between virtual and physical wind tunnel tests due to their smaller values at small wind attack angles. Therefore, the requirements for their errors are currently not specified. For virtual wind tunnel flutter tests, whether the flutter critical wind speed is estimated by the flutter derivatives obtained using the forced vibration method or directly acquired using the free vibration method, the issue of fluid-structure interaction needs to be addressed, in which mesh generation and flow field distribution are more complex, resulting in slightly larger relative errors.

Case Study 1: Static three-component force testing of bridge deck sections

The main girder in the Sutong Yangtze River Bridge adopts a steel box girder configuration with the cross-sectional dimensions shown in Figure D-1. In the virtual wind tunnel testing, appurtenances

such as railings, traffic barriers, and maintenance vehicle tracks are included, and the model cross-section is shown in Figure D-2. The meshing for the flow field is illustrated in Figure D-3. The parameters selected for the analysis are presented in Table D-1. The results of the virtual wind tunnel test are shown in Table D-2.

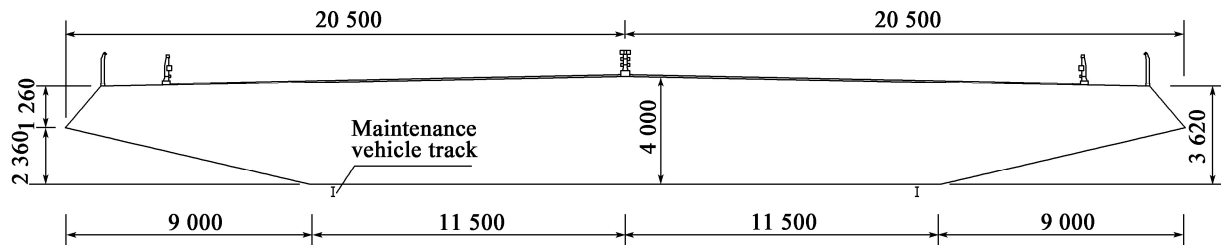


Figure D-1 Dimensions of girder cross-section (Unit: mm)

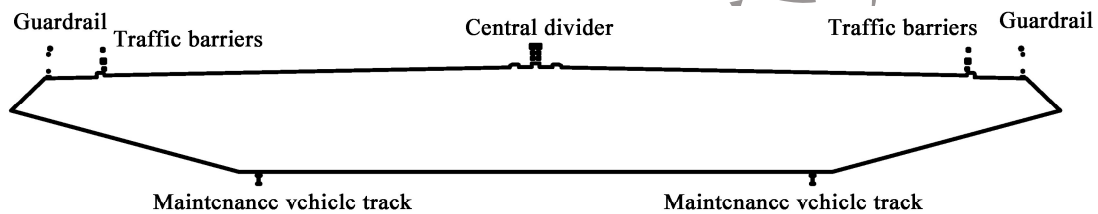


Figure D-2 Schematic of girder shape

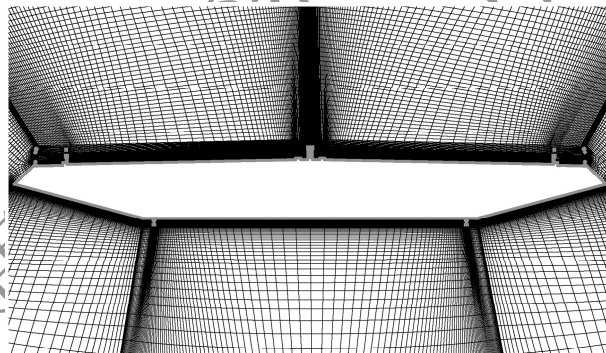


Figure D-3 Schematic for the meshing of the flow field around the cross-section

Table D-1 Analysis methods and parameters

Analysis method	Finite volume method (FVM)
Spatial discretization scheme	Second-order central difference scheme
Time discretization scheme	Second-order implicit scheme
Pressure and velocity coupling	Simple algorithm
Turbulence model	Standard Smagorinsky subgrid scale (SGS) model ($C_s = 0.1$)
Number of meshes	About 120000
Time step, Δt	$\Delta t = 0.005$ s
Total computation time	$T = 50$ s

Table D-2 Test results of three static force components on the cross-section

Wind attack angle (°)	Drag coefficient (C_D)		Lift coefficient (C_L)		Torsional moment coefficient (C_M)	
	Virtual wind tunnel	Physical wind tunnel	Virtual wind tunnel	Physical wind tunnel	Virtual wind tunnel	Physical wind tunnel
-5	0.994	1.018	-0.502	-0.454	-0.081	-0.071
-3	0.935	0.953	-0.436	-0.328	-0.014	-0.028
-1	0.891	0.925	-0.251	-0.188	0.037	0.012
0	0.881	0.911	-0.125	-0.107	0.047	0.028
+1	0.906	0.946	0.046	-0.014	0.055	0.045
+3	0.923	1.056	0.091	0.142	0.069	0.064
+5	1.347	1.229	0.368	0.231	0.071	0.069

Note: The reference height for the drag coefficient is taken as the girder depth of 4 m, and the reference width for the lift coefficient is taken as the girder width of 41 m.

Case Study 2: Sectional model vibration testing—forced vibration method

The main girder of the Aizhai Bridge adopts a steel truss configuration with the cross-sectional dimensions shown in Figure D-4. The cross-sectional shape was selected, taking into account the layout of the trusses at the characteristic positions as well as the appurtenances such as railings, traffic barriers, and maintenance vehicle tracks. The model cross-section is shown in Figure D-5. The meshing for the flow field is illustrated in Figure D-6. With flutter derivatives identified by the forced vibration method, a flutter critical wind speed of 51.8 m/s was obtained through flutter analysis, and the corresponding flutter critical wind speed obtained from wind tunnel tests was 52.5 m/s.

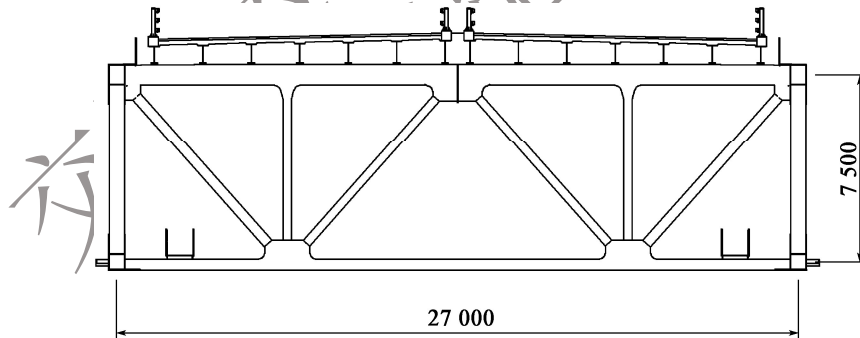


Figure D-4 Cross-sectional dimensions (Unit: mm)

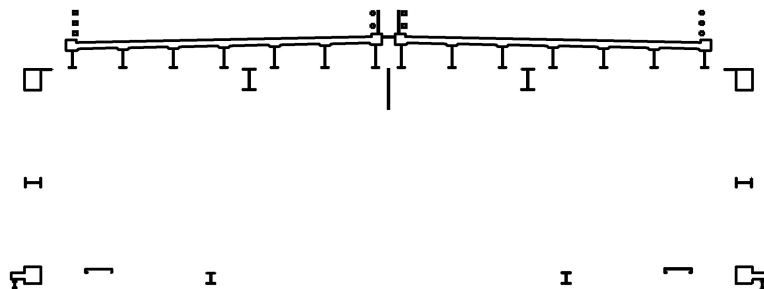


Figure D-5 Schematic of cross-sectional shape

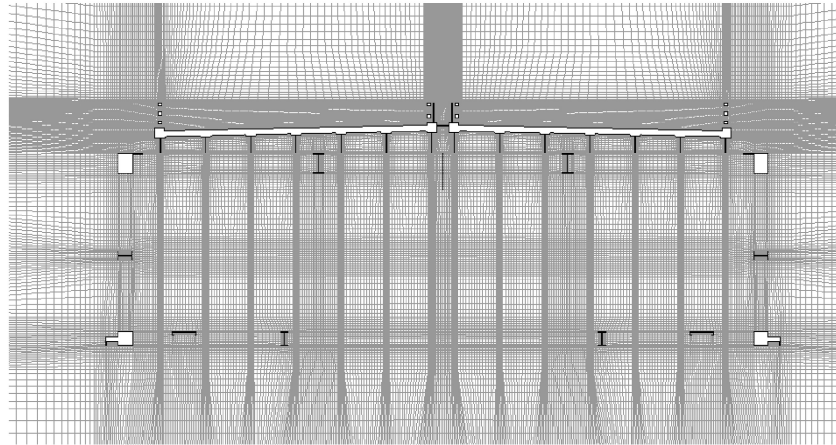


Figure D-6 Schematic for meshing of the flow field around the cross-section

Case Study 3: Sectional model vibration testing——free vibration method

The main girder of the Daxie Second Bridge adopts a steel box girder configuration with the cross-sectional dimensions shown in Figure D-7. The cross-sectional shape was selected, taking into account appurtenances such as railings, traffic barriers, and maintenance vehicle tracks. The model cross-section is illustrated in Figure D-8. The model design parameters are presented in Table D-3. Through a virtual wind tunnel test with the free vibration method, the flutter critical wind speed was obtained as 57.0 m/s, and the corresponding flutter critical wind speed obtained from the wind tunnel test was 54.8 m/s.

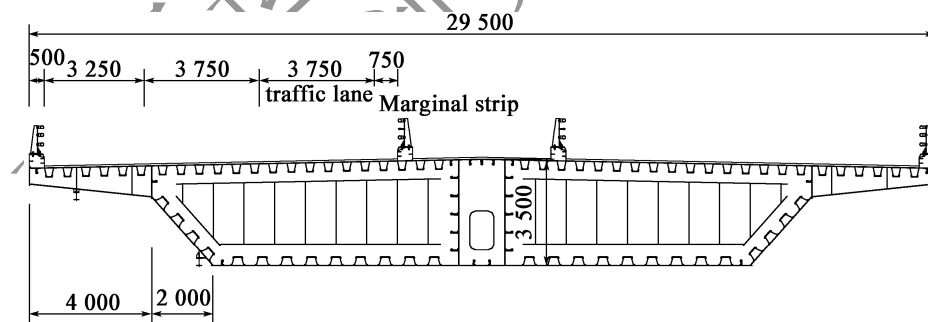


Figure D-7 Main girder cross-section of Daxie Second Bridge (Unit: mm)

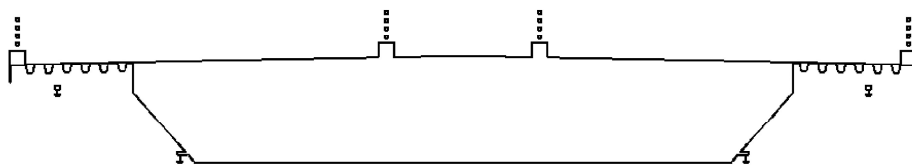


Figure D-8 Schematic for the cross-sectional shape of the Daxie Second Bridge

Table D-3 Design parameters of virtual wind tunnel test model for Daxie Second Bridge

Parameter	Model	Prototype bridge
Geometric scale	1 : 29.5	
Wind speed scale	1 : 10	
Deck width (m)	1	29.5
Vertical bending frequency (Hz)	1.4154	0.4798
Effective mass of vertical bending mode (kg)	23.7978	20710
Torsional frequency (Hz)	2.54	0.861
Equivalent torsional moment of inertia (kg · m ²)	1.7961	1360260
Damping ratio of vertical bending mode (%)	0.5	0.5
Damping ratio of torsional mode (%)	0.5	0.5

D.1.4 Models established for virtual wind tunnel testing shall conform to the principle of similarity in terms of geometric shape, elastic parameters, inertial parameters, damping parameters, etc. The principle of similarity may comply with the relevant requirements for wind tunnel testing in Appendix C of the *Specifications*.

Commentary

The geometric shape of a bridge structure or component has a crucial influence on the flow pattern around the structure, and the established model needs to maintain geometric similarity to the prototype structure as much as possible. The simulation of the bridge structure or member needs to be as detailed as possible, taking into account appurtenances such as guardrails and maintenance vehicle tracks.

D.2 Virtual Wind Tunnel Test Area and Boundary Conditions

D.2.1 The computational domain of the virtual wind tunnel should not be smaller than the ranges specified in Table D.2.1, and the blockage ratio of the geometric model in the virtual wind tunnel shall not exceed 5% .

Table D.2.1 Ranges for the computational domain of virtual wind tunnel

Type of testing	Distance from the inlet to the model	Distance from the outlet to the model	Distance from the two sides to the model	Distance from the top or bottom to the model
Aerostatic force testing/sectional model vibration testing	5 <i>B</i>	20 <i>B</i>	5 <i>B</i>	5 <i>B</i>

continued

Type of testing	Distance from the inlet to the model	Distance from the outlet to the model	Distance from the two sides to the model	Distance from the top or bottom to the model
Bridge tower model testing	$2H$	$10H$	$5B$	$3H$
Full-bridge aeroelastic testing	$10B$	$20B$	$10B$	$3H$
Topographic wind environment model testing	$5L$ or $5B$, whichever is greater	$20L$ or $20B$, whichever is greater	$2L$ or $2B$, whichever is greater	$5H$
Wind environment testing for traffic safety on bridge deck	$5B$	$20B$	$5B$	$3H$

Note: L , B , and H are the length, width, and height of the model, respectively.

Commentary

The basic principles for determining the computational domain include: (1) The inlet location should be reasonably distant from the structural model to avoid the influence of its presence on the inlet wind speed. (2) Due to the strong eddies or high-intensity turbulence typically present at the model downstream, the outlet location should be as far away from the model as possible to reduce the impact of the eddies on the outlet. If the outlet location is insufficiently distant, the computation may result in backflow at the outlet, contradicting the actual situation. (3) The positions of the sides of the computational domain should be selected to minimize the significant blockage effect on the airflow within the entire virtual wind tunnel caused by the presence of the model.

D.2.2 Reasonable boundary conditions and appropriate boundary parameters shall be applied in virtual wind tunnel testing.

Commentary

In virtual wind tunnel testing, the boundary conditions applied to the computational domain typically include: velocity inlet for wind, far-field pressure outlet, symmetry or slip boundaries on both sides, and wall boundaries for the bridge structure or members. The rationality of the boundary parameter settings is determined by their ability to minimize the unphysical influences of the boundaries on internal physical quantities within the computational domain. For instance, improper settings of turbulence intensity or turbulence dissipation rate at the inlet may lead to unreasonable unphysical solutions or even cause solution divergence. A schematic of the boundary setup for the virtual wind tunnel testing of the sectional model is shown schematically in Figure D-9.

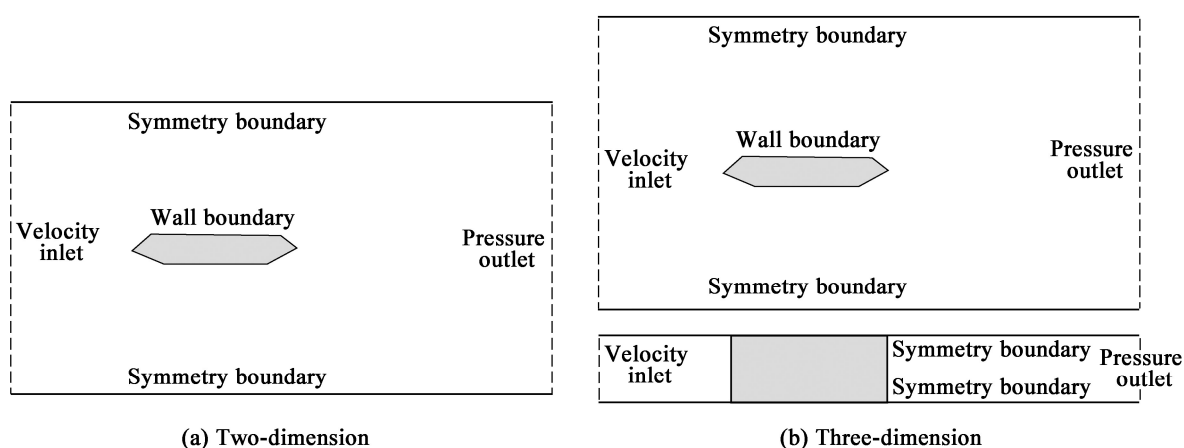


Figure D-9 Schematic of boundary setup for virtual wind tunnel testing of sectional model

D.2.3 The inlet boundary for the wind flow shall meet the requirements of the experimental wind field, and the turbulent flow fields shall satisfy the similarity conditions for turbulence, which may refer to the provisions in Appendix B.1.4 of the *Specifications*.

Commentary

The configuration of the wind speed inlet boundary for virtual wind tunnel testing needs to correspond to the specific test contents being conducted. For aerostatic model testing and sectional model vibration testing, the inlet boundary is typically set as a uniform flow. For bridge tower model testing, full-bridge aeroelastic model testing, topographic wind environment testing, and wind environment testing for traffic safety on bridge decks, the wind speed profile corresponding to a specific terrain category is generally adopted for the wind speed inlet. For test conditions that require simulation of the approach turbulent flow, the approach turbulent flow also needs to satisfy similarity conditions for parameters such as turbulence intensity and turbulent integral length scale.

D.2.4 Before conducting virtual wind tunnel testing, the reasonableness of the boundary conditions such as inlet, outlet, and ground of the unoccupied wind tunnel for the corresponding flow field shall be verified, and it shall be ensured that the flow characteristics do not vary significantly with the flow direction.

Commentary

Before conducting virtual wind tunnel testing, it is necessary to perform flow field simulations of the corresponding computational domain. Based on the simulation results, the variations in airflow characteristics such as wind speed, wind speed profile, and turbulence intensity along the flow

direction within the computational domain are examined to ensure that these characteristics do not change significantly along the flow direction. If significant changes are observed, the rationality of the boundary conditions set for the inlet, outlet, and walls should be checked, as well as the correctness of the parameters such as inlet wind speed, turbulence intensity, and outlet pressure gradient corresponding to these boundaries.

D.3 Mesh Generation

D.3.1 For virtual wind tunnel testing using mesh-based numerical methods, the mesh generation of the computational domain shall conform to the following principles:

- 1 Sufficiently fine meshes shall be generated in the areas adjacent to the surfaces of the structural or member model.
- 2 Mesh refinement shall be applied to the areas of the structural model that contain small members.
- 3 Relatively fine meshes shall be employed in the vicinity of the model.
- 4 Relatively coarse meshes may be used in areas far away from the model.

Commentary

The virtual wind tunnel test results solved by methods such as the finite element method, finite volume method or finite difference method are greatly influenced by the meshing scheme, with the principle being to avoid introducing excessive numerical errors. Generally, in the core flow regions near bridge structures or members, especially at the corners of the main girder and bridge towers, where airflow often separates, the mesh needs to be sufficiently fine to allow the test to resolve potential large gradient flow field patterns in these areas. In the area near the model surface, where the airflow forms a very thin boundary layer, a sufficiently fine mesh is required to improve the solution accuracy in this area, typically with no less than 5 layers of mesh elements. In the areas of the structural model containing small members, such as railings on the bridge deck, maintenance vehicle tracks, and other appurtenances or aerodynamic countermeasures added to enhance the wind-resistant performance of the bridge structure, these members are usually smaller in size compared to the main girder or bridge towers, but their impact on the aerodynamic performance of the structure cannot be ignored. Therefore, mesh refinement is necessary in these areas. As the flow field moves further away from the model area, the interference between the surrounding flow

field and the flow field in the model area gradually weakens. To save computational resources and improve efficiency, a transition to coarser meshing can be made uniformly. Figure D-10 shows an example of meshing for a flow field around a blunt steel box girder section.

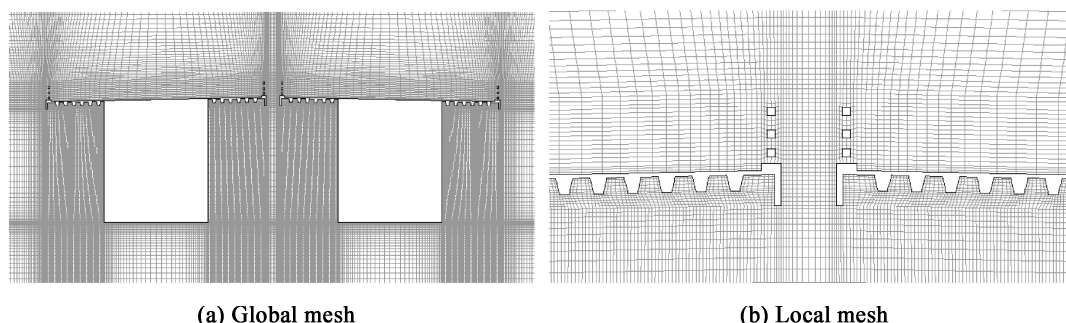


Figure D-10 Mesh generation for the flow field around blunt steel box girder section

D.3.2 When using a mesh-based numerical method, the growth ratio of edge lengths between adjacent mesh elements should not exceed 1.2. The aspect ratio of mesh elements should not exceed 5. The skewness should not exceed 0.2 for two-dimensional meshes and 0.5 for three-dimensional meshes.

Commentary

The quality of mesh generation has a significant impact on the convergence and accuracy of test results. In virtual wind tunnel testing, since the solving process is carried out by computers and the processing of test results is relatively straightforward, test personnel should devote themselves to improving the quality of mesh generation in the computational domain to achieve better test results. There are numerous methods and parameters for evaluating mesh quality, and different numerical methods and software adopt varying criteria for the mesh quality evaluation. Three commonly used criteria are selected in this clause, including adjacent mesh edge growth ratio, mesh aspect ratio, and mesh skewness. The mesh aspect ratio is defined as the ratio of the longest to shortest edges of an element, with a value closer to 1 indicating a more ideal element shape. The adjacent mesh edge growth ratio is the ratio of the edge change between two collinear or coplanar mesh elements, with a value closer to 1 being preferable to ensure smooth transitions in mesh distribution. The mesh skewness is typically defined as $\max \{ (\theta_{\max} - \theta_{eq}) / (180 - \theta_{eq}), (\theta_{eq} - \theta_{\min}) / \theta_{eq} \}$, where θ_{\max} and θ_{\min} are the maximum and minimum angles formed by the element edges, and θ_{eq} is a characteristic angle of a similar equilateral element shape, taken as 60° for triangles and tetrahedrons, and 90° for quadrilaterals and hexahedrons. A mesh skewness closer to 0 indicates a superior element shape, while a value closer to 1 indicates a poorer element shape.

It should be emphasized that even a few highly skewed elements (skewness > 0.95) within the

computational domain can lead to solution divergence or unreliable results for the entire flow field. The adjacent mesh edge growth ratio exceeding 1.2 may degrade computational accuracy and cause residual convergence difficulties. The aspect ratios exceeding 5 tend to increase the stiffness of the discretized equations, resulting in slower iteration convergence or even failure to converge. Figure D-11 illustrates triangles and quadrilaterals with varying aspect ratios. Figure D-12 schematically shows the uniformity of transitions between adjacent meshes. Figure D-13 presents examples of two-dimensional and three-dimensional meshes with different skewness levels.

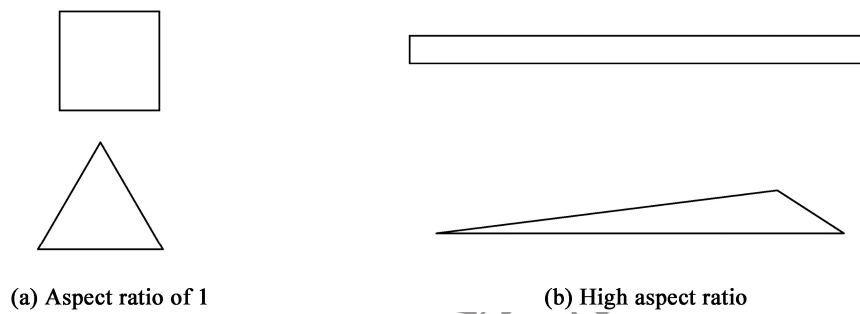


Figure D-11 Schematic of different mesh aspect ratios

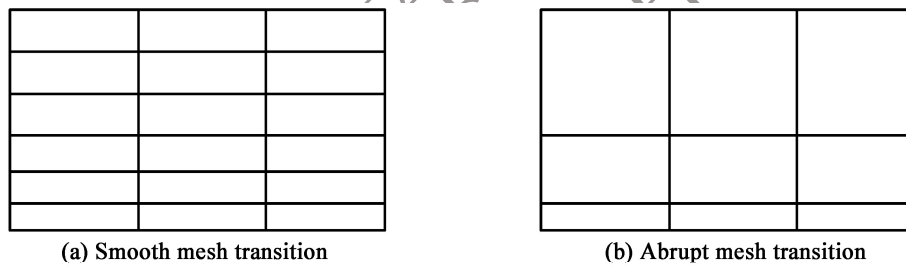


Figure D-12 Schematic of different transitions between adjacent meshes

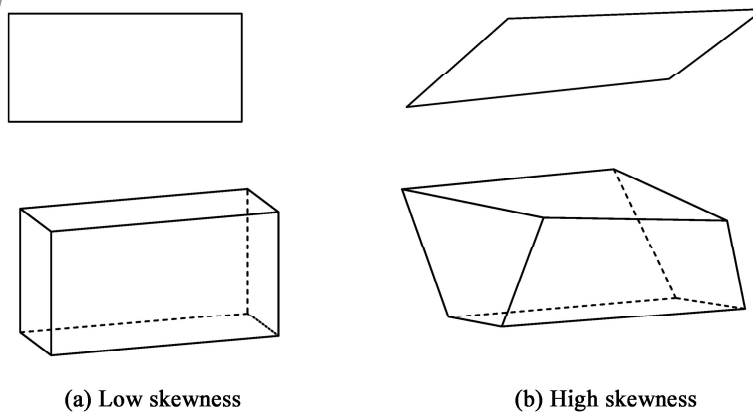


Figure D-13 Schematic of meshes with different skewness levels

D.3.3 When using mesh-based numerical methods to solve aeroelastic problems, dynamic mesh simulation techniques capable of accounting for boundary movement effects shall be employed. The mesh adjustment or remeshing of the computational domain shall be synchronized with the boundary movement and comply with the requirements specified in Clauses D.3.1 and D.3.2 of the *Specifications*.

Commentary

When using mesh-based numerical methods to solve aeroelastic problems, the displacement of bridge structures under aerodynamic forces will cause boundary movement, rendering the existing mesh incompatible with the computational domain after the boundary movement. In such cases, dynamic mesh techniques are needed to match the moved boundaries. Local mesh adjustments can be made for the moving boundary regions for the existing mesh elements within the computational domain to adapt to the new boundaries. For cases where the boundary changes significantly and local mesh adjustment is difficult to adapt to the new boundaries, remeshing of the computational domain can be required. Typically, dense meshing is employed in the surface regions of structures or members, and boundary movements can easily lead to remeshing that generates elements with sharp angles or even cause mesh inversion, resulting in negative volume elements, impeding solution convergence or causing divergence, thus failing to obtain satisfactory results. In practical implementation, rigorous quality checks are required for the regenerated meshes to prevent these issues. Figure D-14 shows two examples of poor-quality mesh regeneration.

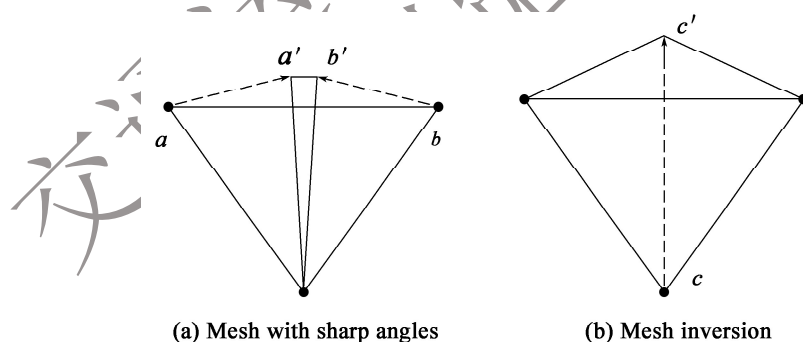


Figure D-14 Examples of poor-quality mesh regeneration

D.4 Numerical Solution

D.4.1 The reasonableness of mesh generation should be validated by comparing two meshing schemes with a mesh density difference of no less than 2 times, ensuring that the discrepancy in test results does not exceed 5%.

Commentary

Ensuring mesh independence is crucial for the validity of numerical solutions, and well-designed meshing schemes have minimal impact on the discrepancy in test results. A common practice is to select a specific condition and generate an initial coarse mesh within the computational domain for subsequent numerical solutions. On this basis, the mesh is typically refined by halving the element size. After solving, the difference between the results obtained from the coarse and refined meshes is required not to exceed 5%. Otherwise, the mesh needs further refinement for the solution until the discrepancy requirement of not exceeding 5% is satisfied.

D.4.2 For numerical solutions, schemes with at least second-order accuracy should be utilized, and the solution convergence shall be guaranteed.

Commentary

The accuracy of numerical solutions depends on the accuracy of the discretization scheme employed. Higher-order schemes deliver better accuracy but present convergence challenges, while lower-order schemes offer faster convergence at the expense of reduced accuracy. A common practice is to conduct initial computation using a first-order scheme to achieve convergence, and then utilize the resulting flow field as the initial condition for subsequent computation with a second-order or higher-order scheme, in order to ensure both the accuracy and convergence of the solution. Convergence is typically judged by requiring that relative residuals of computational variables are not larger than 1×10^{-4} , with attainment of 1×10^{-5} being optimal.

D.4.3 When employing partitioned coupling iteration schemes to solve aeroelastic problems, the conservation of variables shall be ensured during the data exchange between flow field pressures and structural boundary displacements within each time step.

Commentary

The solution of aeroelastic problems involves the coupled calculation of flow field and structural domains, making it relatively complex in numerical simulation. Two primary approaches are commonly employed: the first unifies the flow field and structural equations for simultaneous solution, while the second solves the flow field and structural equations separately. The first approach directly solves the flow field and structural results synchronously. However, due to the

different methods used to formulate the flow field and structural governing equations, developing programs that directly solve these coupled equations remains technically challenging. Although some research achievements exist in this area, the approach has not yet been widely applied. The second approach leverages existing mature standalone solvers for flow field and structural domains, and requires only effective handling of boundary information exchange between the two domains to easily solve the aeroelastic problems. This makes it the prevailing method for solving aeroelastic problems in the structural field. Since the meshing at the coupled boundaries often differs between the flow field and structural domains, and the mesh of the flow field boundary is typically finer than that of the structural boundary, it is important to ensure the balance and coordination in the conversion process of results, for example boundary displacements and pressure distributions, at the coupling between the flow field and structural boundaries within each time step when solving aeroelastic problems.

D.5 Requirements for Virtual Wind Tunnel Testing

D.5.1 Models and test conditions for aerostatic force testing, sectional model vibration testing, bridge tower model testing, full-bridge aeroelastic model testing, topographic wind environment model testing, and wind environment testing for traffic safety on bridge decks may be determined in accordance with the requirements of wind-resistant performance verification by referring to Appendix B of the *Specifications*.

D.5.2 The model coverage for the topographic wind environment model testing should encompass the areas surrounding meteorological stations.

Commentary

Virtual wind tunnel testing for topographic wind environment require establishing the topographic models covering a specified area around the bridge site, generally no less than 10 km. To better analyze wind parameters at the bridge site, the topographic model ideally needs to include areas where surrounding meteorological stations are located. This enables the establishment of correlations between the wind parameters at the meteorological stations and those at the bridge site. By fully utilizing long-term wind parameter observation data from the meteorological stations, a more comprehensive and reasonable assessment of the wind parameters at the bridge site can be provided.

Case Study: Wind speed distribution at the site of the Hezhang Bridge in Guizhou

The Hezhang Bridge in Guizhou is a large river-crossing bridge on the Biwei Expressway. For the virtual wind tunnel testing of the topographic wind environment, a topographic model was established covering a 20 km radius around the bridge site, which also included the nearby Hezhang meteorological station. Through the virtual wind tunnel testing, a correction factor of 1.46 was obtained between the wind speed at the main girder height of the bridge site and the observed wind speed at a height of 10 m from the nearby meteorological station, with Terrain Category C at the bridge site. Figure D-15 shows the virtual wind tunnel simulation results of the wind speed profile at the site of the Hezhang Bridge.

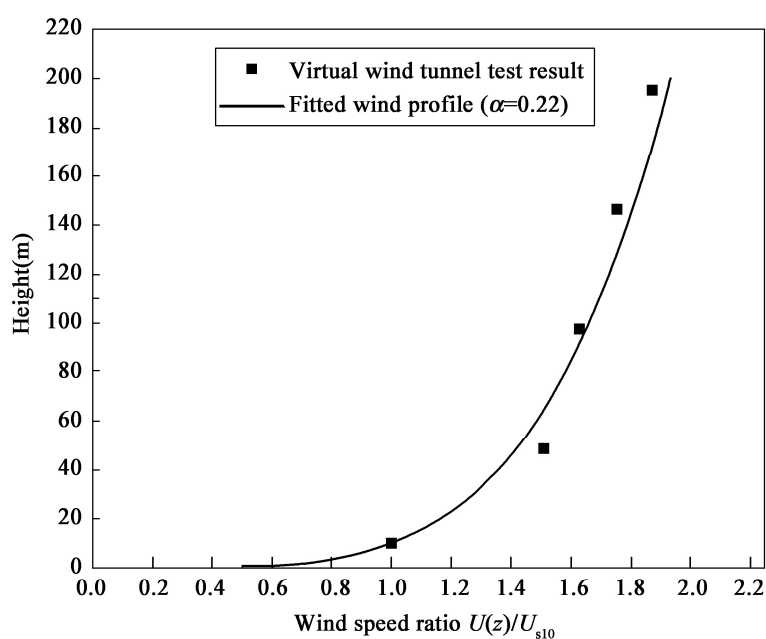


Figure D-15 Virtual wind tunnel simulation results of wind speed profile at the Hezhang Bridge site

D.5.3 In topographic wind environment testing, the simulation of ground vegetation or small-scale obstacles may be moderately simplified, or they may be considered by adding source terms to the fluid governing equations.

Commentary

The topographic wind environment testing for bridges focus on the distribution of wind parameters at the bridge site. Due to current computational resource limitations, it is difficult to accurately simulate ground vegetation or small-scale obstacles in the topographic model. On the premise that their impact on the overall topographic wind environment is insignificant, the terrain surface can be smoothed. If the influence of ground vegetation or small-scale obstacles on the topographic wind environment needs to be considered, an equivalent mathematical model can be used. A common approach is to apply additional source terms in the fluid governing equations.

D. 5. 4 Spatial models of complex terrains may be obtained through reverse engineering by utilizing the positional information of spatial contour lines and elevation points.

Commentary

The virtual wind tunnel testing for a topographic wind environment first requires the establishment of a spatial model of the terrain surface. Existing geographic information databases of terrains typically cannot directly provide three-dimensional spatial models of the terrains, but rather present them in the form of contour lines or elevation points. In such cases, the three-dimensional spatial model of the terrain can be generated with relevant software based on the principles of reverse engineering.

Explanation on Wording in the *Specifications*

1. For the purpose of differentiating treatments when implementing the provisions of the *Specifications*, the following words with different levels of strictness in requirements are explained as follows:

- (1) Must or must not is used for a mandatory requirement in any circumstances.
- (2) Shall or shall not is used for a mandatory requirement in normal circumstances.
- (3) Should or should not is used for an advisory requirement.
- (4) May or may not is used for a permissive condition that no requirement is intended.

2. When other relevant standards or specifications are designated to be followed in the *Specifications*, the phrase used is "shall comply with. . ." or "shall conform to the requirements or provisions of. ..". When it is not mandatory to follow the designated standards or specifications, the phrase used is "may refer to. . .".